
Ancient TL

www.ancienttl.org · ISSN: 2693-0935

Issue 40(1) - June 2022

<https://doi.org/10.26034/la.atl.v40.i1>

This issue is published under a Creative Commons Attribution 4.0 International (CC BY):

<https://creativecommons.org/licenses/by/4.0>



© Ancient TL, 2022

Ancient TL

A periodical devoted to Luminescence and ESR dating

Department of Physics, East Carolina University, 1000 East 5th Street, Greenville, NC 27858, USA
<http://ancienttl.org>

June 2022, Volume 40 No.1

Measuring photo-transferred thermoluminescence from feldspars in post-IR IRSL procedures using a new user defined command for the Risø TL/OSL reader	1
Svenja Riedesel and Geoff A.T. Duller	
Methods Note: An analysis of potassium to rubidium ratios in shoreline sediments: implications for OSL dosimetry	12
Andrew J. Fish and Kenneth Lepper	
Thesis abstracts	15
Bibliography	21
Announcements	53

Ancient TL

Started by the late David Zimmerman in 1977

EDITOR

Regina DeWitt, Department of Physics, East Carolina University, Howell Science Complex, 1000 E. 5th Street
Greenville, NC 27858, USA; Tel: +252-328-4980; Fax: +252-328-0753 (dewittr@ecu.edu)

EDITORIAL BOARD

Ian K. Bailiff, Luminescence Dating Laboratory, Univ. of Durham, Durham, UK (ian.bailiff@durham.ac.uk)

Geoff A.T. Duller, Institute of Geography and Earth Sciences, Aberystwyth University, Ceredigion, Wales, UK
(ggd@aber.ac.uk)

Sheng-Hua Li, Department of Earth Sciences, The University of Hong Kong, Hong Kong, China (shli@hku.hk)

Shannon Mahan, U.S. Geological Survey, Denver Federal Center, Denver, CO, USA (smahan@usgs.gov)

Richard G. Roberts, School of Earth and Environmental Sciences, University of Wollongong, Australia
(rgrob@uow.edu.au)

REVIEWERS PANEL

Richard M. Bailey

Oxford, UK

richard.bailey@ouce.ox.ac.uk

James Feathers

Seattle, WA, USA

jimf@uw.edu

Rainer Grün

Canberra, Australia

rainer.grun@anu.edu.au

David J. Huntley

Burnaby B.C., Canada

huntley@sfu.ca

Sebastian Kreutzer

Heidelberg, Germany

sebastian.kreutzer@uni-heidelberg.de

Michel Lamothe

Montréal, Québec, Canada

lamothe.michel@uqam.ca

Norbert Mercier

Bordeaux, France

norbert.mercier@u-bordeaux-montaigne.fr

Didier Miallier

Aubièrre, France

miallier@clermont.in2p3.fr

Andrew S. Murray

Roskilde, Denmark

anmu@dtu.dk

Vasilis Pagonis

Westminster, MD, USA

vpagonis@mcdaniel.edu

Naomi Porat

Jerusalem, Israel

naomi.porat@gsi.gov.il

Daniel Richter

Leipzig, Germany

drichter@eva.mpg.de

David C.W. Sanderson

East Kilbride, UK

David.Sanderson@glasgow.ac.uk

Andre Sawakuchi

São Paulo, SP, Brazil

andreas@usp.br

Ashok K. Singhvi

Ahmedabad, India

singhvi@prl.res.in

Kristina J. Thomsen

Roskilde, Denmark

krth@dtu.dk

Web coordinators: Joel DeWitt, Regina DeWitt

Article layout and typesetting: Regina DeWitt

Bibliography: Sebastien Huot

Measuring photo-transferred thermoluminescence from feldspars in post-IR IRSL procedures using a new user defined command for the Risø TL/OSL reader

Svenja Riedesel^{1,2}  and Geoff A.T. Duller² 

¹ Institute of Geography, University of Cologne, Cologne, Germany

² Department of Geography and Earth Sciences, Aberystwyth University, United Kingdom

Corresponding Author: riedeselsvenja@gmail.com

Received: February 17, 2022; in final form: May 13, 2022

Abstract

Stimulating a preheated feldspar sample with infrared light causes photo-transfer of charge within the crystal. The resulting photo-transferred luminescence signal is visible in thermoluminescence (TL) and infrared stimulated luminescence (IRSL) measurements, where it results in an increase in the measured luminescence signal intensity. This is particularly relevant when using a post-IR IRSL measurement protocol for dating feldspars, which consists of two consecutive IRSL measurements, one at low temperature (usually at 50 °C) and a second IRSL measurement at elevated temperature. In this case, the lower temperature IRSL measurement causes photo-transfer of charge, which then influences the subsequent higher temperature post-IR IRSL signal. This paper presents a new user defined command to be used with the Sequence Editor software on a Risø TL/OSL reader. This command can be used to assess the amount of photo-transfer that is caused by IR stimulation, and how large a signal this may contribute to a subsequent elevated temperature IRSL measurement. The command can also be useful for identifying the length of time an aliquot should be held at the measurement temperature prior to switching on the IR LEDs in order for any photo-transferred TL to have been reduced to a negligible level. To show the applicability of this new user defined command to feldspar post-IR IRSL measurements, this paper presents results from two feldspar samples measured using the new user defined command as part of three different preheat and post-IR IRSL

temperature combinations.

Keywords: User defined command, photo-transferred TL, feldspar luminescence, post-IR IRSL

1. Introduction

Photo-transferred thermoluminescence (PTTL) or re-excitation (e.g., [Bailiff, 1976](#); [Schlesinger, 1965](#)) describes luminescence that occurs as a result of optical excitation after irradiation and preheating and which is visible in TL curves measured after the optical excitation. It has been associated with redistribution of charge ([Kaylor et al., 1995](#)) and was observed in different minerals, including quartz (e.g., [Kaylor et al., 1995](#); [Schlesinger, 1965](#); [Wintle & Murray, 1997](#)), fluorapatite (e.g., [Bailiff, 1976](#)), zircon (e.g., [Bailiff, 1976](#); [Kristianpoller et al., 2006](#)) and feldspar (e.g., [Duller, 1995](#); [Murray et al., 2009](#); [Robertson et al., 1993](#); [Tsukamoto et al., 2012](#)). PTTL can easily be identified when comparing TL curves recorded after a preheat and TL curves recorded after a preheat and a subsequent optical stimulation step (cf. [Fig. 1](#)).

For feldspars it has been observed that stimulation of a sample with infrared (IR) light can result in an increase in TL signal intensity due to photo-transfer of charge (cf. [Fig. 1](#)). If one subtracts a TL curve measured after a preheat and an IR stimulation step from a TL curve measured after only a preheat (curve A – curve B), a net negative TL signal will be observed in the temperature range of the former preheat (cf. dashed line in [Fig. 1](#); e.g. [Duller 1995](#); [Murray et al. 2009](#); [Robertson et al. 1993](#); [Tsukamoto et al. 2012](#)). Besides affecting TL, PTTL may influence the intensity of the IR stimulated luminescence (IRSL) signal (e.g., [Qin et al., 2015](#); [Wang & Wintle, 2013](#); [Wang et al., 2014](#)), which is particularly important in light of the routine use of the post-IR IRSL

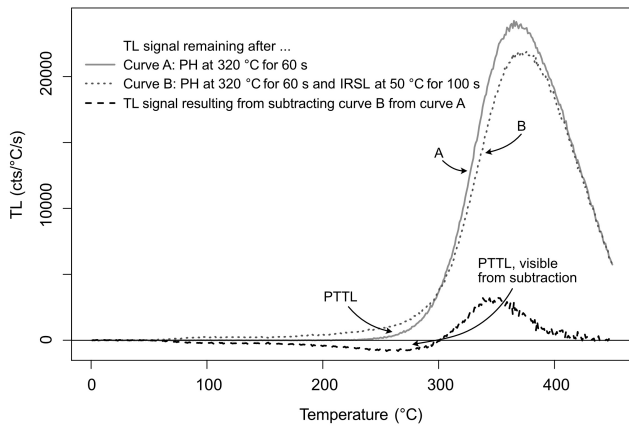


Figure 1: Feldspar TL signal recorded after a preheat of 320 °C for 60 s (solid line). From the dotted line (B) one can see the slight increase in TL signal intensity in the temperature range from ~ 100 °C to 290 °C. This is due to photo-transfer from IR stimulation. The dashed line results from subtracting the dotted line (B) from the solid line (A). Using this approach, the PTTL signal is visible from subtraction.

signal when dating feldspars. Usually, when applying a post-IR IRSL protocol, the signal used for dating is an IRSL signal recorded after a preheat and after one or multiple lower temperature IR stimulation step(s) (cf. Buylaert et al., 2012; Li & Li, 2011; Thiel et al., 2011; Thomsen et al., 2008). The lower temperature IRSL measurements will likely introduce a PTTL signal for the next higher temperature IRSL measurement, where it would then be released during the heating to this higher temperature IRSL measurement, potentially affecting the signal intensity and stability (e.g., Qin et al., 2015; Wang & Wintle, 2013; Wang et al., 2014). PTTL is clearly visible in TL measurements (cf. Fig. 1) and a first impression of PTTL in IRSL can be gained by using blank channels prior to turning on the stimulation light sources. However, the current set of commands for the Risø TL/OSL reader available through the Sequence Editor does not enable recording the PTTL signal to its full extent during IRSL measurements, hindering routine study of this PTTL signal, or any assessment of the likely impact it could have upon the subsequent post-IR IRSL measurement.

To gain further information on the PTTL signal and on its impact on the post-IR IRSL signal, it would be useful to monitor and minimise the impact of PTTL when dating feldspars. Here we present a new user defined command for the Risø TL/OSL reader that makes it possible to record and monitor the PTTL signal during routine IRSL measurements.

2. Previous studies exploring the effect of PTTL on post- IR IRSL signals

Whilst PTTL in feldspars has been known for a long time (e.g., Duller, 1995; Robertson et al., 1993), its presence in and effect on the post-IR IRSL signal has been of interest in

more recent years. To highlight the importance of this photo-transferred signal for IRSL measurements, we here briefly review studies focussing on the PTTL signal arising in the post-IR IRSL measurement procedure.

In 2013 Wang & Wintle associated parts of a measured post-IR IRSL signal of a perthitic feldspar sample with photo-transfer of charge during IR stimulation. These authors suggest that this charge is released thermally during the post-IR IRSL stimulation step at elevated temperature, resulting in a contribution to the overall post-IR IRSL signal. These authors identify contributions of this photo-transferred signal to the overall measured post-IR IRSL signal of up to 20 %. Wang & Wintle (2013) suggest that this photo-transferred TL signal should be removed prior to the measurement of the post-IR IRSL signal, because it is expected that the photo-transferred signal shows fading rates similar to the IRSL signal measured as a first step in the post-IR IRSL measurement procedure. Subsequently these authors suggest to either (i) insert a cut heat, at a temperature slightly below the preheat temperature, between the two IR measurements, or (ii) to hold the sample at the post-IR IRSL measurement temperature for a longer duration prior to switching on the LEDs. However, Wang & Wintle (2013) did not explore this second suggestion.

Wang et al. (2014) further investigated the effect of the photo-transferred signal on the post-IR IRSL signal. These authors suggest that the cut heat proposed by Wang & Wintle (2013) could affect the post-IR IRSL measurement negatively by resulting in re-trapping of some of the thermally excited electrons, which will then contribute to the post-IR IRSL signal. Subsequently, these authors advise against the use of a cut heat as a tool used to remove a PTTL signal. Qin et al. (2015) showed that the presence of a PTTL signal in a post-IR IRSL signal can lead to an underestimation of a given dose in dose recovery experiments and that the presence of a PTTL signal can lead to an underestimation of the thermal stability of the post-IR IRSL signals. Qin et al. (2015) show that increased preheat and post-IR IRSL stimulation temperatures (up to 400 °C) improve dose recovery ratios, compared to a post-IR IRSL₂₉₀ protocol with a preheat at 320 °C.

The application of a cut heat between the two IRSL measurements in a post-IR IRSL protocol results in other issues, as pointed out by Wang et al. (2014). Also, the suggestion by Qin et al. (2015) of using very high preheat and post-IR IRSL stimulation temperatures might influence the feldspar crystal, since exsolution features might be affected by heating the material to temperatures around 400 °C (e.g., Brown & Parsons, 1984; Lin & Yund, 1972; Parsons et al., 2015). Thus, holding the sample at the IRSL measurement temperature for a longer duration (Wang & Wintle, 2013) might be the most gentle and effective solution to remove the PTTL signal and its contribution to a post-IR IRSL signal. If this approach would be attempted, it would be important to evaluate how long such an isothermal holding step prior to switching on the IR LEDs should be. Therefore, a procedure for the routine assessment of the presence and influence of PTTL on post-IR IRSL measurements is needed.

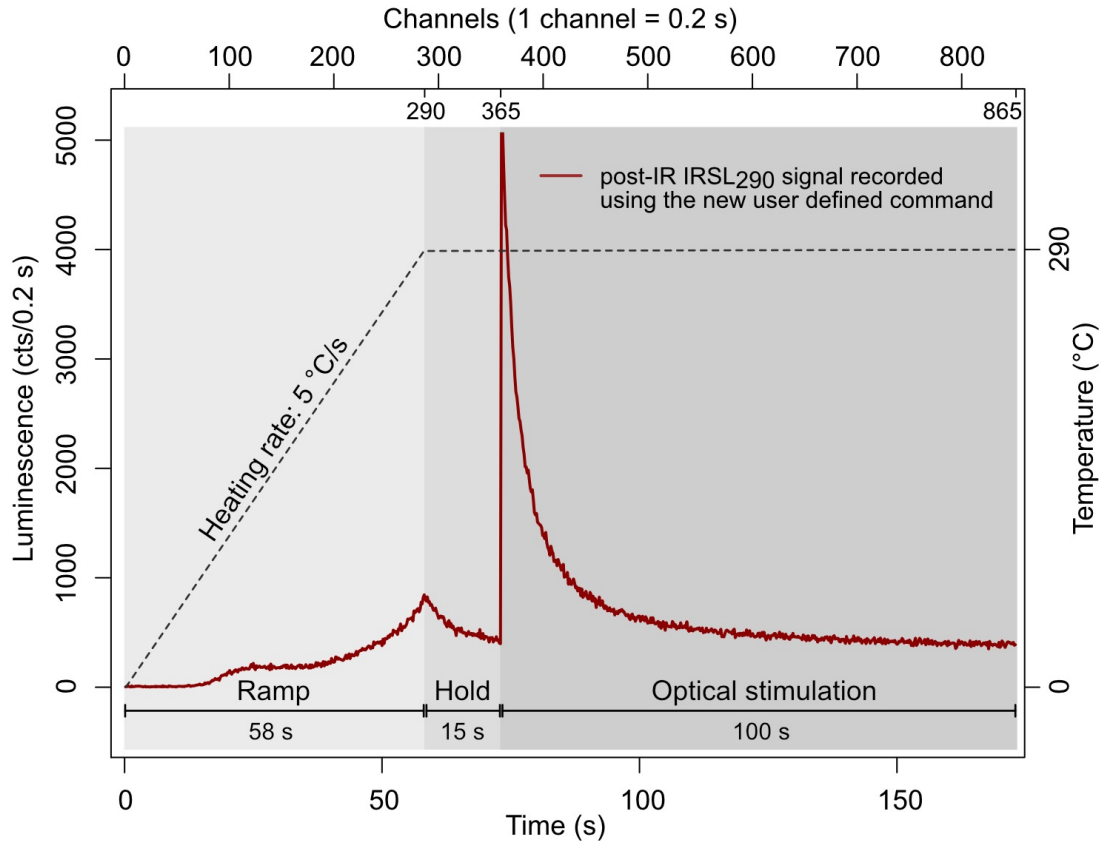


Figure 2: An example of a PTTL signal and IRSL decay curve recorded using the new user defined command. The figure shows the luminescence emitted during ramping of the sample to the measurement temperature (here: 290 °C), then during the 15 s pause prior to the IRSL measurement, and then during the actual IRSL measurement (here: 100 s of IR stimulation).

3. A new user defined command to record and monitor PTTL in feldspar IRSL measurements

3.1. Purpose and performance of the new user defined command

In the following we describe a newly developed user defined command for recording and monitoring PTTL in IRSL measurements using the Risø TL/OSL system. This new user defined command can be used instead of a routine OSL or IRSL measurement, where it will not only record the actual OSL/IRSL measurement, but also any luminescence emitted during heating of the sample to the measurement temperature and during potential isothermal pauses at the measurement temperature prior to optical stimulation. This will enable an estimation to be made of the contribution of this PTTL signal to the elevated temperature IRSL signal.

To enable recording and monitoring of the PTTL signal in OSL/IRSL measurements the Mini-Sys command file for user defined instructions (usermsll.cmd) originally installed with the software needs to be modified (Table 1). The new command results in the same treatment to the aliquot as occurs using the OSL command, but instead of only record-

ing the luminescence emitted during the optical stimulation, this user defined command records data (i) during the ramping of the aliquot temperature from room temperature to the measurement temperature, (ii) during the period of time selected for the ‘Pause’ when the aliquot is held at the measurement temperature prior to starting the optical stimulation, and (iii) during the optical stimulation itself. Data from all three phases of the operation are concatenated, producing a single data record in the BINX file. The data can be viewed using the Analyst software (Duller, 2015), but because they combine together three different phases they are hard to interpret. To present the data more clearly they were exported from Analyst and then further processed using R (R Core Team, 2019). An example of the data produced by this command is shown in Figure 2. Figure 2 shows a post-IR IRSL₂₉₀ signal (red line) recorded using the new user defined command. The shaded areas indicate the three parts of the PTTL and IRSL measurement: (i) ramping to the measurement temperature (here 290 °C, see dashed line), (ii) the isothermal holding measurement for 15 s (also referred to as ‘Pause’) and (iii) the actual optical stimulation for 100 s. The second x-axis on top of the graph shows the channel numbers used, when recording this measurement with a resolution of

0.2 s per channel. We would also advise the user to use the same channel width for all three parts of the measurement using the new command to make data analysis simpler. The post-IR IRSL₂₉₀ signal shows a PTTL signal during the ramp and the isothermal holding measurement. Whilst the PTTL signal increases during the ramp, a decrease is observed during the 15 s pause prior to switching on the LEDs. However, one can see that the PTTL signal has not decreased to the background level after a 15 s pause, thus one can assume a contribution of the PTTL signal to the actual IRSL signal in this example.

3.2. Implementing and using the user defined command

To be able to use this user defined command, the Mini-Sys command file for user defined instructions (usersll.cmd) needs to be changed. Details about user defined commands can be found in [Armitage & Duller \(2004\)](#). Information about the low-level commands that are used in the command file are listed in a handbook provided by Risø via their website (https://www.fysik.dtu.dk/english/research/radphys/research/radiation-instruments/tl_osl_reader/manuals; June 23, 2022). Once the latest Risø software package is installed on the user's hard drive, a PDF ("UserDef.pdf") containing information on how to edit and write user defined commands can be found in the "Manuals" folder of the Risø software package. Before modifying the usersll.cmd file we strongly recommend to back-up the existing file and create a copy for editing. For the purpose of this paper we modified user defined command 4 (UserDef4), which already existed in the usersll.cmd file. The text which needs to be inserted as a user defined command into the usersll.cmd file is given in Table 1. The first part of Table 1 defines which command line in the Sequence Editor software describes which part of the command (see Table 1 and Fig. 3, and compare commands with \$N). The second part contains the instructions for the Mini-Sys, so that the command can be performed. Once the user defined command is implemented, it can be tested. Figure 3 shows the Sequence Editor command window, where all individual commands (\$N) can be edited depending on the settings required for the measurement. Please be aware that it is not possible to modify the title for each command. In the example displayed in Figure 3 an IRSL measurement at 290 °C was performed for 100 s. The corresponding IRSL decay curve and recorded PTTL is shown in Figure 2. Prior to the optical stimulation using IR LEDs, the sample was held at the measurement temperature for 15 s. In this example, command \$5 defines the measurement temperature (*here* 290 °C) and command \$7 the light source (*here* IR LEDs). Depending on the integration time for each channel, all commands referring to the data points recorded have to be adjusted for the respective duration of the individual parts of the measurement. As an example: the duration of the IR stimulation in this example is 100 s (see \$3 in Fig. 3) and we would like the data to be collected with a channel width of 0.2 s, thus the number of data points during

New user defined function in usersll.cmd script

```
; Record luminescence during heating and pause prior to OSL
; $0 Position
; $1 Data points during heating ramp
; $2 Not used
; $3 Length of optical stimulation
; $4 Heating rate during ramp
; $5 Heating temperature
; $6 Length of pause at temperature before optical stimulation
; $7 Light source
; $8 Optical power
; $9 Not used
; $10 Not used
; $11 Data points during optical stimulation
; $12-18 Not used
; $19 Data points during pause before optical stimulation
; $20 = $1 + $11 + $19
```

```
10=PS $0
20=#RS
25=#INITGRAPH $20
30=#TF
40=#RS
50=#WLT
60=LU
70=#RS
75=IR SET $8
80=TL $5 $4 $1 $5
90=#DATA
100=OS N $6 $19
110=#DATB
120=#CONCAT
130=OS $7 $3 $11
140=#DATB
150=#CONCAT
160=#SAVE
170=#ENDGRAPH
180=#WRITE
190=ST 0
200=LD
210=#RS
```

Table 1: User defined command as written for the Mini-Sys command file for user defined instructions (usersll.cmd), which allows recording and monitoring of the PTTL signal in IRSL measurements. Since it is not possible to rename the individual commands in Sequence Editor or the usersll.cmd file, the titles for each command are listed in this table for clarity.

optical stimulation (\$11 in Table 1 and Fig. 3) should be set to 500. Similar calculations and adjustments should be made for the ramp and the isothermal holding step (see corresponding command numbers in Table 1 and Fig. 3). All channels needed to record the ramp (\$1), the isothermal hold (\$19) and the actual stimulation step (\$11) have to be added and the sum needs to be inserted in the field corresponding to \$20 (in this case: $290 + 500 + 75 = 865$).

User Defined ✕

User Command: UserDef4 ▼

User Defined	
<p>Data Points (\$1): 290 ▲▼</p> <p>Lower limit (\$2): 0.0 ▲▼</p> <p>Upper limit (\$3): 100.0 ▲▼</p> <p>Rate (°C/s, %/s) (\$4): 5.0 ▲▼</p> <p>Ph temperature (°C) (\$5): 290 ▲▼</p> <p>Ph time (s) (\$6): 15 ▲▼</p> <p>Lightsource (\$7): IR LEDs ▼</p> <p>Optical Stimulation Power (%) 90.0 ▲▼</p> <p>Delay (\$8): 0 ▲▼</p> <p>Inactive (\$10): 0 ▲▼</p>	<p>Data Points (\$11): 500 ▲▼</p> <p>Lower limit (\$12): 0.0 ▲▼</p> <p>Upper limit (\$13): 0.0 ▲▼</p> <p>Rate (°C/s, %/s) (\$14): 0.0 ▲▼</p> <p>Ph temp. (°C) (\$15): 0 ▲▼</p> <p>Ph time (s) (\$16): 0 ▲▼</p> <p>Lightsource (\$17): None ▼</p> <p>Optical Stimulation Power (%) 0.0 ▲▼</p> <p>Delay (\$18): 75 ▲▼</p> <p>Inactive (\$20): 865 ▲▼</p>

Description:

The user can define a series of parameters. These can then be interpreted as the user defines by writing low level MiniSys code in the USERMSLL.CMD file. Not all parameters need to be used within the code.

The set of parameters on the left of the screen will be placed in the BIN file record in appropriate places, while those on the right hand side will not be stored anywhere.

OK

Cancel

Help

Run Info

N₂ Nitrogen

MiniSys

Figure 3: Screen shot of the Sequence Editor command window, as prepared for a 100 s IRSL measurement at 290 °C (parameter \$5), with a 15 s isothermal measurement step (‘pause’) prior to switching on IR LEDs (parameter \$6). The time included in each channel was defined as 0.2 s for the ramp, the isothermal measurement and the actual IRSL measurement. Each parameter in this window has to be edited to fit desired measurement settings, such as stimulation temperature, duration, channel width and light source.

After ensuring appropriate settings in the Sequence Editor command window, the user defined command can be used instead of the routine IRSL measurement.

4. Application of the new user defined command to explore PTTL

To show the potential use of the new user defined command, the amount of PTTL in TL and IRSL measurements in two feldspar samples (one sedimentary K-rich feldspar sample and one Na-rich feldspar sample extracted from bedrock) was examined using three different preheat and stimulation temperature combinations.

4.1. Samples

The two feldspar samples were selected because of their different chemical composition and because they show very

different laboratory irradiated TL signals (inset Fig. 4a and c) and different PTTL signal intensities (Fig. 4b and d). Both samples are feldspar-rich grain mixtures, such as those commonly used during feldspar luminescence dating. Sample WHB-7 is a sediment extract from the Channelled Scablands, Washington State, USA. The sediment sample WHB-7 was treated using hydrochloric acid (HCl; 10 %) and hydrogen peroxide (H₂O₂; 10 %) to remove carbonates and organic matter. Subsequently the sample was dry sieved to 180-212 μ m and density separated to $2.53 < \rho < 2.58$ g cm⁻³ using sodium polytungstate. Thermoluminescence emissions and anomalous fading rates of sample WHB-7 have been explored previously by Riedesel et al. (2021). KTB-383-C originates from a bedrock core obtained from the KTB borehole in southern Germany. The grain extract of this sample was obtained by crushing the rock; subsequently the material was sieved to isolate the fraction of 180-250 μ m. This

fraction was used to isolate the alkali feldspar grains using sodium polytungstate at a density of 2.58 g cm^{-3} . The density separated sample material of KTB-383-C was etched in 10 % HF for 40 min and subsequently washed in 10 % HCl for 20 min to remove any fluorides (see supplementary material of Guralnik et al. (2015) for details regarding the sample preparation procedure of KTB-383-C). Further information on the luminescence of sample KTB-383-C can be found in Guralnik et al. (2015) and Riedesel et al. (2019).

The chemical compositions of the samples were determined using X-ray fluorescence (XRF) and the mineral phases present in the grain mixtures were determined using X-ray diffraction (XRD). Details regarding these two methods and the respective sample preparation can be found in Riedesel et al. (2021). Sample WHB-7 consists of microcline (8 %), albite (54 %), quartz (15 %) and muscovite (23 %) and its feldspar chemistry has been determined as 64 %

K-feldspar, 32 % Na-feldspar and 5 % Ca-feldspar, when assuming 100 % feldspar (cf. Table 2). Sample KTB-383-C contains 22 % albite, 31 % quartz, 45 % muscovite and 2 % other mineral phases. Its chemical composition is determined as 8 % K-feldspar, 80 % Na-feldspar and 13 % Ca-feldspar, when assuming 100 % feldspar (cf. Table 2).

4.2. Instrumentation and the new user defined command

For luminescence measurements, sample grains were mounted as 2 mm aliquots on stainless steel discs ($\sim 0.095 \text{ g}$ in mass) using silicone oil. The luminescence measurements were performed at the Aberystwyth Luminescence Research Laboratory using a Risø DA20 TL/OSL reader equipped with a $^{90}\text{Sr}/^{90}\text{Y}$ beta source delivering $\sim 0.08 \text{ Gy s}^{-1}$ at the sample position. For stimulation, IR LEDs with an emission at 870 nm (FWHM 40 nm) delivering $\sim 145 \text{ mW cm}^{-2}$ (Risø, D. T.

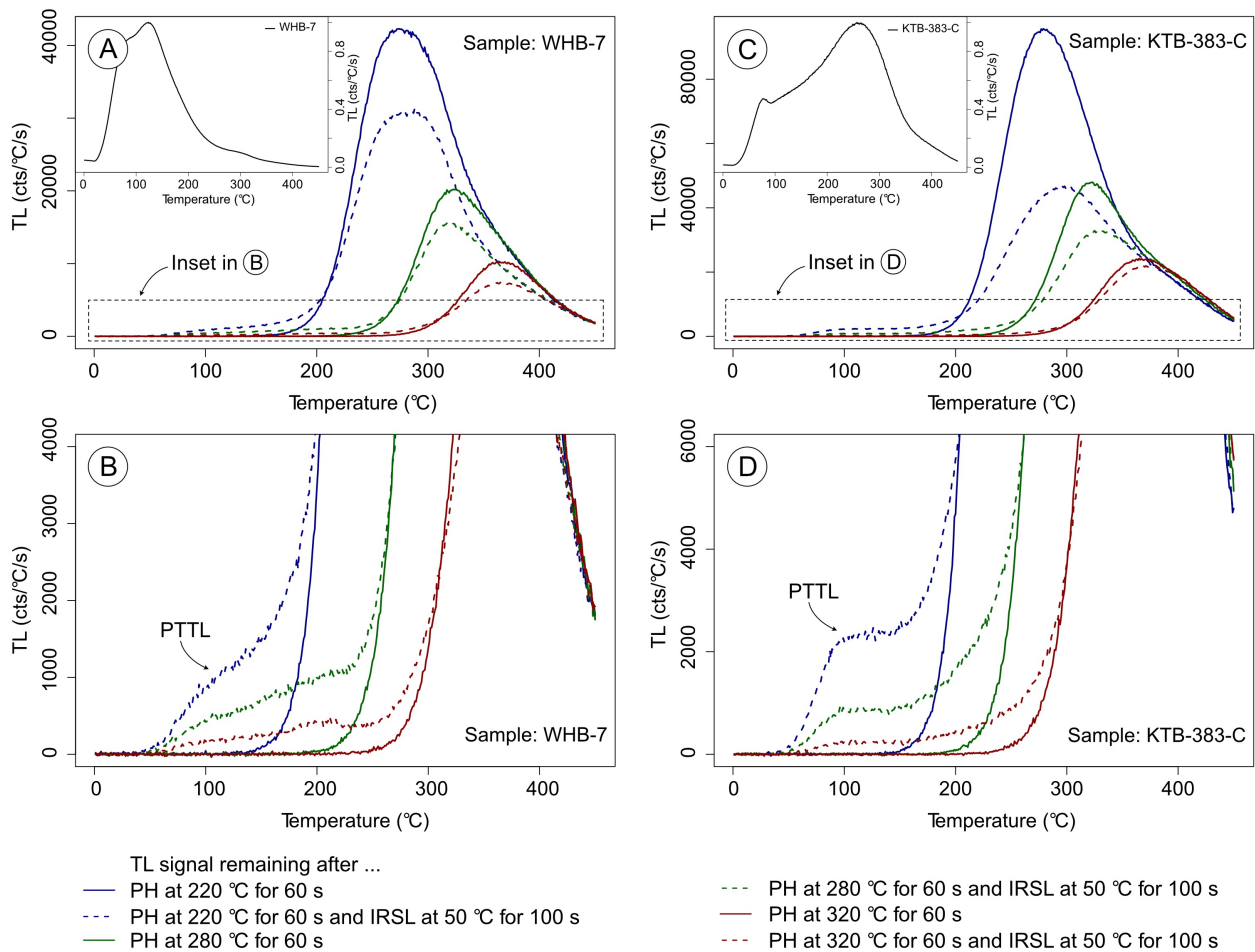


Figure 4: The insets of Figs (A) and (C) show the TL curve recorded immediately after irradiation. (A) TL signal remaining after preheating the laboratory irradiated material to 220 °C (blue line), 280 °C (green line) and 320 °C (red line) and after preheating and IRSL50 (dashed lines of respective colours) of sample WHB-7. Besides the decrease in signal intensity in TL at higher temperatures, an increase in TL intensity is visible in the temperature range below preheat temperature for TL curves recorded after preheating and stimulating with IR photons at 50 °C. This signal increase is associated with photo-transfer and a close-up of this temperature range is shown in (B). (C) and (D) show the same as (A) and (B), but for sample KTB-383-C.

Sample ID	Sampling location	Chemical compositions of feldspars (in %, assuming 100 % feldspar)			Mineral phases present (%)					References
		K-FS	Na-FS	Ca-FS	Microcline	Albite	Quartz	Muscovite	Other	
WHB-7	White Bluffs, Channelled Scablands, Washington State, USA	63.9	31.5	4.6	8	54	15	23	NA	Riedesel et al. (2021)
KTB-383-C	KTB-borehole, Germany	7.9	79.1	13	NA	22	31	45	2	Guralnik et al. (2015), Riedesel et al. (2019)

Table 2: Details of the samples used in this paper. Their chemical composition was determined using XRF and the phases present in the grain mixtures were determined using XRD. References are given to studies in which the luminescence properties of the samples have previously been explored.

Table 3

(a) Measurement protocol used to visualise the impact of photo-transfer on feldspar TL (Curve A in Fig. 1).

Step	Treatment
1	Irradiation (48 Gy)
2	Preheat for 60 s at 220, 280 or 320 °C, 5 °C s ⁻¹
3	Pause for 100 s
4	Pause for 100 s
5	TL to 450 °C, 1 °C s ⁻¹

(b) Measurement protocol used to visualise the impact of photo-transfer on feldspar TL (Curve B in Fig. 1).

Step	Treatment
1	Irradiation (48 Gy)
2	Preheat for 60 s at 220, 280 or 320 °C, 5 °C s ⁻¹
3	IRSL for 100 s at 50 °C
4	Pause for 100 s
5	TL to 450 °C, 1 °C s ⁻¹

(c) Measurement protocol used to visualise the impact of photo-transfer from IRSL₅₀ to post-IR IRSL using the new user defined command to record luminescence during ramping, isothermal holding and IR stimulation steps, as part of the IRSL measurement. A TL signal was recorded after the post-IR IRSL measurement to check for any remaining photo-transferred signal.

Step	Treatment
1	Irradiation (48 Gy)
2	Preheat for 60 s at 220, 280 or 320 °C, 5 °C s ⁻¹
3	IRSL for 100 s at 50 °C – measured using the new user defined command
4	IRSL for 100 s at 190, 250 or 290 °C – measured using the new user defined command
5	TL to 450 °C, 1 °C s ⁻¹

U. Nutech, 2015) were operated at 90 % stimulation power. The TL and IRSL signals were recorded through a combination of Schott BG 39 (2 mm thick, 45 mm in diameter)

and Corning 7-59 (4 mm thick, 45 mm in diameter) optical filters and were detected using an EMI 9235QA photomultiplier tube.

The amount of PTTL in TL and IRSL measurements was examined using three different protocols with three different preheat and stimulation temperature combinations (Table 3a, 3b and 3c). To keep the time differences between irradiation and TL measurements the same for all three protocols, pauses were inserted in Table 3a (steps 3 and 4) and Table 3b (step 4) instead of IRSL commands. TL measurements were recorded up to 450 °C using a heating rate of 1 °C s⁻¹. Measured TL curves were background corrected by subtracting a second TL measurement from the first measurement. This was done automatically, by enabling the command “background subtraction” in the TL command in the Sequence Editor software. TL measurements after an irradiation step, but without any preheat and IRSL stimulation steps were performed before and after the steps outlined in Tables 3a, 3b and 3c to monitor potential sensitivity changes. We observed that once the sample material had been heated to 450 °C all subsequent measurements only display very little change in intensity, and TL measurements could be conducted with good reproducibility.

Preheating of the sample material prior to IRSL measurements was conducted using the TL command available in the Sequence Editor software. The preheat temperatures of 220 °C, 280 °C or 320 °C were reached using a heating rate of 5 °C s⁻¹ and the sample was then kept at the preheat temperature for 60 s. All IRSL measurements were performed using the new user defined command. IRSL measurements were conducted for 100 s at 50 °C (Table 3b and Table 3c). The temperature for the post-IR IRSL stimulation was either 190 °C, 250 °C or 290 °C, depending on the preheat temperature, and the duration of this stimulation was 100 s (Table 3c). The IRSL measurement temperature was reached by heating at a rate of 5 °C s⁻¹ and IR LEDs were switched on after the sample had been kept at the IRSL measurement temperature for 15 s. To visualise the decay of the PTTL signal during the actual IRSL measurements using the user defined

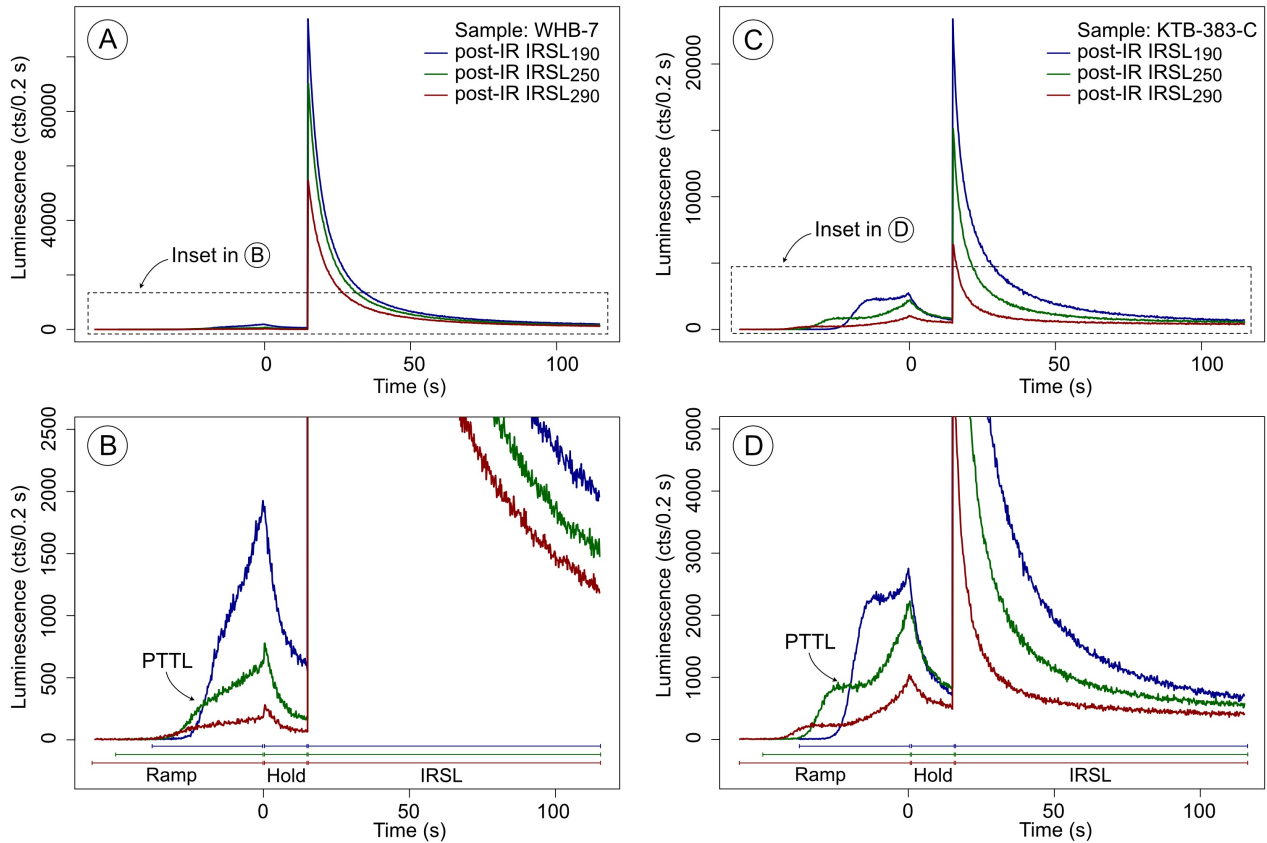


Figure 5: Post-IR IRSL signals recorded of sample WHB-7 (A and B) and of sample KTB-383-C (C and D) using the user defined command (Table 2). Figures (A) and (C) show the intensity of the photo-transferred signal, which is emitted during the ramping up to the IRSL measurement temperature and during isothermal holding of the sample at the measurement temperature prior to switching on the IR LEDs. The close-up figures (B) and (D) show the shape of the photo-transferred signal.

command, the post-IR IRSL measurements were performed using IR stimulation (Fig. 5 and Fig. 6) and without enabling the stimulation light source (Fig. 6, dashed lines) by selecting ‘None’ for the Lightsource (§7 in Fig. 3).

4.3. Results: Monitoring PTTL in TL measurements

Figure 4 shows the effect of $IRSL_{50}$ stimulation on the low temperature part of the TL curve of preheated samples when comparing the TL curves measured with (dashed lines in Fig. 4, Table 3b) and without $IRSL_{50}$ (solid lines in Fig. 4, Table 3a). The TL curves recorded immediately after a preheat (solid lines, Fig. 4) exhibit no TL signal up to $\sim 30^\circ\text{C}$ below the preheat temperature, where the TL signal starts to grow. TL curves recorded after an $IRSL_{50}$ measurement (dashed lines Fig. 4, cf. protocol in Table 3b) show an increase in TL signal intensity from about 50°C until $\sim 20^\circ\text{C}$ below the preheat temperature: this is photo-transfer of charge, induced by IR stimulation.

The shape of the PTTL signal differs slightly for the two samples investigated, with the PTTL signal of KTB-383-C measured in the low temperature protocol showing a clear plateau region, but the TL curves after $IRSL_{50}$ stimulation show a similar trend in both samples: the PTTL signal is

larger when lower temperature preheats were used compared to measurements after higher temperature preheats (Fig. 4B and D).

4.4. Results: Monitoring PTTL as part of IRSL measurements using the new user defined command

In section 4.3 we have shown that both samples show PTTL in TL curves. Especially important for feldspar luminescence dating is the potential influence of PTTL on post-IR IRSL signals, and the influence of this is explored in the following.

Figure 5 illustrates the amount of PTTL in post-IR IRSL signals of the two samples studied here. In Figure 5 the different coloured IRSL curves correspond to the different protocols used, with the blue curve representing the post-IR $IRSL_{190}$ signal, green represents the post-IR $IRSL_{250}$ signal and red the post-IR $IRSL_{290}$ signal. Due to the different temperatures used for these measurements, the time needed to ramp up to the measurement temperature differs, which results in the off-set of the start of the ramp in the three curves (Fig. 5). The different parts of the measurement using the new user defined command are indicated below the x-axis in

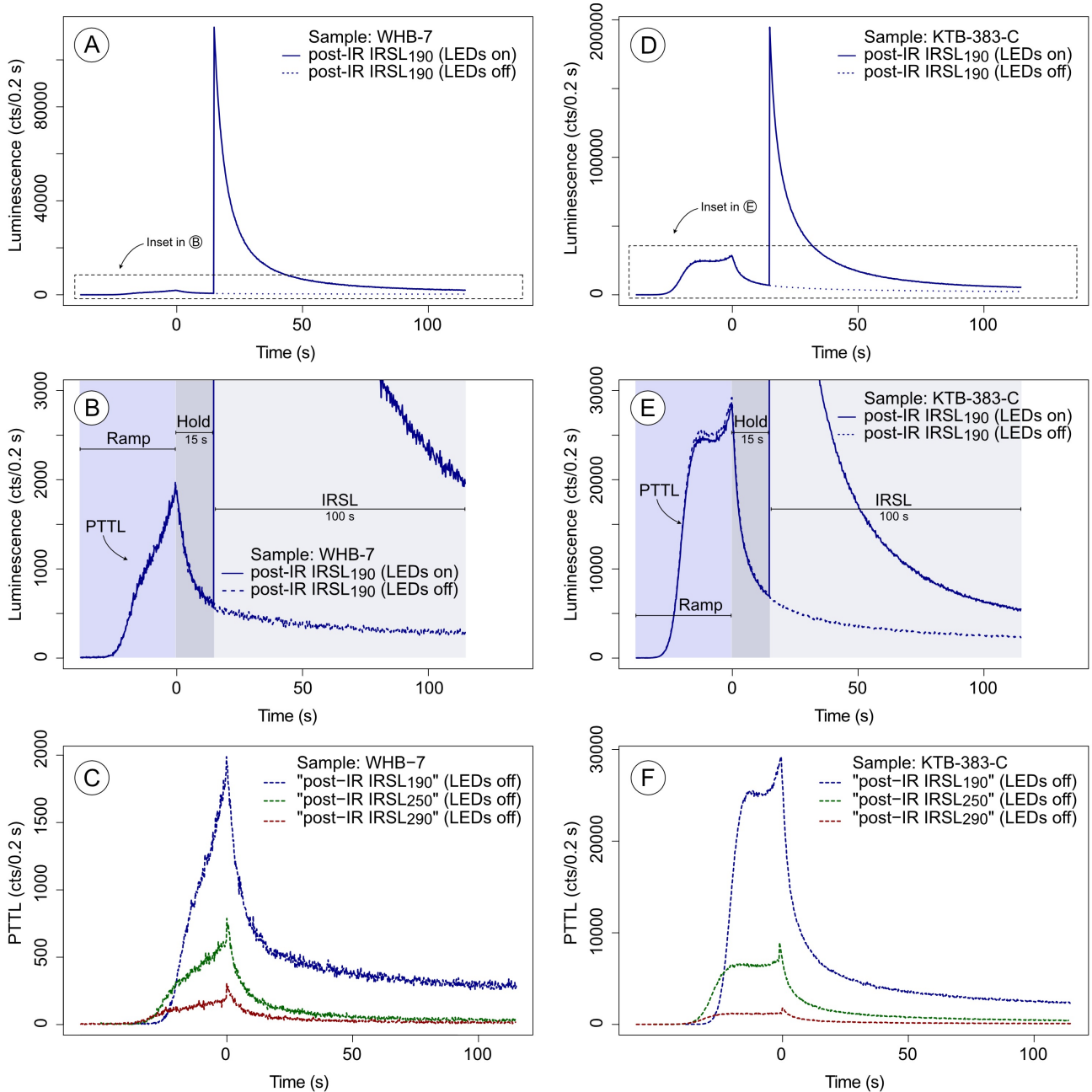


Figure 6: (A) Post-IR IRSL₁₉₀ signal of sample WHB-7 recorded using the protocol shown in Table 3c. The solid line shows the signal recorded with IR LEDs switched on. The dotted line represents the same measurement, but without IR LED stimulation. (B) Close-up of the luminescence signals shown in (A). Subfigures (D) and (E) show results from the same measurements made on sample KTB-383-C. Subfigures (C) and (F) show a comparison of the PTTL “post-IR IRSL” signal recorded for the three different protocols. For these measurements the “post-IR IRSL” signal was recorded using the user defined command, but without optical stimulation.

Figures 5B and 5D.

As already seen for TL, the post-IR IRSL signal recorded using the new user defined command shows a PTTL signal for both samples and for all preheat and post-IR IRSL stimulation temperature combinations. In the recorded post-IR IRSL measurements using the user defined command, the PTTL signal increases during the ramp up to the IRSL mea-

surement temperature. At the end of this ramp the PTTL signal reaches its maximum intensity. During the isothermal holding step, prior to switching on the IR LEDs, the PTTL signal decreases rapidly (Fig. 6). The fastest decay of the PTTL signal is observed in the initial few seconds of the pause, afterwards signal decays more slowly. The intensity and decay behaviour of the PTTL signal is particularly visi-

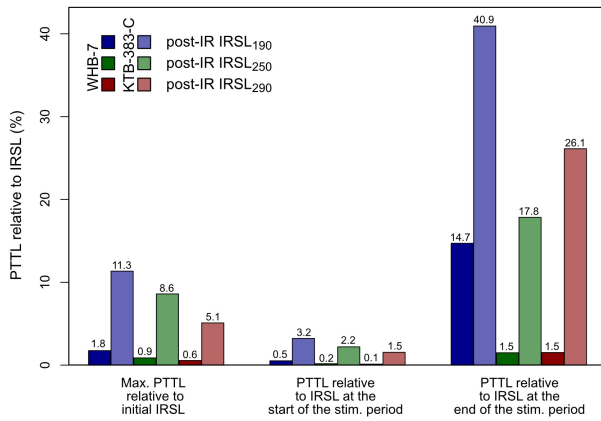


Figure 7: PTTL signal in relation to the measured IRSL signal for WHB-7 and KTB-383-C for all three protocols tested. The respective signals are measured with an integration interval of 0.2 s and the comparison here is based on one channel each. Left: Maximal PTTL signal relative to the maximum IRSL signal intensity. Middle: PTTL signal relative to the IRSL signal, both measured at the time of the start of the stimulation period. Right: Relative comparison of the PTTL and IRSL signal in the last channel of the 100 s stimulation period. The data displayed in the graph corresponds to the data presented in Figure 5

ble in Figure 6, where the PTTL signal is recorded without IR stimulation (dashed curve in Fig. 6) and compared to the corresponding signal with optical stimulation (solid curve in Fig. 6). Figures 6A, B and D, E show the post-IR IRSL₁₉₀ protocol with a 60 s preheat at 220 °C, because this low temperature post-IR IRSL signal shows the largest PTTL signal. For sample WHB-7 the PTTL decreases significantly during the first 5 s of the isothermal holding step, afterwards the decrease stabilises, but remains at a high signal count level, which is even at ~41 % of the post-IR IRSL₁₉₀ signal for KTB-383-C in the later part of the post-IR IRSL₁₉₀ signal (cf. Fig. 6E). Comparing only the PTTL signals for the three different protocols using the new user defined command, it becomes apparent that the PTTL signal of the post-IR IRSL₁₉₀ signal is significantly higher than the PTTL signals of the two higher temperature post-IR IRSL signals (cf. Fig. 6C and F). Whilst for the post-IR IRSL₂₅₀ and post-IR IRSL₂₉₀ a stable background level is reached after 15 to 30 s, dependent on the signal and sample investigated, the PTTL signal of the post-IR IRSL₁₉₀ signal stabilises, but remains at a high level, even after 100 s (cf. Fig. 6C and F; Fig. 7).

Like in TL (Fig. 4), PTTL is largest for the lowest temperature measurement (post-IR IRSL₁₉₀, 220 preheat) and decreases with increasing preheat temperature (Fig. 5). The amount of PTTL present in post-IR IRSL seems to be sample dependent: Whilst the highest PTTL signal intensity is about 11 % of the initial post-IR IRSL₁₉₀ signal for KTB-383-C, it is only 2 % of the initial post-IR IRSL₁₉₀ signal of sample WHB-7 (Fig. 7). However, most important is the finding

that the PTTL signal intensity can be reduced in both samples during an isothermal measurement step prior to switching on the IR LEDs. Comparing the IRSL signal intensity and the PTTL intensity at the start of the stimulation period after the isothermal holding step of 15 s reveals that the relative PTTL signal has decreased to ~0.2 % in WHB-7 and to ~2.2 % in KTB-383-C (Fig. 7) – highlighting the importance of the isothermal holding step prior to turning on the stimulation light source. This suggests that the selection of appropriate isothermal holding durations should be based on the properties of each sample and the protocol used. Our data also shows that dependent on the sample and protocol used, the PTTL signal can remain at a high level even after 100 s (cf. Fig. 7).

5. Conclusions

This paper shows that implementing a user defined command in the Mini-Sys can help to assess the intensity and influence of a photo-transferred luminescence signal on a post-IR IRSL measurement. The user defined command can be used instead of a standard IRSL measurement and will then enable the recording of the ramp up to the IRSL measurement temperature, an isothermal holding step at the IRSL measurement temperature and the IRSL measurement using IR LEDs. To allow the recording of the PTTL signal only, the command can be used without stimulation light source. The measurements with and without stimulation can then be compared, particularly to assess an appropriate isothermal holding step prior to optical stimulation.

Acknowledgement

SR's PhD research was funded through an AberDoc PhD scholarship awarded by Aberystwyth University. The authors would like to thank Dr. Anthony M.T. Bell (Sheffield Hallam University, United Kingdom) for performing the XRF and XRD measurements. Benny Guralnik (DTU, Denmark) is thanked for the provision of KTB-383-C. Sample WHB-7 was collected during a field campaign in 2018 which was financially supported by an RGS-IBG postgraduate research grant awarded to SR. We would like to thank Kristina Thomsen for her constructive feedback and review.

References

- Armitage, S. J. and Duller, G. A. T. *A user defined command for pulsed-irradiation on Risø TL-OSL readers*. *Ancient TL*, 22: 9–12, 2004.
- Bailliff, I. K. *Use of phototransfer for the anomalous fading of thermoluminescence*. *Nature*, 264: 531–533, 1976.
- Brown, W. L. and Parsons, I. *Exsolution and coarsening mechanisms and kinetics in an ordered cryptoperthite series*. *Contributions to Mineralogy and Petrology*, 86: 3–18, 1984.

- Buylaert, J.-P., Jain, M., Murray, A. S., Thomsen, K. J., Thiel, C., and Sohbati, R. *A robust feldspar luminescence dating method for Middle and Late Pleistocene sediments*. *Boreas*, 41: 435–451, 2012.
- Duller, G. A. T. *Infrared bleaching of the thermoluminescence of four feldspars*. *Journal of Physics D: Applied Physics*, 28: 1244–1528, 1995.
- Duller, G. A. T. *The Analyst software package for luminescence data: overview and recent improvements*. *Ancient TL*, 33: 35–41, 2015.
- Guralnik, B., Jain, M., Herman, F., Ankjærgaard, C., Murray, A. S., Valla, P. G., Preusser, F., King, G. E., Chen, R., Lowick, S. E., Kook, M., and Rhodes, E. J. *OSL-thermochronometry of feldspar from the KTB borehole, Germany*. *Earth and Planetary Science Letters*, 423: 232–243, 2015.
- Kaylor, R. M., Feathers, J., Hornyak, W. F., and Franklin, A. D. *Optically stimulated luminescence in Kalahari quartz: Bleaching of the 325 °C peak as the source of the luminescence*. *Journal of Luminescence*, 65: 1–6, 1995.
- Kristianpoller, N., Weiss, D., and Chen, R. *Effects of photostimulation in natural zircon*. *Radiation Measurements*, 41: 961–966, 2006.
- Li, B. and Li, S.-H. *Thermal stability of infrared stimulated luminescence of sedimentary K-feldspar*. *Radiation Measurements*, 46: 29–36, 2011.
- Lin, T.-H. and Yund, R. A. *Potassium and Sodium Self-Diffusion in Alkali Feldspar*. *Contributions to Mineralogy and Petrology*, 34: 177–184, 1972.
- Murray, A. S., Buylaert, J. P., Thomsen, K. J., and Jain, M. *The effect of preheating on the IRSL signal from feldspar*. *Radiation Measurements*, 44: 554–559, 2009.
- Parsons, I., Fitz Gerald, J. D., and Lee, M. R. *Routine characterization and interpretation of complex alkali feldspar intergrowths*. *American Mineralogist*, 100: 1277–1303, 2015.
- Qin, J., Chen, J., and Salisbury, J. B. *Photon transferred TL signals from potassium feldspars and their effects on post-IR IRSL measurements*. *Journal of Luminescence*, 160: 1–8, 2015.
- R Core Team. *R: A Language and Environment for Statistical Computing*. Vienna, Austria, 2019. URL <https://r-project.org>.
- Riedesel, S., King, G. E., Prasad, A. K., Kumar, R., Finch, A. A., and Jain, M. *Optical determination of the width of the band-tail states, and the excited and ground state energies of the principal dosimetric trap in feldspar*. *Radiation Measurements*, 125: 40–51, 2019.
- Riedesel, S., Bell, A. M. T., Duller, G. A. T., Finch, A. A., Jain, M., King, G. E., Pearce, N. J., and Roberts, H. M. *Exploring sources of variation in thermoluminescence emissions and anomalous fading in alkali feldspar*. *Radiation Measurements*, 141: 106541, 2021.
- Risø, D. T. U. Nutech. *Guide to The Risø TL/OSL Reader*. User manual. DTU Nutech. Denmark, 2015.
- Robertson, G. B., Prescott, J. R., and Hutton, J. T. *Bleaching of the thermoluminescence of feldspars by selected wavelengths present in sunlight*. *Nuclear Tracks and Radiation Measurements*, 21: 245–251, 1993.
- Schlesinger, M. *Optical studies of electron and hole trapping levels in quartz*. *Journal of Physics and Chemistry of Solids*, 26: 1761–1766, 1965.
- Thiel, C., Buylaert, J.-P., Murray, A. S., Terhorst, B., Hofer, I., Tsukamoto, S., and Frechen, M. *Luminescence dating of the Stratzing loess profile (Austria) - Testing the potential of an elevated temperature post-IR IRSL protocol*. *Quaternary International*, 234: 23–31, 2011.
- Thomsen, K. J., Murray, A. S., Jain, M., and Bøtter-Jensen, L. *Laboratory fading rates of various luminescence signals from feldspar-rich sediment extracts*. *Radiation Measurements*, 43: 1474–1486, 2008.
- Tsukamoto, S., Jain, M., Murray, A. S., Thiel, C., Schmidt, E., Wacha, L., Dohrmann, R., and Frechen, M. *A comparative study of the luminescence characteristics of polymineral fine grains and coarse-grained K- and Na-rich feldspars*. *Radiation Measurements*, 47: 903–908, 2012.
- Wang, X. L. and Wintle, A. G. *Investigating the contribution of recuperated TL to post-IR IRSL signals in perthitic feldspar*. *Radiation Measurements*, 49: 82–87, 2013.
- Wang, X. L., Wintle, A. G., and Adamiec, G. *Post-IR IRSL production in perthitic feldspar*. *Radiation Measurements*, 64: 1–8, 2014.
- Wintle, A. G. and Murray, A. S. *The relationship between quartz thermoluminescence, photo-transferred thermoluminescence, and optically stimulated luminescence*. *Radiation Measurements*, 27: 611–624, 1997.

Reviewer

Kristina Thomsen

Ancient TL

Methods Note: An analysis of potassium to rubidium ratios in shoreline sediments: implications for OSL dosimetry

Andrew J. Fish¹ and Kenneth Lepper¹

¹ Optical Dating and Dosimetry Laboratory, Department of Geosciences, North Dakota State University,
P.O. Box 6050 / #2745, Fargo, ND 58108-6050
Corresponding Author: andrew.j.fish@ndsu.edu

Received: April 26, 2022; in final form: June 22, 2022

1. Introduction

An integral step in OSL dating is determining the amount of natural radiation to which a sample is subjected in a given amount of time while buried. This value is referred to as a sample's "environmental dose rate," and it is calculated based on the concentration of radioactive elements within the sample, as well as the cosmic ray dose at depth. The four elements of interest for this purpose are uranium (U), thorium (Th), rubidium (Rb), and potassium (K). There are a wide range of analysis methods that can provide concentrations for these elements; one that is frequently used for luminescence dating is gamma spectrometry. While this method is relatively efficient and easy, it has a disadvantage in that it can only measure radionuclides that emit gamma radiation while decaying, a caveat which results in an inability to measure Rb in a sample (⁸⁷Rb, the naturally occurring radionuclide of Rb, is a pure beta emitter). Since Rb concentration is not directly measurable via this method, its value has been commonly approximated by using the measured concentration of K and an assumed K:Rb ratio of 200:1 (Aitken, 1985, 1998; Warren, 1978).

A review of this 200:1 ratio reveals that it is based on measurements of K and Rb concentrations from several published papers from the mid-twentieth century (Warren, 1978). While the results of these past analyses do show a general convergence around a 200:1 ratio, the measurements themselves were only conducted on pottery, shales, clays, and a handful of tektite samples, as shown in Table 1. This is a spread of sample types that were selected for their relevance to TL dating of artifacts, but they do not encapsulate all of OSL's potential geological dating applications. More recent work with OSL dosimetry on shoreline sediments of Glacial Lake Agassiz in North Dakota and Minnesota, USA, and in the Great Lakes region in the northern United States suggested that sediments of this type deviated from the expected ratio. In this analysis, shoreline sand samples from

glacial Lake Agassiz and the Great Lakes region were studied to determine if the archaeology-based 200:1 K:Rb ratio was also applicable to the geology-based samples of this type.

2. Analysis

For the purpose of comparing the assumed 200:1 ratio to the measured K:Rb ratio of the lake shoreline sediments, data from sets of samples used in past projects were compiled and analyzed. In total, 200 dose rate samples were included in the data set; 84 of these samples were collected from beach ridges and spit complexes from Glacial Lake Agassiz. A further 63 samples were taken from strandplains of Lake Huron, and another 53 originated from strandplains of Lake Superior. These samples were collected and analyzed over the course of 17 years.

The potassium and rubidium concentrations of each sample, measured in parts per million (ppm), were determined using instrumental neutron activation analysis (INAA), which involves irradiating samples with neutrons in fission reactors. Neutron irradiation generates new, less-stable radionuclides, which generally have significantly shorter half-lives than the target element's naturally occurring isotopes. The resulting decay of these generated radionuclides emit radiation that can be discerned and measured via gamma spectrometry. The generated radionuclides for the elements of interest in this study were Potassium-42 (⁴²K; half-life 12.355 hours) and Rubidium-86 (⁸⁶Rb, half-life 18.66 days). An overview of the INAA method can be found in Reeves & Brooks (1979).

From 2005 through 2020 samples were dried and prepared for INAA at the Optical Dating and Dosimetry lab at North Dakota State University and then sent for neutron activation (irradiation), gamma spectrometry, and data analysis at The Ohio State University Nuclear Research Laboratory (OSU NRL). OSU NRL measured the naturally occurring gamma

Analysis	K:Rb Ratio (± Std. Dev.)	Sample Type	Sample Count
Tobia & Sayre (1974)	238 ± 99	Soils, clays, shales, and pottery (Egypt)	58
Bieber et al. (1973)	222 ± 68	Clays and pottery (Eastern Mediterranean)	235
Perlman & Asaro (1969)	200	Pottery (Peru, Egypt)	39
Pinson et al. (1965)	200 ± 27	Tektites	54
Taylor & Ahrens (1959)	220 ± 50	Tektites	5
<i>in Pinson et al. (1965)</i>			

Table 1. Summary of past K:Rb analyses.

emission from ^{40}K , rather than the ^{42}K generated radionuclide. From 2020 to the present INAA has instead been conducted by the North Carolina State University Nuclear Reactor Program (NCSU NRP). Dried samples were sent to NCSU NPR where they prepared the samples for neutron activation and analysis. Both facilities have pool-type research reactors. Additional information about their methodology can be found on the laboratories' websites (<https://reactor.osu.edu> and <https://nrp.ne.ncsu.edu>; June 22, 2022).

The potassium and rubidium data from these samples were used to numerically calculate the statistical mean and median of the K:Rb ratios, as well as the standard deviation and standard error. In addition to numerical analysis, the samples were also plotted on scatterplots to help visualize the spread of the data, arranged such that the slope of the line-of-best-fit approximated the average K:Rb ratio for each data set. All 200 samples were plotted together, but selected subsets of the data were also studied independently in an effort to identify any trends that may have arisen. This included separating the samples by lake, which is reflected by the data plotted in Figures 1 and 2.

Figures 1 and 2 present the results of this analysis on a scatterplot and histogram, respectively, while the calculated values are tabulated in Table 2. The average potassium to

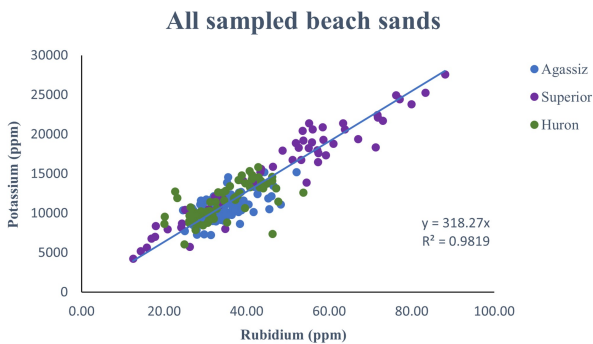


Figure 1. Collective scatterplot of all 200 samples, plotted by potassium against rubidium content. Average K:Rb ratio is represented by the slope of the line-of-best-fit at 318:1.

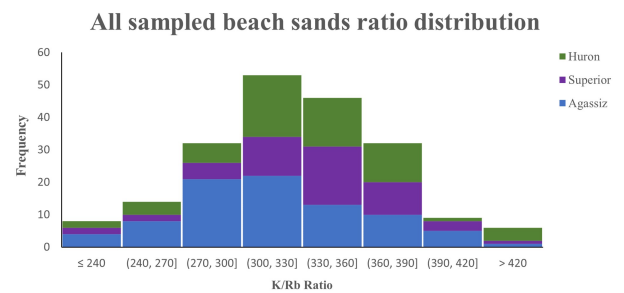


Figure 2. K:Rb ratio frequency distribution.

rubidium ratio of all samples in the data set was 328 ± 3.6 (std. err). Each individual lake yielded similar values as well, with Huron and Superior averaging 336 ± 7.6 (std. err.) and 336 ± 6.0 (std. err.), respectively. Lake Agassiz had a lower K:Rb ratio, down to an average of 316 ± 5.0 (std. err.), but it still fell well within a standard deviation of the overall mean, which was 51.

3. Conclusion

Recall that the overall K:Rb ratio for all 200 samples was 328 ± 3.6 (Table 2), with the mean ratio of each individual lake falling well within one std. dev. (51) of the mean. This average is a considerable difference, 64%, from the ratio proposed by Warren (1978) for his review of pottery, clays, shales, and tektites. If we consider a generalized shoreline sample containing 1% K, 2 ppm Th, and 1 ppm U sampled at a depth of 1m below the surface and having an average water content of 8%, the revised K:Rb ratio would result in a 0.63% difference in the calculated beta dose rate and a 0.36% difference in the total dose rate for the sample. Although these differences are small, it is more applicable to estimate the K:Rb ratios based on data from similar analog materials. The results from this analysis suggest that the commonly assumed 200:1 ratio is not appropriate for approximating the Rb content of shoreline sediments of the Great Lakes and Glacial Lake Agassiz and that an actual measurement of Rb would be necessary if one strives to ensure maximum accuracy of

Shoreline	Number of	Mean	Median	Std. Dev.	Std. Err.
Data Set	Samples	K:Rb Ratio	K:Rb Ratio	K:Rb Ratio	K:Rb Ratio
All Lakes	200	328	326	51	3.6
Agassiz	84	316	310	46	5.0
Superior	53	336	341	44	6.0
Huron	63	336	331	61	7.7

Table 2. Summary of calculated data.

results. Furthermore, these results also indicate that analysis of K:Rb ratios in other sediment types used for OSL dating is warranted.

References

- Aitken, M. J. *Thermoluminescence Dating*. Academic Press, London, 359 pp, 1985.
- Aitken, M. J. *An Introduction to Optical Dating: The dating of Quaternary sediments by the use of photon-stimulated luminescence*. Oxford University Press, New York, 1998.
- Bieber, A. M., Brooks, D. W., Harbottle, G., and Sayre, E. V. *Compositional Groupings of some Ancient Aegean and Eastern Mediterranean pottery*. Brookhaven National Library Report BNL, 1860, 1973.
- Perlman, I. and Asaro, F. *Pottery Analysis by Neutron Activation*. *Archaeometry*, 11: 21–38, 1969. doi: 10.1111/j.1475-4754.1969.tb00627.x.
- Pinson, W. H., Philpotts, J. A., and Schnetzler, C. C. *K/Rb Ratios in Tektites*. *Journal of Geophysical Research*, 70: 2889–2894, 1965. doi: 10.1029/jz070i012p02889.
- Reeves, R. D. and Brooks, R. R. *Trace Element Analysis of Geological Materials*. John Wiley and Sons, Inc., Hoboken, New Jersey, 421 pp, 1979.
- Taylor, S. R. and Ahrens, L. H. *The significance of K/Rb ratios for theories of tektite origin*. *Geochimica Cosmochimica Acta*, 15: 370–3721, 1959.
- Tobia, S. K. and Sayre, E. V. *An Analytical Comparison of Various Egyptian Soils, Clays, Shales and Some Ancient Pottery by Neutron Activation*. *Recent Advances in Science and Technology of Materials*, 1974. doi: 10.1007/978-1-4684-7233-2_7.
- Warren, S. E. *Thermoluminescence Dating of Pottery: An Assessment of the Dose-Rate from Rubidium*. *Archaeometry*, 20: 71–72, 1978. doi: 10.1111/j.1475-4754.1978.tb00215.x.

Reviewer

Sebastien Huot

Thesis Abstracts

Index

Tamás Bartyik	p. 15
Trine Freiesleben	p. 16
Elin Jirdén	p. 16
Raju Kumar	p. 17
Kieran O’Gorman	p. 18
Choudhurimayum Pankaj Sharma	p. 18
Nupur Tiwari	p. 19

Tamás Bartyik

Reconstruction of fluvial processes in the Maros River basin, with special respect to the applicability of OSL sensitivity

June 2022

Institute of Geography and Earth Sciences, University of Szeged,
Hungary

Degree: Ph.D.

Supervisor: Dr. György Sipos

Recently, it has been shown that the luminescence properties of minerals, in particular quartz, can be used as an indicator of fluvial erosion and/or sediment origin for various fluvial processes. One of these properties is the so-called luminescence sensitivity of quartz grains, i.e. the intensity of the luminescence response per unit dose. Laboratory tests have shown that the magnitude of luminescence sensitivity can vary in response to light and heat exposure and radioactive radiation. Thus, in nature, high sensitivity has been associated with a high number of sediment cycles and low sensitivity with their absence. In addition, it has also been shown that the lithological background of quartz, i.e. the source area, can also be a crucial factor, so luminescence sensitivity can be used for the analysis of sediment provenance. Overall, however it is still questionable whether it is the inherited properties of source rocks (as primary factors) or the sedimentary history (as a secondary factor) that determine the luminescence sensitivity of sedimentary quartz. On the other hand, luminescence sensitivity studies have not yet been carried out on the sediments of the Carpathian Basin.

Although the reconstruction of the Late Pleistocene evolution of the lowland alluvial fan of the Maros River in Central Europe, using OSL dating has been done before, such studies have not been carried out in the middle and upper section of the river. The Retezat Mountains in the mountainous catchment of the river are one of the members of the Carpathians that were heavily glaciated during the Pleistocene glaciations. Changes in the glaciation and deglaciation phases in the area may have affected the ability of river

to work downstream. Thus, sediment accumulation in the Hateg Basin in the foothills of the Retezat may be related to deglaciation. The terraces of the Middle Maros may also reflect these phases. In addition, a number of paleochannel patterns can be identified on the prominent alluvial fan of the lowland area of the Maros River. Their temporal and spatial displacements, water yields and channel types are indicators that the sediment discharge and sediment transport capacity of the river increased significantly from the Late Glacial to the Early Holocene and was higher than the present. However, at the regional level, the geomorphological processes in the lower catchment have not yet been compared with those in the upper catchment.

An own luminescence sensitivity measurement protocol was applied to 90–300 µm fluvial quartz grains in parallel with standard OSL age measurements to reconstruct geomorphological evolution.

In the thesis, was found the following correlations with luminescence sensitivity: The sensitivity of Alpine and Carpathian fluvial quartz in the lower section of the catchments show clear differences in terms of CW-OSL, TL 110 °C peak and LM-OSL techniques. Among the sensitivity parameters, the results of total LM-OSL and fast component ratio is the most applicable for the separation of sediments with different provenances. The sedimentary quartz grains of the Danube show a higher sensitivity with increasing age, while the Maros shows a lower sensitivity with increasing age. In the case of the Maros River, luminescence parameters are strongly influenced by sub-basin and river section scale factors. No general trend in the variation of the different sensitivity parameters is observed over the 565 rkm stretch studied. Along the Maros, the residual dose from quartz grains shows a clear downstream decrease, but the trend may be broken by tributaries and erosion.

In the terms of geomorphological reconstruction of Late Pleistocene and Holocene of Maros catchment: The MIS 3 stage in the Maros catchment was dominated by coarse-grained, gravel-sand sedimentation. A higher degree of fluvial incision in the middle catchment of the Maros was observed during the MIS 3-MIS 2 and the MIS 2-MIS 1 transition. Based on the data obtained, fluvial processes along the Middle Maros were mainly influenced by climatic conditions. There is no temporal relationship between the deglaciation phases in the Retezat Mountains and the water yield of the paleochannels of the lowland alluvial fan, but the sediment mobilised by the increase in precipitation may have influenced the channel pattern of the lowland section.

A PDF of this thesis can be downloaded from: <http://doktori.bibl.u-szeged.hu/id/eprint/11145/>

Trine Freiesleben

Developing and testing models for rock surface dating using optically stimulated luminescence

July 2021

Technical University of Denmark, Physics, Roskilde, Denmark

Degree: Ph.D.

Supervisors: Kristina Jørkov Thomsen, Co-supervisor: Andrew Sean Murray

Luminescence dating of rock surfaces is an emerging absolute chronological technique that has the potential to determine how long a rock surface has been exposed to daylight and/or how long it has been buried. The development of this technique into a robust dating method will give the opportunity to determine the ages of previously un-datable stone structures/formations in both archaeology and geology, including megaliths, chambered burial mounds, cairns, cobble fans, ice-scoured bedrock, and many others. When a rock surface is exposed to light, the latent optically stimulated luminescence (OSL) signal is reset to different degrees depending on the distance from the surface and the duration of daylight exposure. Thus, by measuring the OSL signal as a function of depth into the rock surface, it is possible to determine how long the rock surface has been exposed to daylight, and how long it was subsequently buried, by modelling the measured luminescence-depth profile. The challenges involved in this procedure are addressed here, and in particular, the ability of a rock surface to record multiple sequential burial and exposure events is investigated experimentally. Existing models are examined and new, potentially more appropriate models introduced. These models are tested using both simulated and experimental data. Based on these tests it is concluded that exposure ages are very dependent on the exact model assumptions and that fitting parameters previously assumed to be constant with depth are in fact not.

It is shown that, although correct model assumptions improve the quality of exposure age estimates, significant discrepancies between observed and expected fitting parameter values remain and these discrepancies lead to inaccurate age estimation. This is particularly the case when post-IR signals from feldspar are used. The spectral dependency of luminescence signals is examined to better understand these problems. The demonstrated depth dependency of fitting parameters previously assumed to be constant with depth, also gives rise to discrepancies in parameter values. The surprising observation that, in rocks, the IR50 signal is apparently more easily bleached than the quartz fast-component OSL signal is explained in terms of light attenuation effects other than absorption (e.g. scattering and refraction) increasing the effective path length for shorter wavelengths, and so changing the shape of the light spectrum with penetration depth. This complicates parameter estimates in exposure dating even further.

Alternative approaches (rather than parameter estimation) for estimating how long a rock surface has been exposed to light are considered, based on modelling the shape and po-

sition of the measured luminescence-depth profile. It is concluded that the most accurate exposure age is derived by interpolating the depth of an unknown profile onto a curve of profile depths from known age profiles (the Exposure Response Curve, or ERC, approach). Generating ERCs by artificially illuminating surfaces at very high intensities to bracket the unknown profile, may provide calibration profiles of arbitrary 'age', determined by the total number of incident photons. Such an approach is very likely to give more accurate and precise light-exposure ages than using parameters calculated from first principles, or than using a single natural calibration profile (as is current practice).

The model dependency of rock surface burial dating is also investigated, and encouragingly it is concluded that the accuracy of burial dating is not significantly affected by the application of inappropriate models to determine the exposure history of a buried surface (and thus the degree of bleaching before burial).

Dating rock surfaces accurately requires that the environmental dose rate is modelled, because the dose rate is also depth dependent and influenced by the size of the rock itself. A simple analytical model designed with this in mind is presented and applied.

To investigate the accuracy and precision of rock surface dating, both rock surface and standard OSL dating are applied to two important archaeological sites in Central France. These two different applications determine: 1) the timing of the changeover from Neanderthal to anatomically modern humans, and 2) that Neanderthals were capable of making symbolic engravings on cave walls. In the first case, rock surface dating is successful, but in the other, the signal of interest recorded by the rock surfaces appear to have been erased by a prolonged exposure to daylight prior to sampling, or removed by significant erosion of the surface, and only the sediments retain the chronological information. These two application studies illustrate both the potential and some of the limitations of the method.

A PDF of this thesis can be downloaded from *Ancient TL*.

Elin Jirdén

OSL dating of the Mesolithic site Nilsvikdalen 7, Bjørøy, Norway.

June 2022

Lund University, Lund, Sweden

Degree: M.Sc.

Supervisors: Helena Alexanderson and Amber Hood

Luminescence dating is a well-established dating method within geological and archaeological research. However, the use of luminescence dating, and more specifically optically stimulated luminescence (OSL), is currently underutilised in Norwegian archaeology. This study set about determining the suitability of this dating method as a viable option for excavations of Norwegian coastal Stone Age sites. This is done

by OSL dating six samples from three superimposed cultural layers at a settlement (Nilsvikdalen 7) at Bjorøy, SW Norway, which has previously been radiocarbon dated to the Late Mesolithic period, and subsequently evaluating the method suitability from the results.

The cultural layers all consist of varying degrees of humus-rich sand with charcoal, where OSL samples were taken from inside and outside an interpreted hut structure. Quartz OSL dating was carried out using the Single Aliquot Regenerative-dose (SAR) protocol for all six samples and yielded successful results. The samples displayed a strong quartz signal with excellent characteristics. The water content of the site yielded the highest uncertainties for the dose rate determination and was after thorough evaluation determined to ~63–114%. Dose rate was determined to ~2–4 Gy/ka. Different age models were applied, where the mean age was chosen for the final age determination. The bottom cultural layer was dated to the Late Mesolithic, with OSL ages of 8.07 ± 0.51 ka and 7.02 ± 0.43 ka inside the hut, as well as 6.60 ± 0.40 ka outside the hut boundary. The middle and upper layers were dated to Late Mesolithic – Early Neolithic, where the middle unit displayed an age of 6.25 ± 0.36 ka and the upper layer yielded ages of 5.56 ± 0.32 ka and 6.94 ± 0.36 ka (all dates inside the hut). Three of the samples overlap with the corresponding radiocarbon dates, whilst the other three do not statistically agree (values outside of 2 σ) with the radiocarbon dates. For the samples without statistical agreement, the OSL ages produced are younger than the corresponding radiocarbon dates.

For future OSL dating it is suggested to, if possible, take a control sample of recent or known age from a site area to reduce possible uncertainties in the luminescence age determination process. Given the successful dating of the Nilsvikdalen 7 site, this project demonstrates how OSL dating could provide a good solution for future dating of Norwegian coastal Stone Age sites.

Raju Kumar

A new understanding of luminescence processes in feldspar using novel site-selective spectroscopic techniques

March 2020

Department of Physics, Technical University of Denmark, Risø Campus, Denmark

Degree: Ph.D.

Supervisors: Dr. Mayank Jain and Dr. Myungho Kook

Metastable states in solids are widely used for dosimetry and photonic applications. Feldspar, a ubiquitous naturally occurring aluminosilicate, consists of many defects and impurities; some of these transform into metastable states by capturing electrons or holes, when exposed to ionizing radiation. These metastable states can have lifetimes of millions of years rendering feldspar useful for luminescence geochronology. In this dating technique, the dose-dependent

concentration of the metastable states (generated by ionizing radiation) is measured via optically stimulated luminescence (OSL) or infrared stimulated luminescence (IRSL) signals. These signals are generated by charge transfer across the metastable states, followed by electron-hole recombination resulting in the emission of light.

Despite many decades of research, the luminescence mechanisms and the associated defect system in feldspar are poorly understood; for example, the defect responsible for the main dosimetric trap (i.e. principal trap) and its physical characteristics are still unknown. This lack of knowledge may largely be attributed to the inherent physical processes involved in OSL and IRSL generation. The OSL/IRSL technique is not ideal for characterizing the principal trap (e.g. optical trap depth, electronic states, number of defects and their concentration, etc.) as it involves both electron and hole sites as well as the charge transport dynamics, making any interpretation of the electron-trapping state ambiguous. Therefore, it is desirable to use site-selective methods that can directly probe the principal trap without involving any hole sites in the emission process. The main purpose of this Ph.D. research is to advance our current understanding of the luminescence processes in feldspar and the associated defect system using site-selective multi-spectroscopic techniques.

This work shows that there are two principal traps in K-Na feldspar. These traps emit Stokes-shifted infrared photoluminescence (IRPL) bands centered at 1.41 eV (880 nm) and 1.30 eV (955 nm). The two trapping centers have similar electron capture cross-sections and excited-to-ground state relaxation lifetimes, but different trap depths and excited-state energies. These results suggest that the 1.41 eV and 1.30 eV emission centers consist of the same defect that resides in two different sites and, thus, experiences different crystal fields. Cathodoluminescence (CL) microscopy explores the question on the spatial variability of the two principal traps and their link to feldspar composition. CL investigations suggest that the two emission centers (i.e. the two traps) vary spatially even within a single-grain of feldspar and their relative emission peak intensity (1.30 eV vs. 1.41 eV) shows a correlation with the K-Na content. This work sheds new light on the long-standing issues of estimation of trap depth in feldspar, and whether there are single or multiple traps giving rise to the OSL/IRSL signals.

This Ph.D. research also establishes a link between the IRPL emission bands (1.41 eV and 1.30 eV) and the OSL/IRSL phenomenon. Tracking of changes in IRPL (i.e. trapped electron population) due to IRSL (i.e. electron and hole populations) shows that a) both the 1.41 eV and 1.30 eV centers participate in IRSL, and b) only a fraction of the principal trap population participates in the IRSL at a given measurement temperature. A comparison of thermal depletion of IRSL and IRPL signals suggests that the trapped electrons in the principal trap are quite stable up to about 400 °C. The decrease in IRSL because of preheating to 300–400 °C occurs due to the depletion of holes; the holes are used up during the TL measurement (i.e., preheating) prior to the IRSL measurement. Furthermore, it is observed that the electron trap-

ping probability in the principal trap is both a function of its electron capture cross-section and its distance to the nearest hole. This new understanding is anticipated to play a crucial role in the development of mathematical models of luminescence phenomena involving metastable states. Finally, the test of the potential of IRPL in sediment dating suggests that IRPL can be successfully adapted to a SAR protocol; it recovers accurate equivalent doses from 100 to 300 Gy (age range 20-128 ka) without a fading correction.

In terms of practical utility, a new measurement facility for detecting infrared photoluminescence (IRPL) at 1.41 eV (880 nm) and 1.30 eV (955 nm) for routine dosimetric measurements has been developed. Furthermore, a dose measurement protocol, i.e. coupled IRPL-IRSL SAR protocol, is developed to measure natural doses in feldspar using IRPL. This work establishes a fundamentally different dating technique based only on trapped electrons, compared to the existing OSL and IRSL dating techniques.

A PDF of this thesis can be downloaded from: <https://orbit.dtu.dk/en/publications/a-new-understanding-of-luminescence-processes-in-feldspar-using-n> and from Ancient TL.

Kieran O’Gorman

Internal dose rates of single feldspar and composite mineral grains: Methodological developments and optical dating applications

August 2021

University of Wollongong, Wollongong, Australia

Degree: Ph.D.

Supervisors: Zenobia Jacobs, Bo Li, Dominique Tanner

Optical dating of feldspar grains is playing a pivotal role in establishing timelines for hominin occupations in many parts of the world, including the Altai and Wallacea—two regions that are research hotspots for the study of human evolution, ancient dispersals and inter-group hominin interactions. A key challenge of optical dating of feldspar grains is determining the radioactivity within individual grains that are used for dating. Feldspar grains can contain up to ~14 wt% potassium (K) and considerable concentrations of rubidium (Rb), thorium (Th) and uranium (U), all of which have radioactive isotopes that give rise to an internal dose rate component. The internal dose rate can have a major impact on both the precision and accuracy of optical age estimates.

Feldspar grains are often composed of multiple mineral phases of variable compositions. Previous techniques used to determine K concentrations of feldspar grains are time-consuming, and either lack the spatial resolution to classify discrete mineral phases within grains or the coverage to obtain whole-of-grain average K concentrations. Samples from two sites (Ust’-Karakol-1 in the Altai and Leang Bulu Bettue in Wallacea), located in contrasting geological settings (plutonic versus volcanic terranes), are used to develop an approach where quantitative evaluation of minerals

using energy-dispersive spectroscopy (QEM-EDS) is used to rapidly determine whole-of-grain average K concentrations of individual luminescent feldspar grains.

This approach is also applied to samples from two iconic archaeological sites: Denisova Cave in the Altai and Liang Bua in Wallacea. Individual luminescent grains from Denisova Cave are dominated by low-temperature feldspar varieties, which are characteristic of plutonic terranes; most grains are K-rich. Individual luminescent grains from Liang Bua are composite mineral grains composed of a range of feldspar varieties, quartz, clay minerals, heavy minerals and volcanic glass. These grains have a broad range of whole-of-grain average K concentrations—most are low-K. A novel approach, using QEM-EDS and laser ablation inductively coupled plasma mass spectrometry, is developed to investigate the K, Rb, Th and U concentrations of these grains, and determine single-grain and sample-average internal dose rates. Samples from different sedimentary contexts at the site have different internal dose rate distributions.

The potential of using infrared stimulated luminescence (IRSL) and post-infrared IRSL signal behaviours as proxies for K concentrations, as an alternative to directly measuring K concentrations, is investigated for one sample with a broad range of K concentrations. Signal intensity and fading rates are poor proxies, whereas thermal stability shows good potential for selecting the most K-rich grains with the most thermally stable IRSL signals.

Finally, optical dating of K-rich feldspar grains from 32 sediment samples is used to construct a better-resolved chronology for the sedimentary deposits of the South Chamber of Denisova Cave. The internal and external dose rates and equivalent dose distributions of samples from three sedimentary profiles are scrutinised. The resulting chronology is compared to those previously obtained for Main and East chambers. Together, the data provide further insights into the timing of occupation of this iconic site by Denisovans, Neanderthals and modern humans.

Choudhurimayum Pankaj Sharma

Paleoclimatic Reconstruction from the Late Pleistocene-Holocene Sedimentary Archives of Ladakh Himalaya.

April 2022

Wadia Institute of Himalayan Geology, Dehradun, India, and Banaras Hindu University, Varanasi, India

Degree: Ph.D.

Supervisors: Dr. Pradeep Srivastava and Prof. Uma Kant Shukla

The climate which is as old as the earth itself has been ever-changing and the current understanding of climate and its variation which is based on barely three-century-old instrumental data is insufficient to assess the wider pattern, major forcing, and its effects. This demands better exploration of geological archives of climate variability. At present

mountainous areas such as the Himalaya is evidently responding to climate change mainly in the form of widespread glacial retreat. These events are not unnatural since comparatively larger changes were known to occur in the recent geologic past. However, with the rise in the population where the global 15% is dependent on the freshwater supply from Himalayan Glaciers and rivers, a slight change becomes crucial.

The Himalaya has been acting as a barrier to the Indian Summer Monsoon (ISM) rainfall where the area north of its highest peak remains a rain shadow. It is influenced by the three climatic systems Vis ISM, Westerlies, and the East Asian Summer Monsoon (EASM). Ladakh in its western part is one of such areas influenced partly by westerlies and partly by the ISM. Recently, Ladakh is known to be highly susceptible to hydroclimatic hazards and subjected to occasional catastrophic hydrological events, and is known to endanger lives and properties of people residing there. Detailed investigation of geological archives of climate is imperative to expand our knowledge of climatic variability and extreme events that rarely occur on the human timescale. Ladakh is known to be affected almost annually by debris flows ranging from minor to catastrophic scale events. Though triggered by abnormal climatic conditions the long-term causative factor has been its topography. The present thesis deals with past climate reconstruction, understanding flood history, and past extreme hydrological forces that directly impact the infrastructures and lives of inhabitants of Ladakh.

To reconstruct the past climate, a chronologically well-constrained sedimentary archive from Upshi (Ladakh) was studied using a multi-proxy approach i.e. (palynological, geochemical-stable isotopic analysis, and environmental magnetism). Several slack water deposits (SWDs) preserved along the Indus River at Ladakh were explored to reconstruct past floods. SWDs are stacks of sand-silt couplets deposited rapidly during large flooding events in areas where local geomorphic conditions cause a sharp reduction of flow velocity. Each couplet represents a flood and here the age is constrained using Optically Stimulated Luminescence (OSL) for sand and AMS ^{14}C for charcoal specks from hearths. Lastly, in an attempt to understand the role of debris flows in landscape evolution through time and space, past events were investigated using sedimentary facies analysis and luminescence chronology. All ages fall in the Holocene Epoch. Three independent methods namely Weights of Evidence (WOE), index of connectivity (IC), and Flow-R model were used to examine the vulnerability of the region to debris flow hazards.

So based on these studies the last three millennia is known to witness three major climatic oscillation- (1) warm from ~2.7 to 1.8 ka, (2) cold from ~1.8 to 1.1 ka, and (3) warm from ~1.1 to present and the record is comparable to the climatic history of the Ganga and its foreland. After the last glacial maximum, three phases of increased extreme flood recurrence happened – from ~14 to 11, ~10 to 8, and ~7 to 4 ka with increased penetration of ISM. The provenance study suggests Zaskar River is highly erosive during floods. The

presence of hearths also indicates ancient human activity and the timeframes were established using the ^{14}C ages opening up the question of past Human existence in this region for further studies. The warm climatic phases were found to be influenced by planetary warming and solar insolation in the last three millennia. The high flooding phases were also found to be connected with the dynamics of the arctic region. The study of debris flow indicates they were an important agent of denudation and aggradations and such events will continue to occur regardless of human activities. The susceptibility and risk analysis suggest presently Phayang, Shakti and Kharoo are conducive for frequent gully centric flows whereas the rest is likely to get buffered. However, this might lead to higher magnitude but lesser frequency mass flow events.

Nupur Tiwari

Technology, chronology and landscape archaeology of microlithic occurrences in the central Narmada Basin, Madhya Pradesh, India

May 2022

Indian Institute of Science Education and Research, Mohali (IISER), Punjab, India

Degree: Ph.D.

Supervisor: Dr. Parth R. Chauhan

The research carried out for this PhD thesis aimed to survey open-air microlithic sites in Sehore and Hoshangabad Districts of the central Narmada Basin or river valley in Madhya Pradesh, India. Geographically, the surveys were targeted along the Vindhyan Hills to the north of the basin, along the Gondwanas or Satpuras to the south of the basin and the intermediate Narmada floodplain zone in the centre, thus dividing the study area into three distinct zones, i.e. northern, central and southern. The study area selected for this study is located in the central region of the Indian Subcontinent. This region must have served as a corridor for various faunal species and hominins (abundant vertebrate and invertebrate fossils and the only-known archaic hominin fossil, a partial cranium, was discovered in this region). The goal of this research was threefold: (1) to understand the geoarchaeological and spatial contexts of the microlithic record and associated attributes in the central Narmada Basin, (2) to establish a preliminary geochronological framework of microliths in this region and spatially document the evidence to reconstruct the landscape adaptations by hominins in the north, central and south of the Narmada River in this part of the basin and (3) to address specific characters of the regional microlithic typology, technology and chronology in the study area and broad comparisons with other regions of India.

Luminescence dating was applied at key sites to understand the temporal context of the microlithic record in the study area. This provided a broad antiquity to the distribution of microliths in the valley, contributing to more robust interpretations of the region's occupational history. There are no

lengthy stratigraphic sections bearing microliths *in situ*, except for a few sloping sedimentary horizons that were eroding. These sedimentary horizons regularly yielded microliths and were least disturbed; few of these sites were selected for OSL dating.

The scarcity of dateable microlithic sites was observed during the explorations and surveys. Most of the sites appeared in the pediment zone of Vindhyan and Gondwana foothills. The context of all these sites and occurrences are varied, which points towards a significant and intensive use of the landscape and highly mobile groups of hunter-gatherers. The immense spread of microliths around this region and their absence in some pockets is now better understood through intensive surveys. Sites for OSL sampling were selected after exploring all accessible regions with thick sediment accumulation and the appearance of associated microliths eroding out. The selected sites were visited multiple times before deciding upon specific locations for sample collection. Hence, the least disturbed sites with microlithic occurrences were selected to understand the nature and timing of the burial of these microliths as well as the general age of their sedimentary contexts.

Specific criteria were fixed before sampling was carried out, including the assemblage size and artefact condition. Four sites from the northern region, i.e. Pilikarar-I, Pilikarar-II, Naganpur-I and Chikli, and two sites from the southern region, i.e. Morpani and Parcha were selected.

Infra-red (870–40 nm) stimulated luminescence (IRSL) was measured using the combination of Schott BG 39 and Corning 7-59 (320–460 nm). Optically stimulated luminescence (OSL) from quartz was measured using a 7.5 mm Hoya U-340 (330–35 nm) after blue light stimulation (470–20 nm). Single aliquot regenerative dose (SAR) procedure was used to estimate the equivalent dose using IRSL as suggested by Murray and Wintle (2003). Any sensitivity changes that occurred during the multiple heating, stimulation and irradiation in the sample may be corrected by a constant subsequent test dose luminescence signals. Pre-heat temperature for polymineral fine grains and coarse grain quartz grains were 250 °C and 240 °C, respectively. Each aliquot was subjected to a strict set of criteria before being accepted, and those criteria are 10% of test dose error, 10% of recycling dose and 5% recuperation dose. These fine grains are polymineral in nature, and only feldspar grains emit IRSL. IRSL of irradiated feldspar exhibit fading with time, and hence fading rate of IRSL for each sample was estimated as per the method adopted by Auclair et al. (2003). All the luminescence measurements were carried out in Risoe TL/OSL Reader Model DA-20 (Bøtter-Jensen, 2003). Luminescence ages were calculated using equivalent dose divided by dose rate, and the fading corrected ages were obtained using the calculated fading rates following the procedure established by Huntley and Lamothe (2001). Dates obtained through fine-grained IRSL confirm microliths' last burial age between Late Pleistocene to Late Holocene (~50 ka–2 ka).

A PDF of this thesis can be requested from: nupurti-

Bibliography

Compiled by Sebastien Huot

From 1st December 2021 to 31th May 2022

Various geological applications

- aeolian

- Cresswell, A.J., Sanderson, D.C.W., Carling, P.A., Darby, S.E., 2022. Quartz age extension applied to SE Asian cover sands. *Quaternary Geochronology* 69, 101271, <http://doi.org/10.1016/j.quageo.2022.101271>
- Felix-Henningsen, P., 2019. OSL-ages and paleo-climatic evidence of ancient dunes with paleosols along a SW–NE transect from the southern Sahel to the central Sahara in Niger. *Zeitschrift für Geomorphologie, Supplementary Issues* 62, 85-118, http://doi.org/10.1127/zfg_suppl/2019/0533
- Heinrich, H., Schmidt, C., Ziemer, F., Mikolajewicz, U., Roettig, C.-B., 2021. Massive deposition of Sahelian dust on the Canary Island Lanzarote during North Atlantic Heinrich Events. *Quaternary Research* 101, 51-66, <http://doi.org/10.1017/qua.2020.100>
- Hu, F., Jianhui, J., Xie, M., Xiao, Z., Cao, M., Zhou, Y., Liang, J., 2022. Insights into the age and genesis of the clay dunes in the Suhongtu Basin, Alashan Plateau, China. *Geomorphology* 408, 108241, <http://doi.org/10.1016/j.geomorph.2022.108241>
- Jin, J., Ling, Z., Li, Z., Zuo, X., Fan, X., Huang, Y., Wang, X., Wei, C., Ren, Y., Qiu, J., 2022. Spatiotemporal distribution of sea-island prehistoric dune sites, Holocene sea levels, and aeolian sand activities in Fujian Province, China. *Journal of Geographical Sciences* 32, 1157-1176, <http://doi.org/10.1007/s11442-022-1990-9>
- Klinge, M., Schneider, F., Li, Y., Frechen, M., Sauer, D., 2022. Variations in geomorphological dynamics in the northern Khangai Mountains, Mongolia, since the Late Glacial period. *Geomorphology* 401, 108113, <http://doi.org/10.1016/j.geomorph.2022.108113>
- Lancaster, N., Bacon, S.N., Bullard, T.F., Neudorf, C.M., Keen-Zebert, A.K., Decker, D.L., Boggs, M.L., 2022. Tectonic, hydrogeologic, and climatic controls on Late Holocene dune formation, China Lake basin, Indian Wells Valley, California, USA. *Quaternary Research* 106, 11-27, <http://doi.org/10.1017/qua.2021.62>
- Lewis, R.J., Tibby, J., Arnold, L.J., Gadd, P., Jacobsen, G., Barr, C., Negus, P.M., Mariani, M., Penny, D., Chittleborough, D., Moss, E., 2021. Patterns of aeolian deposition in subtropical Australia through the last glacial and deglacial periods. *Quaternary Research* 102, 68-90, <http://doi.org/10.1017/qua.2020.117>
- McIntosh, P.D., Neudorf, C., Lian, O.B., Snee, A.J., Walker, B., Eberhard, R., Doyle, R., Dixon, G., 2021. Late Pleistocene and Early Holocene aeolian deposits of Tasmania and their climatic implications. *Quaternary Research* 102, 91-114, <http://doi.org/10.1017/qua.2020.83>
- Peng, J., Wang, X., Adamiec, G., 2022. Test of high sampling density OSL dating of aeolian samples from the south margin of the Tengger Desert using the global standardised growth curve (gSGC) method. *Quaternary Geochronology* 69, 101275, <http://doi.org/10.1016/j.quageo.2022.101275>
- Sathiyaseelan, S., Panda, D.K., Banerjee, D., Ramesh, D., Shukla, A.D., 2021. Chronology of coastal dune ridges in Vaigai prodelta region, southeastern Tamil Nadu, India. *Current Science* 120, 382-388, <http://doi.org/10.18520/cs/v120/i2/382-388>
- Shu, P., Wang, H., Zhou, W., Ao, H., Niu, D., Wen, X., Li, B., 2021. Seasonal rainfall patterns in stable carbon isotopes in the Mu Us Desert, northern China during the early and middle Holocene. *Climate Dynamics* 56, 799-812, <http://doi.org/10.1007/s00382-020-05504-y>
- Sipos, G., Marković, S.B., Gavrilov, M.B., Balla, A., Filyó, D., Bartyik, T., Mészáros, M., Tóth, O., van Leeuwen, B., Lukić, T., Urdea, P., Onaca, A., Mezósi, G., Kiss, T., 2022. Late Pleistocene and Holocene aeolian activity in the Deliblato Sands, Serbia. *Quaternary Research* 107, 113-124, <http://doi.org/10.1017/qua.2021.67>
- Wang, L., Wu, Q., Fu, Z., Jiang, G., Liu, Y., Xu, K., 2022. Aeolian sand accumulation and land desertification over the past 1,500 years as revealed by two aeolian dunes in the Beiluhe Basin on interior Qinghai-Tibet Plateau, SW China. *Quaternary International* 613, 101-117, <http://doi.org/10.1016/j.quaint.2021.11.013>
- Zong, H., Fu, X., Li, Z., Guo, Y., Yang, X., 2022. Multi-method pIRIR dating of sedimentary sequences at the southern edge of the Gurbantunggut Desert, NW China and its palaeoenvironmental implications. *Quaternary Geochronology* 70, 101300, <http://doi.org/10.1016/j.quageo.2022.101300>

- cave

- Arnold, L.J., Demuro, M., Power, R., Priya, Duval, M., Guilarte, V., Weij, R., Woodhead, J., White, L., Bourne, S., Reed, E.H., 2022. Examining sediment infill dynamics at Naracoorte cave megafauna sites using multiple luminescence dating signals. *Quaternary Geochronology* 70, 101301, <http://doi.org/10.1016/j.quageo.2022.101301>
- Conrad, C., Shoocongdej, R., Marwick, B., White, J.C., Thongcharoenchaikit, C., Higham, C., Feathers, J.K., Tumpeesuwan, S., Castillo, C.C., Fuller, D.Q., Jones, E.L., 2022. Re-evaluating Pleistocene–Holocene occupation of cave sites in north-west Thailand: new radiocarbon and luminescence dating. *Antiquity* 96, 280-297, <http://doi.org/10.15184/aqy.2021.44>
- Douka, K., Slon, V., Jacobs, Z., Ramsey, C.B., Shunkov, M.V., Derevianko, A.P., Mafessoni, F., Kozlikin, M.B., Li, B., Grün, R., Comeskey, D., Devièse, T., Brown, S., Viola, B., Kinsley, L., Buckley, M., Meyer, M., Roberts, R.G., Pääbo, S., Kelso, J., Higham, T., 2019. Age estimates for hominin fossils and the onset of the Upper Palaeolithic at Denisova Cave. *Nature* 565, 640-644, <http://doi.org/10.1038/s41586-018-0870-z>
- Falguères, C., Barkai, R., Tombret, O., Gopher, A., 2022. New ESR/U-series dates of the lowest Acheuleo-Yabrudian levels of Qesem cave. *Quaternary Geochronology* 69, 101266, <http://doi.org/10.1016/j.quageo.2022.101266>
- Priya, Arnold, L.J., Guilarte, V., Duval, M., Demuro, M., Weij, R., Reed, E.H., 2022. ESR and OSL dating of fossil-bearing deposits from Naracoorte Cave Complex palaeontological sites, south Australia. *Quaternary Geochronology* 69, 101270, <http://doi.org/10.1016/j.quageo.2022.101270>
- Shao, Q., Philippe, A., He, C., Jin, M., Huang, M., Jiao, Y., Voinchet, P., Lin, M., Bahain, J.-J., 2022. Applying a Bayesian approach for refining the chronostratigraphy of the Yumidong site in the Three Gorges region, central China. *Quaternary Geochronology* 70, 101304, <http://doi.org/10.1016/j.quageo.2022.101304>

- coastal

- Bateman, M.D., Kinnaird, T.C., Hill, J., Ashurst, R.A., Mohan, J., Bateman, Rebecca B.I., Robinson, R., 2021. Detailing the impact of the Storegga Tsunami at Montrose, Scotland. *Boreas* 50, 1059-1078, <http://doi.org/10.1111/bor.12532>
- Ben Arous, E., Duval, M., Bateman, M.D., 2022. ESR dating of optically bleached quartz grains from Plio-Pleistocene to Holocene coastal dune deposits (Wilderness-Knysna area, South Africa): a comparison with luminescence. *Quaternary Geochronology* 70, 101293, <http://doi.org/10.1016/j.quageo.2022.101293>
- Brill, D., Ageby, L., Obert, C., Hollerbach, R., Duval, M., Kolb, T., Bartz, M., 2022. Investigating the resetting of IRSL signals in beach cobbles and their potential for rock surface dating of marine terraces in Northern Chile. *Marine Geology* 443, 106692, <http://doi.org/10.1016/j.margeo.2021.106692>
- Brill, D., May, S.M., Mhammedi, N., King, G., Lehmann, B., Burow, C., Wolf, D., Zander, A., Brückner, H., 2021. Evaluating optically stimulated luminescence rock surface exposure dating as a novel approach for reconstructing coastal boulder movement on decadal to centennial timescales. *Earth Surface Dynamics* 9, 205-234, <http://doi.org/10.5194/esurf-9-205-2021>
- Cheng, Y., Zou, X., Li, X., Zhao, Z., Zhang, X., Guo, G., Lin, J., 2021. Sedimentary characteristics and evolution process of the Huangqiao sand body in the Yangtze River Delta, China. *Estuarine, Coastal and Shelf Science* 254, 107330, <http://doi.org/10.1016/j.ecss.2021.107330>
- Dadalto, T.P., Carvalho, B.C., Guerra, J.V., Reis, A.T.d., Silva, C.G., 2022. Holocene morpho-sedimentary evolution of Marambaia Barrier Island (SE Brazil). *Quaternary Research* 105, 182-200, <http://doi.org/10.1017/qua.2021.43>
- Dourado, F., Costa, P.J.M., Baptista, M.A., Omira, R., Cezario, A.P., Veloso, A.V., Fatela, F., 2022. Possible evidence of the 1755 CE transatlantic tsunami in Brazil. *Journal of South American Earth Sciences* 116, 103823, <http://doi.org/10.1016/j.jsames.2022.103823>
- Erginal, A.E., Kiyak, N.G., Makaroğlu, Ö., Bozcu, M., Öztürk, M.Z., Selim, H.H., Nowaczyk, N.R., Kaya, N., Öztürk, T., Karabıyıkoglu, M., Polymeris, G.S., 2022. Aeolian imprints of multiple Mediterranean invasions of the Black Sea during Pleistocene. *Palaeogeography, Palaeoclimatology, Palaeoecology* 592, 110902, <http://doi.org/10.1016/j.palaeo.2022.110902>
- Gugliotta, M., Saito, Y., Ta, T.K.O., Nguyen, V.L., La Croix, A.D., Wang, Z., Tamura, T., Nakashima, R., Lieu, K.P., 2022. Late Holocene stratigraphic evolution and sedimentary facies of an active to abandoned tide-dominated distributary channel and its mouth bar. *Sedimentology* 69, 1151-1178, <http://doi.org/10.1111/sed.12940>
- Hanebuth, T.J.J., Kudrass, H.R., Zander, A.M., Akhter, H.S., Neumann-Denzau, G., Zahid, A., 2022. Stepwise, earthquake-driven coastal subsidence in the Ganges–Brahmaputra Delta (Sundarbans) since the eighth

- century deduced from submerged in situ kiln and mangrove remnants. *Natural Hazards* 111, 163-190, <http://doi.org/10.1007/s11069-021-05048-2>
- Heinrich, H., Schmidt, C., Ziemeň, F., Mikolajewicz, U., Roettig, C.-B., 2021. Massive deposition of Sahelian dust on the Canary Island Lanzarote during North Atlantic Heinrich Events. *Quaternary Research* 101, 51-66, <http://doi.org/10.1017/qua.2020.100>
- Jankowski, N.R., Cohen, T.J., Larsen, J., Larsen, A., May, J.H., 2021. Revisiting the abandoned shorelines of Lake George, Australia: a refined optical dating framework. *Journal of Quaternary Science* 36, 1052-1072, <http://doi.org/10.1002/jqs.3348>
- Kim, J.C., Yoo, D.-G., Hong, S.-H., Yoon, H.H., Shin, S., Han, M., Choi, J., Cheong, D., Lee, J.-Y., Choi, H., 2021. Chronostratigraphic and palaeogeographic interpretation of Nakdong deltaic sequences in the south-eastern Korean Peninsula. *Palaeogeography, Palaeoclimatology, Palaeoecology* 584, 110654, <http://doi.org/10.1016/j.palaeo.2021.110654>
- Liu, R., Nian, X., Zhang, W., Qiu, F., Wang, Z., Lin, Q., Shu, J., Liu, N., 2022. Luminescence dating of the late Quaternary sediments in Hangzhou Bay, China. *Quaternary Geochronology* 70, 101302, <http://doi.org/10.1016/j.quageo.2022.101302>
- Lü, T., Sun, J., Feathers, J.K., Sun, D., Cui, C., Shen, X., 2022. OSL dating of coastal sand dunes in southeastern China provides new insights into the relationship between aeolian activity and eustatic sea-level fluctuations. *Palaeogeography, Palaeoclimatology, Palaeoecology* 600, 111082, <http://doi.org/10.1016/j.palaeo.2022.111082>
- Molodkov, A., Bolikhovskaya, N., 2022. Palaeoenvironmental changes and their chronology during the latter half of MIS 5 on the south-eastern coast of the Gulf of Finland. *Quaternary International* 616, 40-54, <http://doi.org/10.1016/j.quaint.2021.10.016>
- Nazarov, D.V., Nikolskaia, O.A., Gladysheva, A.S., Zhigmanovskiy, I.V., Ruchkin, M.V., Merkuljev, A.V., Thomsen, K.J., 2022. Evidence for the intrusion of marine Atlantic waters into the West Siberian Arctic during the Middle Pleistocene. *Boreas* 51, 402-425, <http://doi.org/10.1111/bor.12558>
- Oliver, T.S.N., Donaldson, P., Tamura, T., 2022. Embayment-scale coastal evolution and shoreline progradation in southeast Tasmania, Australia. *Marine Geology* 444, 106725, <http://doi.org/10.1016/j.margeo.2021.106725>
- Oliver, T.S.N., Tamura, T., 2021. Sub-centennially resolved behavior of an accreting sandy shoreline over the past ~ 1000 years. *Journal of Sedimentary Research* 91, 211-218, <http://doi.org/10.2110/jsr.2020.074>
- Prizomwala, S.P., Gandhi, D., Bhatt, N., Winkler, W., Kumar, M.R., Makwana, N., Bhatt, N., 2018. Geological evidence for AD 1008 tsunami along the Kachchh coast, Western India: Implications for hazard along the Makran Subduction Zone. *Scientific Reports* 8, 16816, <http://doi.org/10.1038/s41598-018-35193-x>
- Prizomwala, S.P., Vedpathak, C., Tandon, A., Das, A., Makwana, N., Joshi, N., 2022. Geological footprints of the 1945 Makran tsunami from the west coast of India. *Marine Geology* 446, 106773, <http://doi.org/10.1016/j.margeo.2022.106773>
- Qiaola, S., Nguyen, T.M.L., Ta, T.K.O., Nguyen, V.L., Gugliotta, M., Saito, Y., Kitagawa, H., Nakashima, R., Tamura, T., 2022. Luminescence dating of Holocene sediment cores from a wave-dominated and mountainous river delta in central Vietnam. *Quaternary Geochronology* 70, 101277, <http://doi.org/10.1016/j.quageo.2022.101277>
- Sechi, D., Andreucci, S., De Giudici, G., Pascucci, V., 2018. Luminescence dating of a Middle Late Holocene lower shoreface, SW Sardinia (Italy). *Alpine and Mediterranean Quaternary* 31, 189-192, <https://amq.aiqua.it/index.php/amq/article/view/215>
- Sharma, S., Chauhan, G., Shukla, A.D., Nambiar, R., Bhushan, R., Desai, B.G., Pandey, S., Dabhi, M., Bhandari, S., Bhosale, S., Lakhote, A., Juyal, N., 2021. Causes and implications of Mid- to Late Holocene relative sea-level change in the Gulf of Kachchh, western India. *Quaternary Research* 100, 98-121, <http://doi.org/10.1017/qua.2020.86>
- Shtienberg, G., Gadol, O., Levy, T.E., Norris, R.D., Rittenour, T.M., Yasur-Landau, A., Tamberino, A., Lazar, M., 2022. Changing environments and human interaction during the Pleistocene–Early Holocene from the shallow coastal area of Dor, Israel. *Quaternary Research* 105, 64-81, <http://doi.org/10.1017/qua.2021.30>
- Suursaar, Ü., Rosentau, A., Hang, T., Tõnisson, H., Tamura, T., Vaasma, T., Vandel, E., Vilumaa, K., Sugita, S., 2022. Climatically induced cyclicity recorded in the morphology of uplifting Tihu coastal ridgeplain, Hiiumaa Island, eastern Baltic Sea. *Geomorphology* 404, 108187, <http://doi.org/10.1016/j.geomorph.2022.108187>
- Tamura, T., Nguyen, V.L., Ta, T.K.O., Bateman, M.D., Gugliotta, M., Anthony, E.J., Nakashima, R., Saito, Y., 2020. Long-term sediment decline causes ongoing shrinkage of the Mekong megadelta, Vietnam. *Scientific Reports* 10, 8085, <http://doi.org/10.1038/s41598-020-64630-z>

- Tibby, J., Haynes, D., Gibbs, M., Mosley, L., Bourman, R.P., Fluin, J., 2022. The terminal lakes of the Murray River, Australia, were predominantly fresh before large-scale upstream water abstraction: Evidence from sedimentary diatoms and hydrodynamical modelling. *Science of The Total Environment* 835, 155225, <http://doi.org/10.1016/j.scitotenv.2022.155225>
- Tsakalos, E., Athanassas, C., Tsipas, P., Triantaphyllou, M., Geraga, M., Papatheodorou, G., Filippaki, E., Christodoulakis, J., Kazantzaki, M., 2018. Luminescence geochronology and paleoenvironmental implications of coastal deposits of southeast Cyprus. *Archaeological and Anthropological Sciences* 10, 41-60, <http://doi.org/10.1007/s12520-016-0339-7>
- Tsakalos, E., Dimitriou, E., Kazantzaki, M., Anagnostou, C., Christodoulakis, J., Filippaki, E., 2018. Testing optically stimulated luminescence dating on sand-sized quartz of deltaic deposits from the Sperchios delta plain, central Greece. *Journal of Palaeogeography* 7, 130-145, <http://doi.org/10.1016/j.jop.2018.01.001>
- Xu, X., Zhong, J., Huang, X., Li, H., Ding, Z., Lai, Z., 2022. Age comparison by luminescence using quartz and feldspar on core HPQK01 from the Pearl River delta in China. *Quaternary Geochronology* 71, 101320, <http://doi.org/10.1016/j.quageo.2022.101320>

- colluvial

- Cunningham, A.C., Khashchevskaya, D., Semikolenykh, D., Kurbanov, R., Murray, A.S., 2022. Luminescence dating of mass-transport sediment using rock-surface burial methods: a test case from the Baksan valley in the Caucasus Mountains. *Quaternary Geochronology* 68, 101253, <http://doi.org/10.1016/j.quageo.2022.101253>
- de Godoi Pinton, L., Lupinacci, C.M., 2022. Geochronological and paleoenvironmental reconstruction of colluvial deposits in a cuesta landscape in south-eastern Brazil. *Journal of Quaternary Science* 37, 489-502, <http://doi.org/10.1002/jqs.3395>
- Henkner, J., Ahlrichs, J., Downey, S., Fuchs, M., James, B., Junge, A., Knopf, T., Scholten, T., Kühn, P., 2018. Archaeopedological analysis of colluvial deposits in favourable and unfavourable areas: reconstruction of land use dynamics in SW Germany. *Royal Society Open Science* 5, 171624, <http://doi.org/10.1098/rsos.171624>
- May, S.M., Norpoth, M., Pint, A., Shumilovskikh, L., Raith, K., Brill, D., Rixhon, G., Moret, P., Jiménez-Vialás, H., Grau-Mira, I., García-Jiménez, I., Marzoli, D., León-Martín, C., Reicherter, K., Brückner, H., 2021. Mid- to late Holocene environmental changes and human-environment interactions in the surroundings of La Silla del Papa, SW Spain. *Geoarchaeology* 36, 573-600, <http://doi.org/10.1002/gea.21846>
- Medialdea, A., Brill, D., King, G.E., Zander, A., Lopez-Ramirez, M.R., Bartz, M., Brückner, H., 2022. Violet stimulated luminescence as an alternative for dating complex colluvial sediments in the Atacama Desert. *Quaternary Geochronology* 71, 101337, <http://doi.org/10.1016/j.quageo.2022.101337>
- Zou, J., He, H., Yokoyama, Y., Shirahama, Y., Sproson, A.D., Wei, Z., Shi, F., Hao, H., Miyairi, Y., Lü, L., Su, P., Zhou, C., 2020. Seismic history of a bedrock fault scarp using quantitative morphology together with multiple dating methods: A case study of the Luoyunshan piedmont fault, southwestern Shanxi Rift, China. *Tectonophysics* 788, 228473, <http://doi.org/10.1016/j.tecto.2020.228473>

- earthquake (and fault related)

- Erginal, A.E., Erenoğlu, R.C., Yıldırım, C., Selim, H.H., Kıyak, N.G., Erenoğlu, O., Ulugergerli, E., Karabıyıkoglu, M., 2021. Co-seismic beachrock deformation of 8th century AD Earthquake in Middle Strand of North Anatolian Fault, Lake Iznik, NW Turkey. *Tectonophysics* 799, 228690, <http://doi.org/10.1016/j.tecto.2020.228690>
- Gray, H., DuRoss, C., Nicovich, S., Gold, R., 2022. Luminescence sediment tracing reveals the complex dynamics of colluvial wedge formation. *Science Advances* 8, eabo0747, <http://doi.org/10.1126/sciadv.abo0747>
- Hatem, A.E., Dolan, J.F., Zinke, R.W., Langridge, R.M., McGuire, C.P., Rhodes, E.J., Brown, N., Van Dissen, R.J., 2020. Holocene to latest Pleistocene incremental slip rates from the east-central Hope fault (Conway segment) at Hossack Station, Marlborough fault system, South Island, New Zealand: Towards a dated path of earthquake slip along a plate boundary fault. *Geosphere* 16, 1558-1584, <http://doi.org/10.1130/GES02263.1>
- Jara-Muñoz, J., Melnick, D., Li, S., Socquet, A., Cortés-Aranda, J., Brill, D., Strecker, M.R., 2022. The cryptic seismic potential of the Pichilemu blind fault in Chile revealed by off-fault geomorphology. *Nature Communications* 13, 3371, <http://doi.org/10.1038/s41467-022-30754-1>

- Karlsson, K.W., Rockwell, T.K., Fletcher, J.M., Figueiredo, P.M., Cambron Rosas, J.F., Gontz, A.M., Prasanajit Naik, S., Lacan, P., Spelz, R.M., Owen, L.A., Peña Villa, I.A., Loya, R.L., 2021. Large Holocene ruptures on the Cañada David detachment, Baja California, Mexico; implications for the seismogenesis of low-angle normal faults. *Earth and Planetary Science Letters* 570, 117070, <http://doi.org/10.1016/j.epsl.2021.117070>
- Kothyari, G.C., Kandregula, R.S., Chauhan, G., Desai, B.G., Taloor, A.K., Pathak, V., Swamy, K.V., Mishra, S., Thakkar, M.G., 2021. Quaternary Landform Development in the Central segment of tectonically active Kachchh Mainland Fault zone, Western India. *Quaternary Science Advances* 3, 100018, <http://doi.org/10.1016/j.qsa.2020.100018>
- Kumar, A., Srivastava, P., Sen, K., Morell, K., Hazarika, D., 2020. Evidence for late Quaternary brittle deformation and back thrusting within the Indus Suture Zone, Ladakh Himalaya. *Tectonophysics* 792, 228597, <http://doi.org/10.1016/j.tecto.2020.228597>
- Lei, Q., Yu, J., Zhang, P., Zheng, W., Zhang, Z., Du, P., Wang, Y., 2022. Tectonic geomorphology and prehistoric earthquakes of the West Helanshan fault, West Ordos, and its implications for regional tectonics and seismic hazard. *Tectonophysics* 833, 229375, <http://doi.org/10.1016/j.tecto.2022.229375>
- Li, J., Yuan, S., Liu, Y., Liu, X., Bai, X., Jiang, J., Li, Y., Zhao, Z., 2019. Tectonic Uplift of the Yili Basin during the Last Stage of the Late Pleistocene: Evidence from ESR and OSL Dating of Sediments in the Huocheng Area, Xinjiang. *Acta Geologica Sinica - English Edition* 93, 1219-1227, <http://doi.org/10.1111/1755-6724.14355>
- Liu, X., Yuan, D., Su, Q., Zhang, B., 2020. Late Quaternary Tectonic Activity and Slip Rates of Active Faults in the Western Hexi Corridor, NW China. *Journal of Earth Science* 31, 968-977, <http://doi.org/10.1007/s12583-020-1287-9>
- Pandita, S.K., Haq, A.U., Bhat, G.M., Singh, Y., Singh, A., 2021. Identification of active fault topography along the Kishtwar Fault, Jammu and Kashmir, Northwest Himalaya, India. *Environmental Earth Sciences* 80, 140, <http://doi.org/10.1007/s12665-021-09427-7>
- Philibosian, B.E., Sickler, R.R., Prentice, C.S., Pickering, A.J., Gannon, P., Broudy, K.N., Mahan, S.A., Titular, J.N., Turner, E.A., Folmar, C., Patterson, S.F., Bowman, E.E., 2022. Photomosaics and logs associated with study of West Napa Fault at Ehlers Lane, north of Saint Helena, California, Open-File Report, Reston, VA, p. 8, <http://doi.org/10.3133/ofr20221002>
- Ren, J., Xu, X., Lv, Y., Wang, Q., Li, A., Li, K., Zhu, J., Cai, J., Liu, S., 2022. Late Quaternary slip rate of the northern Lancangjiang fault zone in eastern Tibet: Seismic hazards for the Sichuan-Tibet Railway and regional tectonic implications. *Engineering Geology* 306, 106748, <http://doi.org/10.1016/j.enggeo.2022.106748>
- Shao, Y., Liu-Zeng, J., Van der Woerd, J., Klinger, Y., Oskin, M.E., Zhang, J., Wang, P., Wang, P., Wang, W., Yao, W., 2021. Late Pleistocene slip rate of the central Haiyuan fault constrained from optically stimulated luminescence, ¹⁴C, and cosmogenic isotope dating and high-resolution topography. *GSA Bulletin* 133, 1347-1369, <http://doi.org/10.1130/B35571.1>
- Yin, G., Liu, C., Yuan, R., Han, F., Ding, R., Bahain, J.-J., 2021. ESR Chronology of Bedrock Fault Activity in Carbonate Area: Preliminary Results from the Study of the Lijiang-Xiaojinhe Fault, Southeastern Tibet, China. *Geochronometria* 48, 215-221, <http://doi.org/10.2478/geochr-2020-0033>
- Zhao, X., Hu, D., Wen, Z., Tang, X., Deng, J., Wang, R., Yi, L., 2021. Geological structures associated with potential gas-hydrate accumulation in the Mohe permafrost, North East China. *Journal of Petroleum Science and Engineering* 197, 108110, <http://doi.org/10.1016/j.petrol.2020.108110>
- Zou, J., He, H., Yokoyama, Y., Shirahama, Y., Sproson, A.D., Wei, Z., Shi, F., Hao, H., Miyairi, Y., Lü, L., Su, P., Zhou, C., 2020. Seismic history of a bedrock fault scarp using quantitative morphology together with multiple dating methods: A case study of the Luoyunshan piedmont fault, southwestern Shanxi Rift, China. *Tectonophysics* 788, 228473, <http://doi.org/10.1016/j.tecto.2020.228473>

- fluvial

- Al-Saqarat, B.S., Abbas, M., Lai, Z., Gong, S., Alkuisi, M.M., Abu Hamad, A.M.B., Carling, P.A., Jansen, J.D., 2021. A wetland oasis at Wadi Gharandal spanning 125–70 ka on the human migration trail in southern Jordan. *Quaternary Research* 100, 154-169, <http://doi.org/10.1017/qua.2020.82>
- Bezerra, I.S.A.A., Nogueira, A.C.R., Motta, M.B., Sawakuchi, A.O., Mineli, T.D., Silva, A.d.Q., Silva, A.G., Domingos, F.H.G., Mata, G.A.T., Lima, F.J., Riker, S.R.L., 2022. Incision and aggradation phases of the Amazon River in central-eastern Amazonia during the late Neogene and Quaternary. *Geomorphology* 399, 108073, <http://doi.org/10.1016/j.geomorph.2021.108073>
- Cajigas, R., Quade, J., Rittenour, T., 2020. Multitechnique dating of earthen irrigation canals at the La Playa site, Sonora, Mexico. *Geoarchaeology* 35, 834-855, <http://doi.org/10.1002/gea.21800>

- Capaldi, T.N., Rittenour, T.M., Nelson, M.S., 2022. Downstream changes in quartz OSL sensitivity in modern river sand reflects sediment source variability: Case studies from Rocky Mountain and Andean rivers. *Quaternary Geochronology* 71, 101317, <http://doi.org/10.1016/j.quageo.2022.101317>
- Dey, S., Bookhagen, B., Thiede, R.C., Wittmann, H., Chauhan, N., Jain, V., Strecker, M.R., 2022. Impact of Late Pleistocene climate variability on paleo-erosion rates in the western Himalaya. *Earth and Planetary Science Letters* 578, 117326, <http://doi.org/10.1016/j.epsl.2021.117326>
- Dey, S., Thiede, R.C., Biswas, A., Chauhan, N., Chakravarti, P., Jain, V., 2021. Implications of the ongoing rock uplift in NW Himalayan interiors. *Earth Surface Dynamics* 9, 463-485, <http://doi.org/10.5194/esurf-9-463-2021>
- Donselaar, M.E., Cuevas Gozalo, M.C., van Tooreneburg, K.A., Wallinga, J., 2022. Spatio-temporal reconstruction of avulsion history at the terminus of a modern dryland river system. *Earth Surface Processes and Landforms* 47, 1212-1228, <http://doi.org/10.1002/esp.5311>
- Erturaç, M.K., 2021. Late Pleistocene-Holocene characteristics of the North Anatolian Fault at Adapazarı Basin: evidence from the age and geometry of the fluvial terrace staircases. *Turkish Journal of Earth Sciences* 30, 93-115, <http://doi.org/10.3906/yer-2006-25>
- Hu, G., Min, R., Zhou, Y., Yang, J., Wang, Y., Wang, C., Wang, H., Wang, P., Wang, L., Fan, A., 2022. Luminescence dating of a megaflood event on a terrace of the Jinsha River, China. *Quaternary Geochronology* 70, 101303, <http://doi.org/10.1016/j.quageo.2022.101303>
- Ishii, Y., 2022. Luminescence dating reveals a rapid response to climate change of fluvial terrace formation along the Ani River, northeastern Japan, during the last glacial period. *Quaternary Geochronology* 70, 101307, <http://doi.org/10.1016/j.quageo.2022.101307>
- Ishii, Y., Tamura, T., Collins, D.S., Ben, B., 2021. Applicability of OSL Dating to Fine-Grained Fluvial Deposits in the Mekong River Floodplain, Cambodia. *Geochronometria* 48, 351-363, <http://doi.org/10.2478/geochr-2020-0006>
- Jin, J., Li, F., Ling, Z., Li, Z., 2022. New chronological evidence reveals a continuously inhabited Neolithic–historical settlement in south China. *Palaeogeography, Palaeoclimatology, Palaeoecology* 600, 111081, <http://doi.org/10.1016/j.palaeo.2022.111081>
- Khosravichenar, A., Fattahi, M., Amini, H., Suchodoletz, H.V., 2020. The Potential of Small Mountain River Systems for Paleoenvironmental Reconstructions in Drylands—An Example from the Binaloud Mountains in Northeastern Iran. *Geosciences* 10, 448, <http://doi.org/10.3390/geosciences10110448>
- Ladeira, F.S.B., Mescolotti, P.C., do Nascimento Pupim, F., de Faria, L.M.D.M., Assine, M.L., 2022. Paleosols record dry and humid paleoenvironments during the Upper Pleistocene in the Brazilian Pantanal. *CATENA* 212, 106113, <http://doi.org/10.1016/j.catena.2022.106113>
- Li, K., Qin, J., Chen, J., Shen, J., Li, S.-H., 2021. Multi-Method Luminescence Dating of Old Fluvial Sediments from Northern Tian Shan, China. *Geochronometria* 48, 339-350, <http://doi.org/10.2478/geochr-2020-0014>
- Li, Y., Wei, C., Li, C., Guo, R., Liu, C., Zhang, Y., 2022. Application and evaluation of multiple-centres ESR dating of Pliocene-Quaternary fluvial sediments: A case study from the Zhoula core from the Jiangnan Basin, middle Yangtze River basin, China. *Quaternary Geochronology* 70, 101297, <http://doi.org/10.1016/j.quageo.2022.101297>
- Liu, X., Wei, M., Pan, B., Wang, J., Zhao, Q., Liu, Y., Wang, Y., 2022. Sedimentary evolution of a foreland basin from the northeastern Qilian Mountains based on the integration of geomorphological and luminescence dating of alluvial conglomerates and fluvial terrace sediments. *Quaternary Geochronology* 69, 101268, <http://doi.org/10.1016/j.quageo.2022.101268>
- May, S.M., Norpoth, M., Pint, A., Shumilovskikh, L., Raith, K., Brill, D., Rixhon, G., Moret, P., Jiménez-Vialás, H., Grau-Mira, I., García-Jiménez, I., Marzoli, D., León-Martín, C., Reicherter, K., Brückner, H., 2021. Mid- to late Holocene environmental changes and human-environment interactions in the surroundings of La Silla del Papa, SW Spain. *Geoarchaeology* 36, 573-600, <http://doi.org/10.1002/gea.21846>
- Peña-Monné, J.L., Cunha, P.P., Sampietro-Vattuone, M.M., Bridgland, D.R., Murray, A.S., Buylaert, J.-P., 2022. The connections between river terraces and slope deposits as paleoclimate proxies: The Guadalaviar - Turia sequence (Eastern, Iberia Chain, Spain). *Global and Planetary Change* 208, 103728, <http://doi.org/10.1016/j.gloplacha.2021.103728>
- Qiaola, S., Nguyen, T.M.L., Ta, T.K.O., Nguyen, V.L., Gugliotta, M., Saito, Y., Kitagawa, H., Nakashima, R., Tamura, T., 2022. Luminescence dating of Holocene sediment cores from a wave-dominated and mountainous river delta in central Vietnam. *Quaternary Geochronology* 70, 101277, <http://doi.org/10.1016/j.quageo.2022.101277>

- Richter, M., Tsukamoto, S., 2022. Investigation of quartz electron spin resonance residual signals in the last glacial and early Holocene fluvial deposits from the Lower Rhine. *Geochronology* 4, 55-63, <http://doi.org/10.5194/gchron-4-55-2022>
- Rui, X., Li, B., Yuan, B., Zhang, J., 2022. Luminescence dating of the Huli River terraces in the Nihewan Basin, North China. *Quaternary Geochronology* 71, 101316, <http://doi.org/10.1016/j.quageo.2022.101316>
- Sam, N., Nimiago, P., McIntosh, P., Wang, N., 2020. Markham river floodplain sediments reveal last glacial maximum erosion in Papua New Guinea uplands followed by landscape stability. *Quaternary Australasia* 37, 19-20, <https://search.informit.org/doi/10.3316/INFORMIT.285736632870949>
- Sharma, C.P., Chahal, P., Kumar, A., Singhal, S., Sundriyal, Y.P., Ziegler, A.D., Agnihotri, R., Wasson, R.J., Shukla, U.K., Srivastava, P., 2022. Late Pleistocene–Holocene flood history, flood-sediment provenance and human imprints from the upper Indus River catchment, Ladakh Himalaya. *GSA Bulletin* 134, 275-292, <http://doi.org/10.1130/B35976.1>
- Tsukamoto, S., Bussert, R., Delagnes, A., Richter, M., Mohammednoor, M., Bedri, O., Kraatz, B., Müller, J., Salih, K., Eisawi, A., Bibi, F., 2022. Luminescence chronology of fossiliferous fluvial sediments along the middle Atbara River, Sudan. *Quaternary Geochronology* 71, 101312, <http://doi.org/10.1016/j.quageo.2022.101312>
- Wang, A., Jiang, Q., Lyu, G., Wang, T., Zhou, B., Wei, J., Li, Y., Gu, G., Wan, L., Liu, K., Pan, H., 2022. Fast valley landscape response to climate change in the Lower Jinsha River, Southeastern Tibetan Plateau: Field investigations and numerical modeling. *Geomorphology* 403, 108158, <http://doi.org/10.1016/j.geomorph.2022.108158>
- Wang, H., Wang, P., Hu, G., Ge, Y., Yuan, R., 2021. An Early Holocene river blockage event on the western boundary of the Namche Barwa Syntaxis, southeastern Tibetan Plateau. *Geomorphology* 395, 107990, <http://doi.org/10.1016/j.geomorph.2021.107990>
- Wang, Y., Oskin, M.E., Li, Y., Zhang, H., 2022. Rapid Holocene bedrock canyon incision of Beida River, North Qilian Shan, China. *Earth Surface Dynamics* 10, 191-208, <http://doi.org/10.5194/esurf-10-191-2022>
- Wei, C., Zhang, H., Li, C.a., Zhang, Y., Li, Y., Jia, M., Li, G., Leng, Y., 2021. Holocene OSL Chronology of Flu-Lacustrine Sediments in Yangtze River Basin, Wuhan Area, China. *Geochronometria* 48, 284-293, <http://doi.org/10.2478/geochr-2020-0012>
- Wei, C.-Y., Liu, C.-R., Yin, G.-M., Li, W.-P., 2021. Electron Spin Resonance (ESR) Signal Intensity of Quartz E' Centre and Its Potential Use in Fluvial Sediments Provenance Tracing. *Geochronometria* 48, 197-204, <http://doi.org/10.2478/geochr-2020-0040>
- Yan, Y.-Y., Zhang, J.-F., Hu, G., Zhou, L.-P., 2021. Luminescence Chronology of the Yellow River Terraces in the Heiyukou Area, China, and Its Implication for the Uplift Rate of the Ordos Plateau. *Geochronometria* 48, 325-338, <http://doi.org/10.2478/geochr-2020-0008>

- glacial and periglacial

- Barrows, T.T., Mills, S.C., Fitzsimmons, K., Wasson, R., Galloway, R., 2022. Low-altitude periglacial activity in southeastern Australia during the late Pleistocene. *Quaternary Research* 107, 125-146, <http://doi.org/10.1017/qua.2021.72>
- Carson, E.C., Attig, J.W., Rawling, J.E., Hanson, P.R., Dodge, S.E., 2020. Chronology of advance and recession dynamics of the southern Green Bay Lobe of the Laurentide Ice Sheet, south-central Wisconsin, USA. *Quaternary Research* 95, 142-153, <http://doi.org/10.1017/qua.2020.8>
- Farquharson, L., Mann, D., Rittenour, T., Groves, P., Grosse, G., Jones, B., 2018. Alaskan marine transgressions record out-of-phase Arctic Ocean glaciation during the last interglacial. *Geology* 46, 783-786, <http://doi.org/10.1130/G40345.1>
- Fisher, T.G., Dziekan, M.R., McDonald, J., Lepper, K., Loope, H.M., McCarthy, F.M.G., Curry, B.B., 2020. Minimum limiting deglacial ages for the out-of-phase Saginaw Lobe of the Laurentide Ice Sheet using optically stimulated luminescence (OSL) and radiocarbon methods. *Quaternary Research* 97, 71-87, <http://doi.org/10.1017/qua.2020.12>
- Gribenski, N., Valla, P.G., Preusser, F., Roattino, T., Crouzet, C., Buoncristiani, J.-F., 2021. Out-of-phase Late Pleistocene glacial maxima in the Western Alps reflect past changes in North Atlantic atmospheric circulation. *Geology* 49, 1096-1101, <http://doi.org/10.1130/G48688.1>
- Hou, Y., Long, H., Zhang, J., Feng, Y., Yang, N., Gu, J., Cai, Y., Yang, F., Shen, J., 2022. Luminescence dating of shoreline sediments indicates a late deglacial lake-level rise of Selin Co on the central Tibetan Plateau. *Quaternary Geochronology* 71, 101313, <http://doi.org/10.1016/j.quageo.2022.101313>

- Ishii, Y., 2022. Luminescence dating reveals a rapid response to climate change of fluvial terrace formation along the Ani River, northeastern Japan, during the last glacial period. *Quaternary Geochronology* 70, 101307, <http://doi.org/10.1016/j.quageo.2022.101307>
- Kenzler, M., Krauß, N., Hüneke, H., 2022. Testing a proposed new chronology for the Jasmund Glacitectonic Complex (SW Baltic Sea): No indication of incipient deformation during MIS 3. *Quaternary Geochronology* 70, 101299, <http://doi.org/10.1016/j.quageo.2022.101299>
- Klinge, M., Schlütz, F., Zander, A., Hülle, D., Batkhisig, O., Lehmkuhl, F., 2021. Late Pleistocene lake level, glaciation and climate change in the Mongolian Altai deduced from sedimentological and palynological archives. *Quaternary Research* 99, 168-189, <http://doi.org/10.1017/qua.2020.67>
- Liu, L., Zhang, H., Zhang, W., Chai, L., 2022. Global Last Glacial Maximum climate inferred from reconstructing the Eryehai Valley, Mount Taibai, Qinling Mountains, eastern China. *Palaeogeography, Palaeoclimatology, Palaeoecology* 590, 110858, <http://doi.org/10.1016/j.palaeo.2022.110858>
- Murton, J.B., Opel, T., Toms, P., Blinov, A., Fuchs, M., Wood, J., Gärtner, A., Merchel, S., Rugel, G., Savvinov, G., Wetterich, S., 2022. A multimethod dating study of ancient permafrost, Batagay megaslump, east Siberia. *Quaternary Research* 105, 1-22, <http://doi.org/10.1017/qua.2021.27>
- Rhodes, E.J., Leathard, J.A., 2022. MET-IRSL used to track pre-depositional sediment transport history. *Quaternary Geochronology* 70, 101294, <http://doi.org/10.1016/j.quageo.2022.101294>
- Rymer, K.G., Rachlewicz, G., Buchwal, A., Temme, A.J.A.M., Reimann, T., van der Meij, W.M., 2022. Contemporary and past aeolian deposition rates in periglacial conditions (Ebba Valley, central Spitsbergen). *CATENA* 211, 105974, <http://doi.org/10.1016/j.catena.2021.105974>
- Schaetzl, R.J., Running Iv, G., Larson, P., Rittenour, T., Yansa, C., Faulkner, D., 2022. Luminescence dating of sand wedges constrains the Late Wisconsin (MIS 2) permafrost interval in the upper Midwest, USA. *Boreas* 51, 385-401, <http://doi.org/10.1111/bor.12550>
- Slee, A., McIntosh, P.D., Woodward, C., Wang, N., Gadd, P., 2022. A rapid sediment pulse induced by glacial melting during the MIS 8/7e transition buried well-developed karst in the Railton Valley, Tasmania, Australia. *Boreas* 51, 185-200, <http://doi.org/10.1111/bor.12538>
- Tamura, T., Ishiwa, T., Tokuda, Y., Itaki, T., Sasaki, S., Suganuma, Y., 2022. Luminescence characteristics of coastal sediments in Langhovde, East Antarctica. *Quaternary Geochronology* 70, 101298, <http://doi.org/10.1016/j.quageo.2022.101298>
- Zhou, S., Xie, J., Ou, X., Xu, L., Sun, Y., Zeng, X., Wen, X., Chen, R., Yang, H., Huang, X., Zhou, Y., Sun, J., 2021. Evidence for glaciation predating MIS-6 in the eastern Nyainqêntanglha Range, southeastern Tibet. *Science China Earth Sciences* 64, 559-570, <http://doi.org/10.1007/s11430-020-9711-2>
- Zinelabedin, A., Riedesel, S., Reimann, T., Ritter, B., Dunai, T.J., 2022. Testing the potential of using coarse-grain feldspars for post-IR IRSL dating of calcium sulphate-wedge growth in the Atacama Desert. *Quaternary Geochronology* 71, 101341, <http://doi.org/10.1016/j.quageo.2022.101341>

- lacustrine

- Fan, Y., Li, Z., Cai, Q., Yang, G., Zhang, Q., Zhao, H., Chen, F., Maghsoudi, M., 2022. Dating of the late Quaternary high lake levels in the Jilantai area, northwestern China, using optical luminescence of quartz and K-feldspar. *Journal of Asian Earth Sciences* 224, 105024, <http://doi.org/10.1016/j.jseaes.2021.105024>
- Feng, Y., Hou, Y., Zhang, J., Yang, N., Cai, Y., Yang, F., Gu, J., Long, H., 2022. Timing of Holocene lake highstands around Dawa Co in inner Tibetan Plateau: Comparison of quartz and feldspar luminescence dating with radiocarbon age. *Quaternary Geochronology* 69, 101267, <http://doi.org/10.1016/j.quageo.2022.101267>
- Hou, Y., Long, H., Gao, L., Shen, J., 2021. Luminescence Dating of Lacustrine Sediments from Cuoe Lake on the Central Tibetan Plateau. *Geochronometria* 48, 304-312, <http://doi.org/10.2478/geochr-2020-0002>
- Hou, Y., Long, H., Zhang, J., Feng, Y., Yang, N., Gu, J., Cai, Y., Yang, F., Shen, J., 2022. Luminescence dating of shoreline sediments indicates a late deglacial lake-level rise of Selin Co on the central Tibetan Plateau. *Quaternary Geochronology* 71, 101313, <http://doi.org/10.1016/j.quageo.2022.101313>
- Hu, F., Jianhui, J., Xie, M., Xiao, Z., Cao, M., Zhou, Y., Liang, J., 2022. Insights into the age and genesis of the clay dunes in the Suhongtu Basin, Alashan Plateau, China. *Geomorphology* 408, 108241, <http://doi.org/10.1016/j.geomorph.2022.108241>
- Huang, L., Chen, Y., Wu, Y., Zeng, T., Wei, G., 2022. Lake level changes of Nam Co since 25 ka as revealed by OSL dating of paleo-shorelines. *Quaternary Geochronology* 70, 101274, <http://doi.org/10.1016/j.quageo.2022.101274>
- López-Avilés, A., Jiménez-Moreno, G., García-Alix, A., García-García, F., Camuera, J., Scott Anderson, R., Sanjurjo-Sánchez, J., Arce Chamorro, C., Carrión, J.S., 2022. Post-glacial evolution of alpine

- environments in the western Mediterranean region: The Laguna Seca record. *CATENA* 211, 106033, <http://doi.org/10.1016/j.catena.2022.106033>
- Oh, J.-S., Seong, Y.B., Hong, S., Yu, B.Y., 2019. Paleo-shoreline changes in moraine dammed lake Khagiin Khar, Khentey Mountains, Central Mongolia. *Journal of Mountain Science* 16, 1215-1230, <http://doi.org/10.1007/s11629-019-5445-4>
- Peti, L., Fitzsimmons, K.E., Hopkins, J.L., Nilsson, A., Fujioka, T., Fink, D., Mifsud, C., Christl, M., Muscheler, R., Augustinus, P.C., 2020. Development of a multi-method chronology spanning the Last Glacial Interval from Orakei maar lake, Auckland, New Zealand. *Geochronology* 2, 367-410, <http://doi.org/10.5194/gchron-2-367-2020>
- Rex, C.L., Staff, R.A., Sanderson, D.C.W., Cresswell, A.J., Marshall, M.H., Hyodo, M., Horiuchi, D., Tada, R., Nakagawa, T., 2022. Controls on luminescence signals in lake sediment cores: A study from Lake Suigetsu, Japan. *Quaternary Geochronology* 71, 101319, <http://doi.org/10.1016/j.quageo.2022.101319>
- Scheidt, S., Lenz, M., Egli, R., Brill, D., Klug, M., Fabian, K., Lenz, M.M., Gromig, R., Rethemeyer, J., Wagner, B., Federov, G., Melles, M., 2022. A 62 kyr geomagnetic palaeointensity record from the Taymyr Peninsula, Russian Arctic. *Geochronology* 4, 87-107, <http://doi.org/10.5194/gchron-4-87-2022>
- Wang, Y., Han, Z., Zhou, Y., Cheng, J., Li, X., Wang, Y., Yi, S., Lu, H., 2022. A quantitative reconstruction of Holocene annual precipitation in the marginal zone of the East Asian summer monsoon. *Palaeogeography, Palaeoclimatology, Palaeoecology* 596, 110968, <http://doi.org/10.1016/j.palaeo.2022.110968>
- Wang, Y., Lu, H., Yi, S., Huber, M., Yang, F., Gu, Y., Dong, X., Lu, F., 2022. Tropical forcing orbital-scale precipitation variations revealed by a maar lake record in South China. *Climate Dynamics* 58, 2269-2280, <http://doi.org/10.1007/s00382-021-06004-3>
- Wei, C., Zhang, H., Li, C.a., Zhang, Y., Li, Y., Jia, M., Li, G., Leng, Y., 2021. Holocene OSL Chronology of Flu-Lacustrine Sediments in Yangtze River Basin, Wuhan Area, China. *Geochronometria* 48, 284-293, <http://doi.org/10.2478/geochr-2020-0012>
- Zhao, H., Wang, X., Yang, H., Wang, K., Geng, J., 2021. Luminescence Dating of Late Pleistocene Lacustrine Deposits in Badain Jaran Desert, North China. *Geochronometria* 48, 294-303, <http://doi.org/10.2478/geochr-2020-0032>
- Zong, H., Fu, X., Li, Z., Guo, Y., Yang, X., 2022. Multi-method pIRIR dating of sedimentary sequences at the southern edge of the Gurbantunggut Desert, NW China and its palaeoenvironmental implications. *Quaternary Geochronology* 70, 101300, <http://doi.org/10.1016/j.quageo.2022.101300>

- loess

- Almond, P.C., Gulyás, S., Sümegei, P., Sümegei, B.P., Covey-Crump, S., Jones, M., Shaw, J., Parker, A., 2021. A palaeoenvironmental record of the Southern Hemisphere last glacial maximum from the Mount Cass loess section, North Canterbury, Aotearoa/New Zealand. *Quaternary Research* 102, 115-129, <http://doi.org/10.1017/qua.2020.95>
- Avram, A., Kabacińska, Z., Micallef, A., Timar-Gabor, A., 2022. Testing the potential of using fine quartz for dating loess in South Island, New Zealand. *Radiation Measurements* 155, 106788, <http://doi.org/10.1016/j.radmeas.2022.106788>
- Buchanan, G.R., Tsukamoto, S., Zhang, J., Long, H., 2022. Testing the natural limits of infrared radiofluorescence dating of the Luochuan loess-palaeosol sequence, Chinese Loess Plateau. *Radiation Measurements* 155, 106797, <http://doi.org/10.1016/j.radmeas.2022.106797>
- Jia, J., Wang, N., Wang, Z., Wang, S., Meadows, M., Wang, L., Fan, Y., Chen, J., 2022. Weakened dust activity in southern Central Asia during Heinrich events. *Palaeogeography, Palaeoclimatology, Palaeoecology* 587, 110805, <http://doi.org/10.1016/j.palaeo.2021.110805>
- Jia, Y.-n., Zhang, Y., Huang, C.C., Wang, N., Qiu, H., Wang, H., Xiao, Q., Chen, D., Lin, X., Liu, C., Wang, C., Nan, Q., Zhu, Y., 2022. Weathering and pedogenesis of the late Pleistocene and Holocene aeolian loess-palaeosol sections in the Yellow River source area, NE Tibetan Plateau. *Palaeogeography, Palaeoclimatology, Palaeoecology* 600, 111065, <http://doi.org/10.1016/j.palaeo.2022.111065>
- Kabacińska, Z., Buylaert, J.P., Yi, S., Timar-Gabor, A., 2022. Revisiting natural and laboratory electron spin resonance (ESR) dose response curves of quartz from Chinese loess. *Quaternary Geochronology* 70, 101306, <http://doi.org/10.1016/j.quageo.2022.101306>
- Li, Y., Zhou, L., 2021. Variations of Thermally and Optically Stimulated Luminescence Sensitivity of Loess and Pedocomplex Samples from Southern Tajikistan, Central Asia. *Geochronometria* 48, 242-252, <http://doi.org/10.1515/geochr-2015-0118>

- Liu, X., Yang, H., Kang, S., Vandenberghe, J., Ai, L., Shi, Z., Cheng, P., Lan, J., Wang, X., Sun, Y., 2022. Centennial-scale East Asian winter monsoon variability within the Younger Dryas. *Palaeogeography, Palaeoclimatology, Palaeoecology* 601, 111101, <http://doi.org/10.1016/j.palaeo.2022.111101>
- Lomax, J., Wolf, D., Meliksetian, K., Wolpert, T., Sahakyan, L., Hovakimyan, H., Faust, D., Fuchs, M., 2022. Testing post-IR-IRSL dating on Armenian loess-palaeosol sections against independent age control. *Quaternary Geochronology* 69, 101265, <http://doi.org/10.1016/j.quageo.2022.101265>
- Lü, T., Sun, J., Feathers, J.K., Sun, D., 2021. Spatiotemporal variations and implications of luminescence sensitivity of quartz grains on the Chinese Loess Plateau since the last interglaciation. *Quaternary Research* 99, 190-203, <http://doi.org/10.1017/qua.2020.53>
- Lu, Y., Sun, X., Zhao, H., Tan, P., 2021. Luminescence dating of Youfangbei early late Pleistocene site, Nihewan Basin, North China. *Quaternary Research* 104, 159-169, <http://doi.org/10.1017/qua.2021.19>
- Marković, S.B., Oches, E.A., Perić, Z.M., Gaudenyi, T., Jovanović, M., Sipos, G., Thiel, C., Buylaert, J.-P., Savić, S., McCoy, W.D., Radaković, M.G., Marković, R.S., Gavrilov, M.B., 2021. The Požarevac loess-palaeosol sequence: a record of increased aridity in the south-eastern margin of the Carpathian Basin during the last 350 ka. *Journal of Quaternary Science* 36, 1436-1447, <http://doi.org/10.1002/jqs.3327>
- Marković, S.B., Vandenberghe, J., Stevens, T., Mihailović, D., Gavrilov, M.B., Radaković, M.G., Zeeden, C., Obrecht, I., Perić, Z.M., Nett, J.J., Lehmkuhl, F., 2021. Geomorphological evolution of the Petrovaradin Fortress Palaeolithic site (Novi Sad, Serbia). *Quaternary Research* 103, 21-34, <http://doi.org/10.1017/qua.2020.88>
- Moine, O., Antoine, P., Coutard, S., Guérin, G., Hatté, C., Paris, C., Saulnier-Copard, S., 2021. Intra-interstadial environmental changes in Last Glacial loess revealed by molluscan assemblages from the Upper Palaeolithic site of Amiens-Renancourt 1 (Somme, France). *Journal of Quaternary Science* 36, 1322-1340, <http://doi.org/10.1002/jqs.3312>
- Perić, Z.M., Marković, S.B., Avram, A., Timar-Gabor, A., Zeeden, C., Nett, J.J., Fischer, P., Fitzsimmons, K.E., Gavrilov, M.B., 2022. Initial quartz OSL and dust mass accumulation rate investigation of the Kisiljevo loess sequence in north-eastern Serbia. *Quaternary International* 620, 13-23, <http://doi.org/10.1016/j.quaint.2020.10.040>
- Rahimzadeh, N., Sprafke, T., Thiel, C., Terhorst, B., Frechen, M., 2021. A comparison of polymineral and K-feldspar post-infrared stimulated luminescence ages of loess from Franconia, southern Germany. *E&G Quaternary Sci. J.* 70, 53-71, <http://doi.org/10.5194/egqsj-70-53-2021>
- Rahimzadeh, N., Tsukamoto, S., Zhang, J., 2022. A comparative study of sand- and silt-sized quartz fractions for MAR-VSL dating using loess-palaeosol deposits in southern Germany. *Quaternary Geochronology* 70, 101276, <http://doi.org/10.1016/j.quageo.2022.101276>
- Sycheva, S.A., Khokhlova, O.S., Pushkina, P.R., 2021. Structure of the Late Pleistocene Climate Rhythm Inferred from the Detailed Soil-Sedimentation Archive of the Extraglacial Region of the East European Plain (Aleksandrov Quarry). *Stratigraphy and Geological Correlation* 29, 368-387, <http://doi.org/10.1134/S0869593821030084>
- Vinnepand, M., Fischer, P., Fitzsimmons, K., Thornton, B., Fiedler, S., Vött, A., 2020. Combining Inorganic and Organic Carbon Stable Isotope Signatures in the Schwalbenberg Loess-Palaeosol-Sequence Near Remagen (Middle Rhine Valley, Germany). *Frontiers in Earth Science* 8, 276, <http://doi.org/10.3389/feart.2020.00276>
- Wacha, L., Laag, C., Grizelj, A., Tsukamoto, S., Zeeden, C., Ivanišević, D., Rolf, C., Banak, A., Frechen, M., 2021. High-resolution palaeoenvironmental reconstruction at Zmajevac (Croatia) over the last three glacial/interglacial cycles. *Palaeogeography, Palaeoclimatology, Palaeoecology* 576, 110504, <http://doi.org/10.1016/j.palaeo.2021.110504>
- Wang, Y., Yang, S., Ding, Z., 2021. Provenance and paleoclimatic implications of loess deposits in Shandong Province, eastern China. *Quaternary Research* 103, 88-98, <http://doi.org/10.1017/qua.2020.113>
- Wolf, D., Kolb, T., Ryborz, K., Heinrich, S., Schäfer, I., Calvo, R., Sanchez, J., Hambach, U., Zech, R., Zöller, L., Faust, D., 2021. Evidence for strong relations between the upper Tagus loess formation (central Iberia) and the marine atmosphere off the Iberian margin during the last glacial period. *Quaternary Research* 101, 84-113, <http://doi.org/10.1017/qua.2020.119>
- Yang, H., Li, G., Gou, S., Qian, J., Deng, Y., Zhang, Y., Jonell, T.N., Wang, Z., Jin, M., 2021. The close-space luminescence dated loess record from SW Junggar Basin indicates persistent aridity during the last glacial-interglacial cycle in lowlands of Central Asia. *Palaeogeography, Palaeoclimatology, Palaeoecology* 584, 110664, <http://doi.org/10.1016/j.palaeo.2021.110664>
- Zhang, J., Liu, Q., Yang, L., Cheng, H., Cai, Y., Long, H., 2022. Regional hydroclimates regulate the Holocene aeolian accumulation processes of the Qinghai Lake basin on the northeastern Tibetan plateau. *CATENA* 210, 105866, <http://doi.org/10.1016/j.catena.2021.105866>

- Zhao, Q., Ding, M., Peng, S., Wang, L., Zhang, W., Song, B., Zhou, R., Yue, J., Zheng, D., 2021. High Resolution Quartz OSL and K-feldspar post-IR IRSL Dating of Loess in the Central Shandong Mountains (Eastern China). *Geochronometria* 48, 232-241, <http://doi.org/10.1515/geochr-2015-0113>
- Zhao, Q., Peng, S., Fan, N., Wang, L., Hao, Q., Liu, X., Zhou, R., Ding, M., Zhang, W., Liu, N., 2022. Luminescence chronology of loess-palaeosol deposits in the Central Shandong Mountains region: Provenances and paleoclimate implications. *Quaternary Geochronology* 70, 101296, <http://doi.org/10.1016/j.quageo.2022.101296>
- Zöller, L., Fischer, M., Jary, Z., Antoine, P., Krawczyk, M., 2022. Chronostratigraphic and geomorphologic challenges of last glacial loess in Poland in the light of new luminescence ages. *E&G Quaternary Science Journal* 71, 59-81, <http://doi.org/10.5194/egqsj-71-59-2022>

- marine

- Farquharson, L., Mann, D., Rittenour, T., Groves, P., Grosse, G., Jones, B., 2018. Alaskan marine transgressions record out-of-phase Arctic Ocean glaciation during the last interglacial. *Geology* 46, 783-786, <http://doi.org/10.1130/G40345.1>
- Long, Z., Wang, Z., Tu, H., Li, R., Wen, Z., Wang, Y., Zhang, Y., Lai, Z., 2022. OSL and radiocarbon dating of a core from the Bohai Sea in China and implication for Late Quaternary transgression pattern. *Quaternary Geochronology* 70, 101308, <http://doi.org/10.1016/j.quageo.2022.101308>

- soil

- Gray, H.J., Keen-Zebert, A., Furbish, D.J., Tucker, G.E., Mahan, S.A., 2020. Depth-dependent soil mixing persists across climate zones. *Proceedings of the National Academy of Sciences* 117, 8750-8756, <http://doi.org/10.1073/pnas.1914140117>
- Ladeira, F.S.B., Mescolotti, P.C., do Nascimento Pupim, F., de Faria, L.M.D.M., Assine, M.L., 2022. Paleosols record dry and humid paleoenvironments during the Upper Pleistocene in the Brazilian Pantanal. *CATENA* 212, 106113, <http://doi.org/10.1016/j.catena.2022.106113>
- Menges, J., Hovius, N., Andermann, C., Dietze, M., Swoboda, C., Cook, K.L., Adhikari, B.R., Vieth-Hillebrand, A., Bonnet, S., Reimann, T., Koutsodendris, A., Sachse, D., 2019. Late Holocene landscape collapse of a trans-Himalayan dryland: Human impact and aridification. *Geophysical Research Letters* 46, 13814-13824, <http://doi.org/10.1029/2019GL084192>
- Rashidi, Z., Karimi, A., Murray, A., Khormali, F., Farpoor, M.H., Sohbaty, R., 2022. Late Pleistocene–Holocene pedogenesis and palaeoclimate in western Asia from palaeosols of the Central Iranian Plateau. *Boreas* 51, 201-218, <http://doi.org/10.1111/bor.12541>
- Román-Sánchez, A., Laguna, A., Reimann, T., Giráldez, J.V., Peña, A., Vanwallegem, T., 2019. Bioturbation and erosion rates along the soil-hillslope conveyor belt, part 2: Quantification using an analytical solution of the diffusion–advection equation. *Earth Surface Processes and Landforms* 44, 2066-2080, <http://doi.org/10.1002/esp.4626>
- Sycheva, S.A., Khokhlova, O.S., Pushkina, P.R., 2021. Structure of the Late Pleistocene Climate Rhythm Inferred from the Detailed Soil-Sedimentation Archive of the Extraglacial Region of the East European Plain (Aleksandrov Quarry). *Stratigraphy and Geological Correlation* 29, 368-387, <http://doi.org/10.1134/S0869593821030084>

- surface exposure dating

- Brill, D., Ageby, L., Obert, C., Hollerbach, R., Duval, M., Kolb, T., Bartz, M., 2022. Investigating the resetting of IRSL signals in beach cobbles and their potential for rock surface dating of marine terraces in Northern Chile. *Marine Geology* 443, 106692, <http://doi.org/10.1016/j.margeo.2021.106692>
- Brill, D., May, S.M., Mhammedi, N., King, G., Lehmann, B., Burrow, C., Wolf, D., Zander, A., Brückner, H., 2021. Evaluating optically stimulated luminescence rock surface exposure dating as a novel approach for reconstructing coastal boulder movement on decadal to centennial timescales. *Earth Surface Dynamics* 9, 205-234, <http://doi.org/10.5194/esurf-9-205-2021>
- Cunningham, A.C., Khashchevskaya, D., Semikolennykh, D., Kurbanov, R., Murray, A.S., 2022. Luminescence dating of mass-transport sediment using rock-surface burial methods: a test case from the Baksan valley in the Caucasus Mountains. *Quaternary Geochronology* 68, 101253, <http://doi.org/10.1016/j.quageo.2022.101253>

- Feathers, J., Muller, N., 2020. Optically stimulated luminescence dating of a probable Native American cairn and wall site in Eastern Pennsylvania. *North American Archaeologist* 41, 33-50, <http://doi.org/10.1177/0197693120920492>
- Fu, X., Romanyukha, A.A., Li, B., Jankowski, N.R., Lachlan, T.J., Jacobs, Z., George, S.P., Rosenfeld, A.B., Roberts, R.G., 2022. Beta dose heterogeneity in sediment samples measured using a Timepix pixelated detector and its implications for optical dating of individual mineral grains. *Quaternary Geochronology* 68, 101254, <http://doi.org/10.1016/j.quageo.2022.101254>
- Fuhrmann, S., Meyer, M.C., Gliganic, L.A., Obleitner, F., 2022. Testing the effects of aspect and total insolation on luminescence depth profiles for rock surface exposure dating. *Radiation Measurements* 153, 106732, <http://doi.org/10.1016/j.radmeas.2022.106732>
- Sellwood, E.L., Kook, M., Jain, M., 2022. Investigating the potential of rock surface burial dating using IRPL and IRSL imaging. *Radiation Measurements* 155, 106783, <http://doi.org/10.1016/j.radmeas.2022.106783>

- tephra (and volcanic related)

- Rodrigues, K., Huot, S., Keen-Zebert, A., 2022. Exploring the application of blue and red thermoluminescence for dating volcanic glasses. *Radiation Measurements* 153, 106731, <http://doi.org/10.1016/j.radmeas.2022.106731>

- thermochronology

- Brown, N.D., Rhodes, E.J., 2022. Developing an internally consistent methodology for K-feldspar MAAD TL thermochronology. *Radiation Measurements* 153, 106751, <http://doi.org/10.1016/j.radmeas.2022.106751>
- Ogata, M., King, G.E., Herman, F., Sueoka, S., 2022. Reconstructing the thermal structure of shallow crust in the Tono region using multi-OSL-thermometry of K-feldspar from deep borehole core. *Earth and Planetary Science Letters* 591, 117607, <http://doi.org/10.1016/j.epsl.2022.117607>
- Tsang, M.-Y., Toyoda, S., Tomita, M., Yamamoto, Y., 2022. Thermal stability and closure temperature of barite for electron spin resonance dating. *Quaternary Geochronology* 71, 101332, <http://doi.org/10.1016/j.quageo.2022.101332>

Archaeology applications

- Agnihotri, R., Patel, N., Srivastava, P., Ambekar, A., Arif, M., Kumar, A., Phartiyal, B., Kumar, A., 2021. A new chronology based on OSL and radiocarbon dating for the archaeological settlements of Vadnagar (western India) along with magnetic and isotopic imprints of cultural sediments. *Journal of Archaeological Science: Reports* 38, 103045, <http://doi.org/10.1016/j.jasrep.2021.103045>
- al Khasawneh, S., Murray, A., Thompson, W., 2022. Dating Neolithic rubble layers from Ba'ja and Basta sites in southern Jordan using luminescence. *Quaternary Geochronology* 70, 101291, <http://doi.org/10.1016/j.quageo.2022.101291>
- Al-Saqarat, B.S., Abbas, M., Lai, Z., Gong, S., Alkuisi, M.M., Abu Hamad, A.M.B., Carling, P.A., Jansen, J.D., 2021. A wetland oasis at Wadi Gharandal spanning 125–70 ka on the human migration trail in southern Jordan. *Quaternary Research* 100, 154-169, <http://doi.org/10.1017/qua.2020.82>
- Ames, C.J.H., Gliganic, L., Cordova, C.E., Boyd, K., Jones, B.G., Maher, L., Collins, B.R., 2020. Chronostratigraphy, Site Formation, and Palaeoenvironmental Context of Late Pleistocene and Holocene Occupations at Grassridge Rock Shelter (Eastern Cape, South Africa). *Open Quaternary* 6, 5, <http://doi.org/http://doi.org/10.5334/oq.77>
- Ardelean, C.F., Becerra-Valdivia, L., Pedersen, M.W., Schwenninger, J.-L., Oviatt, C.G., Macías-Quintero, J.I., Arroyo-Cabrales, J., Sikora, M., Ocampo-Díaz, Y.Z.E., Rubio-Cisneros, I.I., Watling, J.G., de Medeiros, V.B., De Oliveira, P.E., Barba-Pingarón, L., Ortiz-Butrón, A., Blancas-Vázquez, J., Rivera-González, I., Solís-Rosales, C., Rodríguez-Ceja, M., Gandy, D.A., Navarro-Gutierrez, Z., De La Rosa-Díaz, J.J., Huerta-Arellano, V., Marroquín-Fernández, M.B., Martínez-Riojas, L.M., López-Jiménez, A., Higham, T., Willerslev, E., 2020. Evidence of human occupation in Mexico around the Last Glacial Maximum. *Nature* 584, 87-92, <http://doi.org/10.1038/s41586-020-2509-0>
- Arnold, L.J., Demuro, M., Power, R., Priya, Duval, M., Guilarte, V., Weij, R., Woodhead, J., White, L., Bourne, S., Reed, E.H., 2022. Examining sediment infill dynamics at Naracoorte cave megafauna sites using multiple luminescence dating signals. *Quaternary Geochronology* 70, 101301, <http://doi.org/10.1016/j.quageo.2022.101301>
- Bahain, J.-J., Farkh, S., Falguères, C., Shao, Q., Voinchet, P., Ghaleb, B., Hérison, D., Lochet, J.-L., Limondin-Lozouet, N., Auguste, P., Gauthier, A., Dabkowski, J., Deschodt, L., Antoine, P., 2022. ESR/U-series

- dating of Eemian human occupations of Northern France. *Quaternary Geochronology* 71, 101305, <http://doi.org/10.1016/j.quageo.2022.101305>
- Barzilai, O., ברזילי, ע., Goldsmith, Y., גולדסמית, י., Shemer, M., שמר, מ., Porat, N., פורת, נ., Crouvi, O., כרובי, א., 2020. Evidence for a Middle Paleolithic Flint Workshop in Arnona, South Jerusalem. *Journal of the Israel Prehistoric Society* 50, 15-43, <https://www.jstor.org/stable/27074894>
- Boaretto, E., Hernandez, M., Goder-Goldberger, M., Aldeias, V., Regev, L., Caracuta, V., McPherron Shannon, P., Hublin, J.-J., Weiner, S., Barzilai, O., 2021. The absolute chronology of Boker Tachtit (Israel) and implications for the Middle to Upper Paleolithic transition in the Levant. *Proceedings of the National Academy of Sciences* 118, e2014657118, <http://doi.org/10.1073/pnas.2014657118>
- Borić, D., Cristiani, E., Hopkins, R., Schwenninger, J.-L., Gerometta, K., French, C.A.I., Mutri, G., Čalić, J., Dimitrijević, V., Marín-Arroyo, A.B., Jones, J.R., Stevens, R., Masciana, A., Uno, K., Richter, K.K., Antonović, D., Wehr, K., Lane, C., White, D., 2022. Neanderthals on the Lower Danube: Middle Palaeolithic evidence in the Danube Gorges of the Balkans. *Journal of Quaternary Science* 37, 142-180, <http://doi.org/10.1002/jqs.3354>
- Cajigas, R., Quade, J., Rittenour, T., 2020. Multitechnique dating of earthen irrigation canals at the La Playa site, Sonora, Mexico. *Geoarchaeology* 35, 834-855, <http://doi.org/10.1002/gea.21800>
- Chazan, M., Berna, F., Brink, J., Ecker, M., Holt, S., Porat, N., Thorp, J.L., Horwitz, L.K., 2020. Archeology, Environment, and Chronology of the Early Middle Stone Age Component of Wonderwerk Cave. *Journal of Paleolithic Archaeology* 3, 302-335, <http://doi.org/10.1007/s41982-020-00051-8>
- Colarossi, D., Fewlass, H., Stahlschmidt, M.C., Presnyakova, D., Matembo, J., Hein, M., Talamo, S., Archer, W., 2022. A targeted drilling and dating campaign to identify Stone Age archaeological sites before excavation in west coast southern Africa. *Quaternary Geochronology* 71, 101314, <http://doi.org/10.1016/j.quageo.2022.101314>
- Conrad, C., Shoocongdej, R., Marwick, B., White, J.C., Thongcharoenchaikit, C., Higham, C., Feathers, J.K., Tumpeesuwan, S., Castillo, C.C., Fuller, D.Q., Jones, E.L., 2022. Re-evaluating Pleistocene–Holocene occupation of cave sites in north-west Thailand: new radiocarbon and luminescence dating. *Antiquity* 96, 280-297, <http://doi.org/10.15184/aqy.2021.44>
- de Mello Araujo, A.G., Feathers, J.K., Hartmann, G.A., Ladeira, F.S.B., Valezio, É.V., Nascimento, D.L., Ricci, O., de Oliveira Marum, V.J., Ferreira da Trindade, R.I., 2022. Revisiting Alice Boer: Site formation processes and dating issues of a supposedly pre-Clovis site in Southeastern Brazil. *Geoarchaeology* 37, 32-58, <http://doi.org/10.1002/gea.21831>
- Degano, I., Soriano, S., Villa, P., Pollarolo, L., Lucejko, J.J., Jacobs, Z., Douka, K., Vitagliano, S., Tozzi, C., 2019. Hafting of Middle Paleolithic tools in Latium (central Italy): New data from Fossellone and Sant'Agostino caves. *PLOS ONE* 14, e0213473, <http://doi.org/10.1371/journal.pone.0213473>
- Demuro, M., Arnold, L.J., Parés, J.-M., Aranburu, A., Huguët, R., Vallverdú, J., Arsuaga, J.-L., Bermúdez de Castro, J.-M., Carbonell, E., 2022. Extended-range luminescence chronologies for the Middle Pleistocene units at the Sima del Elefante archaeological site (Sierra de Atapuerca, Burgos, Spain). *Quaternary Geochronology* 71, 101318, <http://doi.org/10.1016/j.quageo.2022.101318>
- Douka, K., Slon, V., Jacobs, Z., Ramsey, C.B., Shunkov, M.V., Derevianko, A.P., Mafessoni, F., Kozlikin, M.B., Li, B., Grün, R., Comeskey, D., Deviese, T., Brown, S., Viola, B., Kinsley, L., Buckley, M., Meyer, M., Roberts, R.G., Pääbo, S., Kelso, J., Higham, T., 2019. Age estimates for hominin fossils and the onset of the Upper Palaeolithic at Denisova Cave. *Nature* 565, 640-644, <http://doi.org/10.1038/s41586-018-0870-z>
- Duval, M., Arnold, L.J., Demuro, M., Parés, J.M., Campaña, I., Carbonell, E., Bermúdez de Castro, J.M., 2022. New chronological constraints for the lowermost stratigraphic unit of Atapuerca Gran Dolina (Burgos, N Spain). *Quaternary Geochronology* 71, 101292, <http://doi.org/10.1016/j.quageo.2022.101292>
- Duval, M., Westaway, K., Zaim, J., Rizal, Y., Aswan, Puspaningrum, M.R., Trihascaryo, A., Albers, P.C.H., Smith, H.E., Drawhorn, G.M., Price, G.J., Louys, J., 2021. New Chronological Constraints for the Late Pleistocene Fossil Assemblage and Associated Breccia from Ngala Sampit, Sumatra. *Open Quaternary* 7, 9, <http://doi.org/http://doi.org/10.5334/oq.96>
- Falguères, C., Barkai, R., Tombret, O., Gopher, A., 2022. New ESR/U-series dates of the lowest Acheuleo-Yabrudian levels of Qesem cave. *Quaternary Geochronology* 69, 101266, <http://doi.org/10.1016/j.quageo.2022.101266>
- Feathers, J., Muller, N., 2020. Optically stimulated luminescence dating of a probable Native American cairn and wall site in Eastern Pennsylvania. *North American Archaeologist* 41, 33-50, <http://doi.org/10.1177/0197693120920492>
- Ferro-Vázquez, C., Blanco-Rotea, R., Sanjurjo-Sánchez, J., García-Rodríguez, S., García Quintela, M.V., 2021. Territories of Faith: 1000 Years of Landscape Multifunctionality in Santa Mariña de Augas Santas (NW Spain). *Land* 10, <http://doi.org/10.3390/land10090992>

- Fisher, E.C., Cawthra, H.C., Esteban, I., Jerardino, A., Neumann, F.H., Oertle, A., Pargeter, J., Saktura, R.B., Szabó, K., Winkler, S., Zohar, I., 2020. Coastal occupation and foraging during the last glacial maximum and early Holocene at Waterfall Bluff, eastern Pondoland, South Africa. *Quaternary Research* 97, 1-41, <http://doi.org/10.1017/qua.2020.26>
- Ge, J., Wang, Y., Shan, M., Feng, X., Chen, F., Wu, H., Li, Q., Zhou, X., Li, Y., Tang, R., Olsen, J.W., Deng, C., Gao, X., 2021. Evidence from the Dayao Paleolithic site, Inner Mongolia for human migration into arid northwest China during mid-Pleistocene interglacials. *Quaternary Research* 103, 113-129, <http://doi.org/10.1017/qua.2020.115>
- Guérin, G., Lebrun, B., Marchand, G., Philippe, A., 2022. Age-depth modelling and the effect of including – or not – shared errors across sets of OSL samples: The case study of Beg-er-Vil (Brittany, France). *Quaternary Geochronology* 70, 101311, <http://doi.org/10.1016/j.quageo.2022.101311>
- Han, F., Bahain, J.-J., Voinchet, P., Jin, M., Yin, G., 2022. Radiometric dating of Meipu hominin site in China by coupled ESR/U-series and cosmogenic ²⁶Al/¹⁰Be burial dating methods. *Quaternary Geochronology* 70, 101295, <http://doi.org/10.1016/j.quageo.2022.101295>
- Jin, J., Li, F., Ling, Z., Li, Z., 2022. New chronological evidence reveals a continuously inhabited Neolithic–historical settlement in south China. *Palaeogeography, Palaeoclimatology, Palaeoecology* 600, 111081, <http://doi.org/10.1016/j.palaeo.2022.111081>
- Jin, J., Li, F., Zuo, X., Huang, Y., Ling, Z., Li, Z., 2022. OSL dating of Zhuangbianshan site in the humid subtropical coastal region of China. *Boreas* 51, 149-158, <http://doi.org/10.1111/bor.12544>
- Jin, J., Ling, Z., Li, Z., Zuo, X., Fan, X., Huang, Y., Wang, X., Wei, C., Ren, Y., Qiu, J., 2022. Spatiotemporal distribution of sea-island prehistoric dune sites, Holocene sea levels, and aeolian sand activities in Fujian Province, China. *Journal of Geographical Sciences* 32, 1157-1176, <http://doi.org/10.1007/s11442-022-1990-9>
- Junge, A., Dunseth, Z.C., Shahack-Gross, R., Finkelstein, I., Fuchs, M., 2021. Construction and use of rock-cut cisterns: a chronological OSL approach in the arid Negev Highlands, Israel. *Archaeological and Anthropological Sciences* 13, 150, <http://doi.org/10.1007/s12520-021-01366-5>
- Kadowaki, S., Tamura, T., Kida, R., Omori, T., Maher, L.A., Portillo, M., Hirose, M., Suga, E., Massadeh, S., Henry, D.O., 2022. Lithic technology and chronology of Initial Upper Paleolithic assemblages at Tor Fawaz, southern Jordan. *Journal of Paleolithic Archaeology* 5, 1, <http://doi.org/10.1007/s41982-021-00107-3>
- Karimi Moayed, N., Vandenberghe, D.A.G.J., Buylaert, J.P., Deforce, K., Debeer, A.E., Biernacka, P., De Smedt, P., De Clercq, W., De Grave, J., 2022. A combined OSL and ¹⁴C dating study of charcoal production in the sandy environment of Zoersel forest (N Belgium). *Quaternary Geochronology* 71, 101339, <http://doi.org/10.1016/j.quageo.2022.101339>
- Kot, M., Gryczewska, N., Szymanek, M., Moskal del-Hoyo, M., Szeliga, M., Berto, C., Wojenka, M., Krajcarz, M., Krajcarz, M.T., Wertz, K., Fedorowicz, S., Jaskulska, E., Pilcicka-Ciura, H., 2022. Bramka Rockshelter: An Early Mesolithic cave site in Polish Jura. *Quaternary International* 610, 44-64, <http://doi.org/10.1016/j.quaint.2021.08.015>
- Kot, M., Pavlenok, G., Krajcarz, M.T., Szymanek, M., Fedorowicz, S., Moska, P., Khudjanazarov, M., Szymczak, K., Leloch, M., Kogai, S., Talamo, S., Fewlass, H., Pavlenok, K., 2022. Is there Initial Upper Palaeolithic in Western Tian Shan? Example of an open-air site Katta Sai 2 (Uzbekistan). *Journal of Anthropological Archaeology* 65, 101391, <http://doi.org/10.1016/j.jaa.2021.101391>
- Lai, H.-C., Li, Y.-Y., Zhang, J.-F., Zhou, L., 2021. Chronology of the Huxushan Paleolithic Site in South China: Inferred from Multiple Luminescence Dating Techniques. *Geochronometria* 48, 379-390, <http://doi.org/10.2478/geochr-2020-0039>
- Louys, J., Duval, M., Price, G.J., Westaway, K., Zaim, Y., Rizal, Y., null, A., Puspaningrum, M., Trihascaryo, A., Breitenbach, S.F.M., Kwiecien, O., Cai, Y., Higgins, P., Albers, P.C.H., de Vos, J., Roberts, P., 2022. Speleological and environmental history of Lida Ajer cave, western Sumatra. *Philosophical Transactions of the Royal Society B: Biological Sciences* 377, 20200494, <http://doi.org/10.1098/rstb.2020.0494>
- Malinsky-Buller, A., Glauberman, P., Ollivier, V., Lauer, T., Timms, R., Frahm, E., Brittingham, A., Triller, B., Kindler, L., Knul, M.V., Krakovsky, M., Joannin, S., Hren, M.T., Bellier, O., Clark, A.A., Blockley, S.P.E., Arakelyan, D., Marreiros, J., Paixaco, E., Calandra, I., Ghukasyan, R., Nora, D., Nir, N., Adigyozyan, A., Haydosyan, H., Gasparyan, B., 2021. Short-term occupations at high elevation during the Middle Paleolithic at Kalavan 2 (Republic of Armenia). *PLOS ONE* 16, e0245700, <http://doi.org/10.1371/journal.pone.0245700>
- Malinsky-Buller, A., Glauberman, P., Wilkinson, K., Li, B., Frahm, E., Gasparyan, B., Timms, R., Adler, D.S., Sherriff, J., 2021. Evidence for Middle Palaeolithic occupation and landscape change in central Armenia at the open-air site of Alapars-1. *Quaternary Research* 99, 223-247, <http://doi.org/10.1017/qua.2020.61>

- Marković, S.B., Vandenbergh, J., Stevens, T., Mihailović, D., Gavrilov, M.B., Radaković, M.G., Zeeden, C., Obrecht, I., Perić, Z.M., Nett, J.J., Lehmkuhl, F., 2021. Geomorphological evolution of the Petrovaradin Fortress Palaeolithic site (Novi Sad, Serbia). *Quaternary Research* 103, 21-34, <http://doi.org/10.1017/qua.2020.88>
- Mihailović, D., Kuhn, S.L., Bogičević, K., Dimitrijević, V., Marín-Arroyo, A.B., Marković, J., Mercier, N., Mihailović, B., Morley, M.W., Radović, P., Rink, W.J., Plavšić, S., Roksandic, M., 2022. Connections between the Levant and the Balkans in the late Middle Pleistocene: Archaeological findings from Velika and Mala Balanica Caves (Serbia). *Journal of Human Evolution* 163, 103138, <http://doi.org/10.1016/j.jhevol.2021.103138>
- Mihailović, D., Milošević, S., Blackwell, B.A.B., Mercier, N., Mentzer, S.M., Miller, C.E., Morley, M.W., Bogičević, K., Đurić, D., Marković, J., Mihailović, B., Dragosavac, S., Plavšić, S., Skinner, A.R., Chaity, I.I.C., Huang, Y.E.W., Chu, S., Nenadić, D., Radović, P., Lindal, J., Roksandic, M., 2022. Neanderthal settlement of the Central Balkans during MIS 5: Evidence from Pešturina Cave, Serbia. *Quaternary International* 610, 1-19, <http://doi.org/10.1016/j.quaint.2021.09.003>
- Mologni, C., Purdue, L., Audiard, B., Dubar, M., Kreutzer, S., Texier, P.-J., 2021. Sedimentary processes and palaeoenvironments from La Combette sequence (southeastern France): climatic insights on the Last Interglacial/Glacial transition. *Palaeogeography, Palaeoclimatology, Palaeoecology* 576, 110503, <http://doi.org/10.1016/j.palaeo.2021.110503>
- Nykamp, M., Hardt, J., Hoelzmann, P., May, J., Reimann, T., 2021. Towards timing and stratigraphy of the Bronze Age burial mound royal tomb (Königsgrab) of Seddin (Brandenburg, northeastern Germany). *E&G Quaternary Science Journal* 70, 1-17, <http://doi.org/10.5194/egqsj-70-1-2021>
- Pederzani, S., Britton, K., Aldeias, V., Bourgon, N., Fewlass, H., Lauer, T., McPherron Shannon, P., Rezek, Z., Sirakov, N., Smith Geoff, M., Spasov, R., Tran, N.H., Tsanova, T., Hublin, J.-J., 2021. Subarctic climate for the earliest Homo sapiens in Europe. *Science Advances* 7, eabi4642, <http://doi.org/10.1126/sciadv.abi4642>
- Peña-Monné, J.L., Montes Ramírez, L., Sampietro-Vattuone, M.M., Domingo Martínez, R., Medialdea, A., Bartolomé, M., Rubio Fernández, V., García Giménez, R., Turú, V., Ros, X., Baró, P., Bernal-Wormull, J.L., Edwards, R.L., 2022. Geomorphological, chronological, and paleoenvironmental context of the Mousterian site at Roca San Miguel (Arén, Huesca, Spain) from the penultimate to the last glacial cycle. *Quaternary Research* 106, 162-181, <http://doi.org/10.1017/qua.2021.61>
- Rasmussen, K.L., van der Plicht, J., Degano, I., Modugno, F., Colombini, M.P., de la Fuente, G., Delbey, T., Frumkin, A., Davidovich, U., Porat, R., Shamir, O., Sukenik, N., Doudna, G., Taylor, J., Popović, M., 2022. Defining multiple inhabitations of a cave environment using interdisciplinary archaeometry: the ‘Christmas Cave’ of the Wadi en-Nar/Nahal Qidron, West of the Dead Sea. *Heritage Science* 10, 18, <http://doi.org/10.1186/s40494-022-00652-2>
- Richard, M., Chazan, M., Porat, N., 2022. Single grain TT-OSL ages for the Earlier Stone Age site of Bestwood 1 (Northern Cape Province, South Africa). *Quaternary International* 614, 16-22, <http://doi.org/10.1016/j.quaint.2020.08.019>
- Richard, M., Pons-Branchu, E., Carmieli, R., Kaplan-Ashiri, I., Alvaro Gallo, A., Ricci, G., Caneve, L., Wroth, K., Dapigny, A., Tribolo, C., Boaretto, E., Toffolo, M.B., 2022. Investigating the effect of diagenesis on ESR dating of Middle Stone Age tooth samples from the open-air site of Lovedale, Free State, South Africa. *Quaternary Geochronology* 69, 101269, <http://doi.org/10.1016/j.quageo.2022.101269>
- Rodrigues, A.L., Marques, R., Dias, M.I., Prudêncio, M.I., Cardoso, G., Russo, D., Fontanals, N.R., Soriano, E., 2022. Luminescence and compositional studies for the identification of “fire-setting” features at prehistoric mine La Turquesa (Catalonia, Spain). *Journal of Radioanalytical and Nuclear Chemistry* 331, 1397-1408, <http://doi.org/10.1007/s10967-022-08198-0>
- Sanjurjo-Sánchez, J., Blanco-Rotea, R., García-Quintela, M.V., Burbidge, C.I., 2020. OSL Dating of Earthen Mortars from a Medieval Building in Northwestern Spain: Crypt of Basílica da AscensiÓn (Allariz, Ourense). *Radiocarbon* 62, 679-692, <http://doi.org/10.1017/RDC.2020.70>
- Santamaría, M., Navazo, M., Benito-Calvo, A., Alonso, R., López, G.I., Carbonell, E., 2021. Atapuerca Neanderthal landscape at Fuente Mudarra site in Burgos, Spain, during Marine Isotope Stages 5–3. *Quaternary Research* 99, 248-269, <http://doi.org/10.1017/qua.2020.65>
- Scerri, E.M.L., Niang, K., Candy, I., Blinkhorn, J., Mills, W., Cerasoni, J.N., Bateman, M.D., Crowther, A., Groucutt, H.S., 2021. Continuity of the Middle Stone Age into the Holocene. *Scientific Reports* 11, 70, <http://doi.org/10.1038/s41598-020-79418-4>
- Shao, Q., Philippe, A., He, C., Jin, M., Huang, M., Jiao, Y., Voinchet, P., Lin, M., Bahain, J.-J., 2022. Applying a Bayesian approach for refining the chronostratigraphy of the Yumidong site in the Three Gorges region, central China. *Quaternary Geochronology* 70, 101304, <http://doi.org/10.1016/j.quageo.2022.101304>

- Shemer, M., Greenbaum, N., Taha, N., Brailovsky-Rokser, L., Ebert, Y., Shaar, R., Falgueres, C., Voinchet, P., Porat, N., Faershtein, G., Horwitz, L.K., Rosenberg-Yefet, T., Barkai, R., 2022. Late Acheulian Jaljulia – Early human occupations in the paleo-landscape of the central coastal plain of Israel. *PLOS ONE* 17, e0267672, <http://doi.org/10.1371/journal.pone.0267672>
- Simms, S.R., Rittenour, T.M., Kuehn, C., Cannon, M.B., 2020. Prehistoric Irrigation in Central Utah: Chronology, Agricultural Economics, and Implications. *American Antiquity* 85, 452-469, <http://doi.org/10.1017/aaq.2020.25>
- Solongo, S., Tengis, S., Wagner, G.A., Hüttel, H.-G., 2021. CW-OSL, LM-OSL and TL Dating of Bricks from Karakorum, Mongolia: Insights from TL Spectra. *Geochronometria* 48, 402-414, <http://doi.org/10.2478/geochr-2020-0003>
- Spinapolice, E.E., Zerboni, A., Meyer, M.C., Talamo, S., Mariani, G.S., Gliganic, L.A., Buti, L., Fusco, M., Maiorano, M.P., Silvestrini, S., Sorrentino, R., Vazzana, A., Romandini, M., Fiorini, A., Curci, A., Benazzi, S., 2022. Back to Uluzzo – archaeological, palaeoenvironmental and chronological context of the Mid–Upper Palaeolithic sequence at Uluzzo C Rock Shelter (Apulia, southern Italy). *Journal of Quaternary Science* 37, 217-234, <http://doi.org/10.1002/jqs.3349>
- Sun, M., Sun, Y., Chongyi, E., Hou, G., Zhang, J., Shi, Y., 2021. Luminescence Dating of Nuomuhong Culture Ceramics at Talitaliha Site on the Northeastern Qinghai-Tibetan Plateau. *Geochronometria* 48, 391-401, <http://doi.org/10.2478/geochr-2020-0034>
- Sun, X.-f., Wen, S.-q., Lu, C.-q., Zhou, B.-y., Curnoe, D., Lu, H.-y., Li, H.-c., Wang, W., Cheng, H., Yi, S.-w., Jia, X., Du, P.-x., Xu, X.-h., Lu, Y.-m., Lu, Y., Zheng, H.-x., Zhang, H., Sun, C., Wei, L.-h., Han, F., Huang, J., Edwards, R.L., Jin, L., Li, H., 2021. Ancient DNA and multimethod dating confirm the late arrival of anatomically modern humans in southern China. *Proceedings of the National Academy of Sciences* 118, e2019158118, <http://doi.org/10.1073/pnas.2019158118>
- Tribolo, C., Mercier, N., Martin, L., Taffin, N., Miller, C.E., Will, M., Conard, N., 2022. Luminescence dating estimates for the coastal MSA sequence of Hoedjiespunt 1 (South Africa). *Journal of Archaeological Science: Reports* 41, 103320, <http://doi.org/10.1016/j.jasrep.2021.103320>
- van den Brink, E.C.M., Ackermann, O., Anker, Y., Dray, Y., Itach, G., Jakoel, E., Kapul, R., Roskin, J., Weiner, S., 2019. Chalcolithic groundwater mining in the southern Levant: open, vertical shafts in the Late Chalcolithic central coastal plain settlement landscape of Israel. *Levant* 51, 236-270, <http://doi.org/10.1080/00758914.2020.1818174>
- Wang, C.-X., Ji, X., Wu, Y., Jin, Z., Zhang, Y., Chen, M., Wang, N., Fan, A., 2022. Quartz OSL and TL dating of pottery, burnt clay, and sediment from Beicun archaeological site, China. *Quaternary Geochronology* 70, 101281, <http://doi.org/10.1016/j.quageo.2022.101281>
- Williams, M.A.J., Spooner, N.A., McDonnell, K., O'Connell, J.F., 2021. Identifying disturbance in archaeological sites in tropical northern Australia: Implications for previously proposed 65,000-year continental occupation date. *Geoarchaeology* 36, 92-108, <http://doi.org/10.1002/gea.21822>
- Wiśniewski, T., Krajcarz, M.T., Standzikowski, K., 2020. Turonian flint economy in the easternmost Magdalenian: new data from Stare Baraki, site 1 (eastern Poland). *Archaeological and Anthropological Sciences* 12, 281, <http://doi.org/10.1007/s12520-020-01230-y>
- Withnell, C.B., Joannes-Boyau, R., Bell, C.J., 2020. A reassessment of the age of the fauna from Cumberland Bone Cave, Maryland, (middle Pleistocene) using coupled U-series and electron spin resonance dating (ESR). *Quaternary Research* 97, 187-198, <http://doi.org/10.1017/qua.2020.30>

ESR, applied in various contexts

- Aşlar, E., Şahiner, E., Polymeris, G.S., Meriç, N., 2021. Thermally and optically stimulated luminescence properties of BeO dosimeter with double TL peak in the main dosimetric region. *Applied Radiation and Isotopes* 170, 109635, <http://doi.org/10.1016/j.apradiso.2021.109635>
- Avram, A., Kabacińska, Z., Micallef, A., Timar-Gabor, A., 2022. Testing the potential of using fine quartz for dating loess in South Island, New Zealand. *Radiation Measurements* 155, 106788, <http://doi.org/10.1016/j.radmeas.2022.106788>
- Bahain, J.-J., Farkh, S., Falguères, C., Shao, Q., Voinchet, P., Ghaleb, B., Hérisson, D., Loch, J.-L., Limondin-Lozouet, N., Auguste, P., Gauthier, A., Dabkowski, J., Deschodt, L., Antoine, P., 2022. ESR/U-series dating of Eemian human occupations of Northern France. *Quaternary Geochronology* 71, 101305, <http://doi.org/10.1016/j.quageo.2022.101305>
- Ben Arous, E., Duval, M., Bateman, M.D., 2022. ESR dating of optically bleached quartz grains from Plio-Pleistocene to Holocene coastal dune deposits (Wilderness-Knysna area, South Africa): a comparison with luminescence. *Quaternary Geochronology* 70, 101293, <http://doi.org/10.1016/j.quageo.2022.101293>

- Brill, D., Ageby, L., Obert, C., Hollerbach, R., Duval, M., Kolb, T., Bartz, M., 2022. Investigating the resetting of IRSL signals in beach cobbles and their potential for rock surface dating of marine terraces in Northern Chile. *Marine Geology* 443, 106692, <http://doi.org/10.1016/j.margeo.2021.106692>
- Duval, M., Arnold, L.J., Demuro, M., Parés, J.M., Campaña, I., Carbonell, E., Bermúdez de Castro, J.M., 2022. New chronological constraints for the lowermost stratigraphic unit of Atapuerca Gran Dolina (Burgos, N Spain). *Quaternary Geochronology* 71, 101292, <http://doi.org/10.1016/j.quageo.2022.101292>
- Duval, M., Westaway, K., Zaim, J., Rizal, Y., Aswan, Puspaningrum, M.R., Trihascaryo, A., Albers, P.C.H., Smith, H.E., Drawhorn, G.M., Price, G.J., Louys, J., 2021. New Chronological Constraints for the Late Pleistocene Fossil Assemblage and Associated Breccia from Ngalau Sampit, Sumatra. *Open Quaternary* 7, 9, <http://doi.org/http://doi.org/10.5334/oq.96>
- Falguères, C., Barkai, R., Tombret, O., Gopher, A., 2022. New ESR/U-series dates of the lowest Acheuleo-Yabrudian levels of Qesem cave. *Quaternary Geochronology* 69, 101266, <http://doi.org/10.1016/j.quageo.2022.101266>
- Gonzales, C.A.B., Taño, J.E., Yasuda, H., 2022. Effect of heating on the ESR signal of human fingernails. *Radiation Measurements* 152, 106728, <http://doi.org/10.1016/j.radmeas.2022.106728>
- Guilarte, V., Duval, M., 2021. ESR Dating of Optically Bleached Quartz Grains: Assessing the Impact of Different Experimental Setups on Dose Evaluations. *Geochronometria* 48, 179-190, <http://doi.org/10.2478/geochr-2020-0005>
- Guilarte, V., Fang, F., Grün, R., Duval, M., 2022. ESR dating of quartz grains: Evaluating the performance of various cryogenic systems for dosimetric purpose. *Radiation Measurements* 155, 106802, <http://doi.org/10.1016/j.radmeas.2022.106802>
- Han, F., Bahain, J.-J., Voinchet, P., Jin, M., Yin, G., 2022. Radiometric dating of Meipu hominin site in China by coupled ESR/U-series and cosmogenic ²⁶Al/¹⁰Be burial dating methods. *Quaternary Geochronology* 70, 101295, <http://doi.org/10.1016/j.quageo.2022.101295>
- Kabacińska, Z., Buylaert, J.P., Yi, S., Timar-Gabor, A., 2022. Revisiting natural and laboratory electron spin resonance (ESR) dose response curves of quartz from Chinese loess. *Quaternary Geochronology* 70, 101306, <http://doi.org/10.1016/j.quageo.2022.101306>
- Li, J., Yuan, S., Liu, Y., Liu, X., Bai, X., Jiang, J., Li, Y., Zhao, Z., 2019. Tectonic Uplift of the Yili Basin during the Last Stage of the Late Pleistocene: Evidence from ESR and OSL Dating of Sediments in the Huocheng Area, Xinjiang. *Acta Geologica Sinica - English Edition* 93, 1219-1227, <http://doi.org/10.1111/1755-6724.14355>
- Li, Y., Wei, C., Li, C., Guo, R., Liu, C., Zhang, Y., 2022. Application and evaluation of multiple-centres ESR dating of Pliocene-Quaternary fluvial sediments: A case study from the Zhoulao core from the Jiangnan Basin, middle Yangtze River basin, China. *Quaternary Geochronology* 70, 101297, <http://doi.org/10.1016/j.quageo.2022.101297>
- Louys, J., Duval, M., Price, G.J., Westaway, K., Zaim, Y., Rizal, Y., null, A., Puspaningrum, M., Trihascaryo, A., Breitenbach, S.F.M., Kwiciczen, O., Cai, Y., Higgins, P., Albers, P.C.H., de Vos, J., Roberts, P., 2022. Speleological and environmental history of Lida Ajer cave, western Sumatra. *Philosophical Transactions of the Royal Society B: Biological Sciences* 377, 20200494, <http://doi.org/10.1098/rstb.2020.0494>
- Mihailović, D., Kuhn, S.L., Bogičević, K., Dimitrijević, V., Marín-Arroyo, A.B., Marković, J., Mercier, N., Mihailović, B., Morley, M.W., Radović, P., Rink, W.J., Plavšić, S., Roksandic, M., 2022. Connections between the Levant and the Balkans in the late Middle Pleistocene: Archaeological findings from Velika and Mala Balanica Caves (Serbia). *Journal of Human Evolution* 163, 103138, <http://doi.org/10.1016/j.jhevol.2021.103138>
- Mihailović, D., Milošević, S., Blackwell, B.A.B., Mercier, N., Mentzer, S.M., Miller, C.E., Morley, M.W., Bogičević, K., Đurić, D., Marković, J., Mihailović, B., Dragosavac, S., Plavšić, S., Skinner, A.R., Chaity, I.I.C., Huang, Y.E.W., Chu, S., Nenadić, D., Radović, P., Lindal, J., Roksandic, M., 2022. Neanderthal settlement of the Central Balkans during MIS 5: Evidence from Pešturina Cave, Serbia. *Quaternary International* 610, 1-19, <http://doi.org/10.1016/j.quaint.2021.09.003>
- Priya, Arnold, L.J., Guilarte, V., Duval, M., Demuro, M., Weij, R., Reed, E.H., 2022. ESR and OSL dating of fossil-bearing deposits from Naracoorte Cave Complex palaeontological sites, south Australia. *Quaternary Geochronology* 69, 101270, <http://doi.org/10.1016/j.quageo.2022.101270>
- Richard, M., Pons-Branchu, E., Carmieli, R., Kaplan-Ashiri, I., Alvaro Gallo, A., Ricci, G., Caneve, L., Wroth, K., Dapigny, A., Tribolo, C., Boaretto, E., Toffolo, M.B., 2022. Investigating the effect of diagenesis on ESR dating of Middle Stone Age tooth samples from the open-air site of Lovedale, Free State, South Africa. *Quaternary Geochronology* 69, 101269, <http://doi.org/10.1016/j.quageo.2022.101269>
- Richter, M., Tsukamoto, S., 2022. Investigation of quartz electron spin resonance residual signals in the last glacial and early Holocene fluvial deposits from the Lower Rhine. *Geochronology* 4, 55-63, <http://doi.org/10.5194/gchron-4-55-2022>

- Shao, Q., Philippe, A., He, C., Jin, M., Huang, M., Jiao, Y., Voinchet, P., Lin, M., Bahain, J.-J., 2022. Applying a Bayesian approach for refining the chronostratigraphy of the Yumidong site in the Three Gorges region, central China. *Quaternary Geochronology* 70, 101304, <http://doi.org/10.1016/j.quageo.2022.101304>
- Shemer, M., Greenbaum, N., Taha, N., Brailovsky-Rokser, L., Ebert, Y., Shaar, R., Falgueres, C., Voinchet, P., Porat, N., Faershtein, G., Horwitz, L.K., Rosenberg-Yefet, T., Barkai, R., 2022. Late Acheulian Jaljulia – Early human occupations in the paleo-landscape of the central coastal plain of Israel. *PLOS ONE* 17, e0267672, <http://doi.org/10.1371/journal.pone.0267672>
- Tanaka, K., Muto, J., Yabe, Y., Oka, T., Nagahama, H., 2021. Effect of Fracture on ESR Intensity Using a Low-Velocity Rotary Shear Apparatus. *Geochronometria* 48, 205-214, <http://doi.org/10.2478/geochr-2020-0035>
- Tsang, M.-Y., Toyoda, S., Tomita, M., Yamamoto, Y., 2022. Thermal stability and closure temperature of barite for electron spin resonance dating. *Quaternary Geochronology* 71, 101332, <http://doi.org/10.1016/j.quageo.2022.101332>
- Wei, C.-Y., Liu, C.-R., Yin, G.-M., Li, W.-P., 2021. Electron Spin Resonance (ESR) Signal Intensity of Quartz E' Centre and Its Potential Use in Fluvial Sediments Provenance Tracing. *Geochronometria* 48, 197-204, <http://doi.org/10.2478/geochr-2020-0040>
- Withnell, C.B., Joannes-Boyau, R., Bell, C.J., 2020. A reassessment of the age of the fauna from Cumberland Bone Cave, Maryland, (middle Pleistocene) using coupled U-series and electron spin resonance dating (ESR). *Quaternary Research* 97, 187-198, <http://doi.org/10.1017/qua.2020.30>
- Yin, G., Liu, C., Yuan, R., Han, F., Ding, R., Bahain, J.-J., 2021. ESR Chronology of Bedrock Fault Activity in Carbonate Area: Preliminary Results from the Study of the Lijiang-Xiaojinhe Fault, Southeastern Tibet, China. *Geochronometria* 48, 215-221, <http://doi.org/10.2478/geochr-2020-0033>
- Yu, W., Zhang, J., Herries, A.I.R., Bailey, M., Joannes-Boyau, R., 2022. ESRfrag: A new suite of open access programs for the efficient handling of Electron Spin Resonance spectra of enamel fragments. *Quaternary Geochronology* 71, 101335, <http://doi.org/10.1016/j.quageo.2022.101335>
- Zhao, X., Hu, D., Wen, Z., Tang, X., Deng, J., Wang, R., Yi, L., 2021. Geological structures associated with potential gas-hydrate accumulation in the Mohe permafrost, North East China. *Journal of Petroleum Science and Engineering* 197, 108110, <http://doi.org/10.1016/j.petrol.2020.108110>
- Zhou, S., Xie, J., Ou, X., Xu, L., Sun, Y., Zeng, X., Wen, X., Chen, R., Yang, H., Huang, X., Zhou, Y., Sun, J., 2021. Evidence for glaciation predating MIS-6 in the eastern Nyainqêntanglha Range, southeastern Tibet. *Science China Earth Sciences* 64, 559-570, <http://doi.org/10.1007/s11430-020-9711-2>

Basic research

- Akpan, D.N., Aka, M.U., Effiong, C.I., Ekpo, S.S., 2022. A two-stage thermally-assisted optically stimulated luminescence (TA-OSL). *International Journal of Science and Research Archive* 5, 254-265, <http://doi.org/10.30574/ijrsra.2022.5.2.0066>
- Alexanderson, H., 2022. Luminescence characteristics of Scandinavian quartz, their connection to bedrock provenance and influence on dating results. *Quaternary Geochronology* 69, 101272, <http://doi.org/10.1016/j.quageo.2022.101272>
- Avram, A., Kabacińska, Z., Micallef, A., Timar-Gabor, A., 2022. Testing the potential of using fine quartz for dating loess in South Island, New Zealand. *Radiation Measurements* 155, 106788, <http://doi.org/10.1016/j.radmeas.2022.106788>
- Buchanan, G.R., Tsukamoto, S., Zhang, J., Long, H., 2022. Testing the natural limits of infrared radiofluorescence dating of the Luochuan loess-palaeosol sequence, Chinese Loess Plateau. *Radiation Measurements* 155, 106797, <http://doi.org/10.1016/j.radmeas.2022.106797>
- Caicedo Mateus, F.D., Asfora, V.K., Guzzo, P.L., Barros, V.S.M., 2021. Investigation of the spectrally resolved TL signals of natural quartz single crystals sensitized by high-dose of gamma-radiation and moderate heat-treatments. *Nuclear Instruments and Methods in Physics Research Section B: Beam Interactions with Materials and Atoms* 486, 37-47, <http://doi.org/10.1016/j.nimb.2020.11.001>
- Chandler, J.R., Sholom, S., McKeever, S.W.S., Bakhanova, E., Chumak, V., Velásquez, D., Hall, H.L., 2022. Dose conversion factors for absorbed dose in a mobile phone to absorbed dose in critical organs in an anthropomorphic phantom for emergency dosimetry applications: OSL and TL experimental results, and Monte Carlo simulations. *Radiation Measurements* 154, 106781, <http://doi.org/10.1016/j.radmeas.2022.106781>
- Chauhan, N., Selvam, T.P., Anand, S., Shinde, D.P., Mayya, Y.S., Feathers, J.K., Singhvi, A.K., 2021. Distribution of natural beta dose to individual grains in sediments. *Proceedings of the Indian National Science Academy* 87, 613-627, <http://doi.org/10.1007/s43538-021-00057-y>

- Chen, R., Lawless, J.L., Pagonis, V., 2022. On the various-heating-rates method for evaluating the activation energies of thermoluminescence peaks. *Radiation Measurements* 150, 106692, <http://doi.org/10.1016/j.radmeas.2021.106692>
- Cheng, T., Zhang, D., Zhao, H., Yang, S., Li, B., 2022. Bleachability of pIRIR signal from single-grain K-feldspar. *Quaternary Geochronology* 71, 101321, <http://doi.org/10.1016/j.quageo.2022.101321>
- Chruścińska, A., Palczewski, P., 2020. OSL characteristics: Theory and experiments. *Radiation Protection Dosimetry* 192, 266-293, <http://doi.org/10.1093/rpd/ncaa205>
- Cresswell, A.J., Sanderson, D.C.W., Carling, P.A., Darby, S.E., 2022. Quartz age extension applied to SE Asian cover sands. *Quaternary Geochronology* 69, 101271, <http://doi.org/10.1016/j.quageo.2022.101271>
- Durcan, J.A., Duller, G.A.T., 2022. The variability of single grain quartz luminescence properties investigated using EMCCD imaging. *Radiation Measurements* 153, 106748, <http://doi.org/10.1016/j.radmeas.2022.106748>
- El-Faramawy, N., Alazab, H.A., Gad, A., Sabry, M., 2022. Study of the thermoluminescence kinetic parameters of a β -irradiated natural calcite. *Radiation Physics and Chemistry* 190, 109793, <http://doi.org/10.1016/j.radphyschem.2021.109793>
- Espitia, Y., Cogollo, R., Osorio, A., Gutiérrez, O.D., 2022. Kinetic analysis of the main thermoluminescence glow peak in α -Al₂O₃. *Radiation Measurements* 153, 106749, <http://doi.org/10.1016/j.radmeas.2022.106749>
- Gray, H.J., Keen-Zebert, A., Furbish, D.J., Tucker, G.E., Mahan, S.A., 2020. Depth-dependent soil mixing persists across climate zones. *Proceedings of the National Academy of Sciences* 117, 8750-8756, <http://doi.org/10.1073/pnas.1914140117>
- Gu, Y., Wang, M., Zhang, Q., Ge, L., Xu, L., Lu, H., 2022. Accurate-parametric SAR-TL dating protocols for older sediments using quartz. *Applied Radiation and Isotopes* 181, 110072, <http://doi.org/10.1016/j.apradiso.2021.110072>
- Guilarte, V., Duval, M., 2021. ESR Dating of Optically Bleached Quartz Grains: Assessing the Impact of Different Experimental Setups on Dose Evaluations. *Geochronometria* 48, 179-190, <http://doi.org/10.2478/geochr-2020-0005>
- Guilarte, V., Fang, F., Grün, R., Duval, M., 2022. ESR dating of quartz grains: Evaluating the performance of various cryogenic systems for dosimetric purpose. *Radiation Measurements* 155, 106802, <http://doi.org/10.1016/j.radmeas.2022.106802>
- Herrera, J., Cogollo, R., Gutiérrez, O.D., Chithambo, M.L., 2022. Thermoluminescence of aquamarine: A preliminary study. *Radiation Measurements* 155, 106806, <http://doi.org/10.1016/j.radmeas.2022.106806>
- Huang, C., Zhang, J., Wang, L., Zhao, H., Li, S.-H., 2022. Equivalent dose estimation of calcite using isothermal thermoluminescence signals. *Quaternary Geochronology* 70, 101310, <http://doi.org/10.1016/j.quageo.2022.101310>
- Kalita, J.M., Chithambo, M.L., 2022. Thermally-assisted optically stimulated luminescence from deep electron traps in microcline. *Radiation Measurements* 154, 106786, <http://doi.org/10.1016/j.radmeas.2022.106786>
- Kitis, G., Peng, J., Li, B., Pagonis, V., 2022. Testing new analytical expression for dose response curves originating from the OTOR model. *Journal of Luminescence* 244, 118747, <http://doi.org/10.1016/j.jlumin.2022.118747>
- Klavnsen, M.F., Ankjærgaard, C., Behrens, C.P., Vogelius, I.R., Boye, K., Hansen, R.H., Andersen, C.E., 2022. Time-resolved plastic scintillator dosimetry in MR linear accelerators without image distortion. *Radiation Measurements* 154, 106759, <http://doi.org/10.1016/j.radmeas.2022.106759>
- Konstantinidis, P.G., Tsoutsoumanos, E., Polymeris, G.S., Kitis, G., 2022. Recombination pathways in a BeO yielding two main dosimetric TL peaks. *Radiation Measurements* 151, 106716, <http://doi.org/10.1016/j.radmeas.2022.106716>
- Lawless, J.L., Chen, R., Pagonis, V., 2022. Effect of radiation physics on inherent statistics of glow curves from small samples or low doses. *Radiation Measurements* 151, 106698, <http://doi.org/10.1016/j.radmeas.2021.106698>
- Martin, L., Sanderson, D., Paling, S., Cresswell, A., Murphy, S., 2022. Advancing dosimetry for Dating Environmental Materials: Development of an ultra-sensitive beta dosimeter system and potential for beta autoradiography. *Radiation Measurements* 154, 106760, <http://doi.org/10.1016/j.radmeas.2022.106760>
- Mercier, N., Galharret, J.-M., Tribolo, C., Kreutzer, S., Philippe, A., 2022. Luminescence age calculation through Bayesian convolution of equivalent dose and dose-rate distributions: the De_Dr model. *Geochronology* 4, 297-310, <http://doi.org/10.5194/gchron-4-297-2022>
- Odlum, M.L., Rittenour, T., Ault, A.K., Nelson, M., Ramos, E.J., 2022. Investigation of quartz luminescence properties in bedrock faults: Fault slip processes reduce trap depths, lifetimes, and sensitivity. *Radiation Measurements* 155, 106784, <http://doi.org/10.1016/j.radmeas.2022.106784>

- Pogue, J.A., DeWitt, R., 2022. Optical and thermal luminescence efficiencies of BeO exposed to low-energy protons and carbon ions. *Radiation Measurements* 154, 106758, <http://doi.org/10.1016/j.radmeas.2022.106758>
- Polymeris, G.S., Giannoulatou, V., Paraskevopoulos, K.M., Pagonis, V., Kitis, G., 2022. Anomalous fading in thermoluminescence signal of ten different K-feldspar samples and correlation to structural state characteristics. *Radiation Measurements* 155, 106789, <http://doi.org/10.1016/j.radmeas.2022.106789>
- Qin, J., Chen, J., Li, K., 2021. Characteristics of Pulsed Blue and Green Light Stimulated Luminescence Signals of Quartz and Feldspars. *Geochronometria* 48, 138-146, <http://doi.org/10.2478/geochr-2020-0038>
- Sadek, A.M., 2022. A more in-depth visualization for the heat transfer across the thermoluminescence detectors. *Radiation Measurements* 150, 106677, <http://doi.org/10.1016/j.radmeas.2021.106677>
- Sellwood, E.L., Kook, M., Jain, M., 2022. Investigating the potential of rock surface burial dating using IRPL and IRSL imaging. *Radiation Measurements* 155, 106783, <http://doi.org/10.1016/j.radmeas.2022.106783>
- Sontag-González, M., Frouin, M., Li, B., Schwenninger, J.-L., 2021. Assessing the Dating Potential of Violet Stimulated Luminescence Protocols. *Geochronometria* 48, 121-128, <http://doi.org/10.1515/geochr-2015-0115>
- Sontag-González, M., Fuchs, M., 2022. Spectroscopic investigations of infrared-radiofluorescence (IR-RF) for equivalent dose estimation. *Radiation Measurements* 153, 106733, <http://doi.org/10.1016/j.radmeas.2022.106733>
- Tanaka, K., Muto, J., Yabe, Y., Oka, T., Nagahama, H., 2021. Effect of Fracture on ESR Intensity Using a Low-Velocity Rotary Shear Apparatus. *Geochronometria* 48, 205-214, <http://doi.org/10.2478/geochr-2020-0035>
- Tsoutsoumanos, E., Konstantinidis, P.G., Polymeris, G.S., Karakasidis, T., Kitis, G., 2022. Electron trap filling and emptying through simulations: Studying the shift of the maximum intensity position in Thermoluminescence and Linearly Modulated Optically Stimulated Luminescence curves. *Radiation Measurements* 153, 106735, <http://doi.org/10.1016/j.radmeas.2022.106735>
- Williams, O.M., Smith, B.W., Spooner, N.A., 2022. A role for oxygen vacancies in quartz luminescence. *Radiation Measurements* 154, 106774, <http://doi.org/10.1016/j.radmeas.2022.106774>
- Williams, O.M., Spooner, N.A., 2022. Quartz mid-temperature thermoluminescence configurational coordinate model. *Radiation Measurements* 150, 106701, <http://doi.org/10.1016/j.radmeas.2021.106701>

Beyond quartz and K-feldspar: non-traditional minerals

- Calcite

- El-Faramawy, N., Alazab, H.A., Gad, A., Sabry, M., 2022. Study of the thermoluminescence kinetic parameters of a β -irradiated natural calcite. *Radiation Physics and Chemistry* 190, 109793, <http://doi.org/10.1016/j.radphyschem.2021.109793>
- Huang, C., Zhang, J., Wang, L., Zhao, H., Li, S.-H., 2022. Equivalent dose estimation of calcite using isothermal thermoluminescence signals. *Quaternary Geochronology* 70, 101310, <http://doi.org/10.1016/j.quageo.2022.101310>

- Salt

- Muhamad Azim, M.K., Abdul Sani, S.F., Daar, E., Khandaker, M.U., Almugren, K.S., Alkallas, F.H., Bradley, D.A., 2020. Luminescence properties of natural dead sea salt pellet dosimetry upon thermal stimulation. *Radiation Physics and Chemistry* 176, 108964, <http://doi.org/10.1016/j.radphyschem.2020.108964>

Dose rate interests

- Chauhan, N., Selvam, T.P., Anand, S., Shinde, D.P., Mayya, Y.S., Feathers, J.K., Singhvi, A.K., 2021. Distribution of natural beta dose to individual grains in sediments. *Proceedings of the Indian National Science Academy* 87, 613-627, <http://doi.org/10.1007/s43538-021-00057-y>
- Fu, X., Romanyukha, A.A., Li, B., Jankowski, N.R., Lachlan, T.J., Jacobs, Z., George, S.P., Rosenfeld, A.B., Roberts, R.G., 2022. Beta dose heterogeneity in sediment samples measured using a Timepix pixelated detector and its implications for optical dating of individual mineral grains. *Quaternary Geochronology* 68, 101254, <http://doi.org/10.1016/j.quageo.2022.101254>
- Kolb, T., Tudyka, K., Kadereit, A., Lomax, J., Poręba, G., Zander, A., Zipf, L., Fuchs, M., 2022. The μ Dose system: determination of environmental dose rates by combined alpha and beta counting – performance tests and practical experiences. *Geochronology* 4, 1-31, <http://doi.org/10.5194/gchron-4-1-2022>

- Kumar, R., Frouin, M., Gazack, J., Schwenninger, J.L., 2022. OxGamma: A MATLAB based application for the analysis of gamma-ray spectra. *Radiation Measurements* 154, 106761, <http://doi.org/10.1016/j.radmeas.2022.106761>
- Mauz, B., Nolan, P.J., Appleby, P.G., 2022. Technical note: Quantifying uranium-series disequilibrium in natural samples for dosimetric dating – Part 1: gamma spectrometry. *Geochronology* 4, 213-225, <http://doi.org/10.5194/gchron-4-213-2022>
- Tribolo, C., Mercier, N., Martin, L., Taffin, N., Miller, C.E., Will, M., Conard, N., 2022. Luminescence dating estimates for the coastal MSA sequence of Hoedjiespunt 1 (South Africa). *Journal of Archaeological Science: Reports* 41, 103320, <http://doi.org/10.1016/j.jasrep.2021.103320>

Dosimetry

- Aşlar, E., Şahiner, E., Polymeris, G.S., Meriç, N., 2021. Thermally and optically stimulated luminescence properties of BeO dosimeter with double TL peak in the main dosimetric region. *Applied Radiation and Isotopes* 170, 109635, <http://doi.org/10.1016/j.apradiso.2021.109635>
- Chandler, J.R., Sholom, S., McKeever, S.W.S., Bakhanova, E., Chumak, V., Velásquez, D., Hall, H.L., 2022. Dose conversion factors for absorbed dose in a mobile phone to absorbed dose in critical organs in an anthropomorphic phantom for emergency dosimetry applications: OSL and TL experimental results, and Monte Carlo simulations. *Radiation Measurements* 154, 106781, <http://doi.org/10.1016/j.radmeas.2022.106781>
- Gonzales, C.A.B., Taño, J.E., Yasuda, H., 2022. Effect of heating on the ESR signal of human fingernails. *Radiation Measurements* 152, 106728, <http://doi.org/10.1016/j.radmeas.2022.106728>
- Khabaz, R., Vega-Carrillo, H.R., 2020. Assessment of Kerma coefficients for OSL dosimeters by analytical and Monte Carlo approaches. *Radiation Physics and Chemistry* 173, 108875, <http://doi.org/10.1016/j.radphyschem.2020.108875>
- Kim, H., Yu, H., Discher, M., Kim, M.C., Choi, Y., Lee, H., Lee, J.T., Lee, H., Kim, Y.-s., Kim, H.S., Lee, J., 2022. A small-scale realistic inter-laboratory accident dosimetry comparison using the TL/OSL from mobile phone components. *Radiation Measurements* 150, 106696, <http://doi.org/10.1016/j.radmeas.2021.106696>
- Konstantinidis, P.G., Tsoutsoumanos, E., Polymeris, G.S., Kitis, G., 2022. Recombination pathways in a BeO yielding two main dosimetric TL peaks. *Radiation Measurements* 151, 106716, <http://doi.org/10.1016/j.radmeas.2022.106716>
- Martin, L., Sanderson, D., Paling, S., Cresswell, A., Murphy, S., 2022. Advancing dosimetry for Dating Environmental Materials: Development of an ultra-sensitive beta dosimeter system and potential for beta autoradiography. *Radiation Measurements* 154, 106760, <http://doi.org/10.1016/j.radmeas.2022.106760>
- Meriç, N., Şahiner, E., Kitis, G., Polymeris, G.S., 2021. Component-Resolved Analysis Towards Correlation between Thermoluminescence and Optically Stimulated Luminescence in Commercial Magnesium Oxide. *Geochronometria* 48, 222-231, <http://doi.org/10.2478/geochr-2020-0011>
- Muhamad Azim, M.K., Abdul Sani, S.F., Daar, E., Khandaker, M.U., Almugren, K.S., Alkallas, F.H., Bradley, D.A., 2020. Luminescence properties of natural dead sea salt pellet dosimetry upon thermal stimulation. *Radiation Physics and Chemistry* 176, 108964, <http://doi.org/10.1016/j.radphyschem.2020.108964>
- Pakari, O.V., Yukihara, E.G., Gawryluk, D.J., Bossin, L., 2022. On the feasibility of polymer fibers with mineral filler as emergency dosimeters. *Radiation Measurements* 153, 106718, <http://doi.org/10.1016/j.radmeas.2022.106718>

Portable instruments

- Gray, H., DuRoss, C., Nicovich, S., Gold, R., 2022. Luminescence sediment tracing reveals the complex dynamics of colluvial wedge formation. *Science Advances* 8, eabo0747, <http://doi.org/10.1126/sciadv.abo0747>
- van den Brink, E.C.M., Ackermann, O., Anker, Y., Dray, Y., Itach, G., Jakoel, E., Kapul, R., Roskin, J., Weiner, S., 2019. Chalcolithic groundwater mining in the southern Levant: open, vertical shafts in the Late Chalcolithic central coastal plain settlement landscape of Israel. *Levant* 51, 236-270, <http://doi.org/10.1080/00758914.2020.1818174>

Computer coding

- Dietze, M., Kreutzer, S., Fuchs, M.C., Meszner, S., 2022. sandbox – creating and analysing synthetic sediment sections with R. *Geochronology* 4, 323-338, <http://doi.org/10.5194/gchron-4-323-2022>

- Kumar, R., Frouin, M., Gazack, J., Schwenninger, J.L., 2022. OxGamma: A MATLAB based application for the analysis of gamma-ray spectra. *Radiation Measurements* 154, 106761, <http://doi.org/10.1016/j.radmeas.2022.106761>
- Pagonis, V., Kitis, G., 2022. Standardizing the computerized analysis and modeling of luminescence phenomena: New open-access codes in R and Python. *Radiation Measurements* 153, 106730, <http://doi.org/10.1016/j.radmeas.2022.106730>
- Prevezanou, K., Kioselaki, G., Tsoutsoumanos, E., Konstantinidis, P.G., Polymeris, G.S., Pagonis, V., Kitis, G., 2022. Implementation of expressions using Python in stimulated luminescence analysis. *Radiation Measurements* 154, 106772, <http://doi.org/10.1016/j.radmeas.2022.106772>
- Yu, W., Zhang, J., Herries, A.I.R., Bailey, M., Joannes-Boyau, R., 2022. ESRfrag: A new suite of open access programs for the efficient handling of Electron Spin Resonance spectra of enamel fragments. *Quaternary Geochronology* 71, 101335, <http://doi.org/10.1016/j.quageo.2022.101335>

Review

- Bailey, R.M., 2020. Luminescence Dating, in: Britton, K., Richards, M.P. (Eds.), *Archaeological Science: An Introduction*. Cambridge University Press, Cambridge, pp. 424-438, <http://doi.org/10.1017/9781139013826.019>
- Mauz, B., Nolan, P.J., Appleby, P.G., 2022. Technical note: Quantifying uranium-series disequilibrium in natural samples for dosimetric dating – Part 1: gamma spectrometry. *Geochronology* 4, 213-225, <http://doi.org/10.5194/gchron-4-213-2022>
- Sandeva, I., Dimčev, V., Ginovska, M., Stojanovska, L., Krleski, A., Spasevska, H., 2020. Age determination of a sediment sample by optically stimulated luminescence. *Journal of Electrical Engineering and Information Technologies* 5, 79-84, <http://doi.org/10.51466/JEEIT2052079s>
- Singhvi, A.K., Kaushal, R.K., Parida, S., 2022. Luminescence dating and Quaternary Geology: The Indian Narrative. *Journal of the Palaeontological Society of India* 67, 183-210, https://palaeontologicalsociety.in/vol67_1/14.%20JPSI-IBSV-Singhvi.pdf
- Skinner, A.R., Blackwell, B.A.B., Blickstein, J.I.B., Lundberg, J., 2021. Using Dentine as well as Enamel in ESR Dating. *Brazilian Journal of Physics* 52, 25, <http://doi.org/10.1007/s13538-021-01030-2>
- Woor, S., 2022. Optically stimulated luminescence dating of ancient landscapes. *Nature Reviews Earth & Environment* 3, 362-362, <http://doi.org/10.1038/s43017-022-00307-7>

Comment of interest for all

- Liritzis, I., 2022. Sources of error and bias in luminescence dating. *Mediterranean Archaeology and Archaeometry* 22, 193-194, <http://doi.org/10.5281/zenodo.6464966>

Books

- McKeever, S.W.S., 2022. *A Course in Luminescence Measurements and Analyses for Radiation Dosimetry*. Wiley, 416p, <https://www.wiley.com/en-us/A+Course+in+Luminescence+Measurements+and+Analyses+for+Radiation+Dosimetry-p-9781119646921>

Conference Announcements: UKLUM 2022



UK Luminescence and ESR meeting 2022

Royal Holloway University of London

This is the first announcement for the 2022 UK luminescence and ESR dating meeting (UKLUM2022) which will be held at Royal Holloway University of London between the 7th and 9th of September, 2022.

The meeting will provide an informal forum for discussing luminescence and ESR research, with an emphasis on recent developments, ongoing work and student projects. Oral and poster presentations will be welcome, particularly from student and early career researchers. To register an interest or request further details please contact Simon Armitage using the conference specific e-mail address: UKLum2022@rhul.ac.uk

We look forward to welcoming you to Royal Holloway.

UK Luminescence and ESR meeting 2022



ROYAL
HOLLOWAY
UNIVERSITY
OF LONDON

Conference Announcements: **APLED 2022**

Dear Colleagues,

It is our pleasure to announce **The Sixth Asia-Pacific Conference on Luminescence and Electron Spin Resonance Dating - APLED 2022, which will be held online on 26-28 September 2022, organized by Ankara University.** The theme for the conference is to bring together academic researchers and scientists worldwide. The language of the conference is English. The topics of the conference are the following:

1. Basic physical processes for luminescence dosimetry and dating
2. Material characterization for luminescence dosimetry and dating
3. Innovative dating and dosimetry approaches
4. Advances in dose rate determination
5. Instrumentation and procedures
6. Luminescence and ESR Dosimetry
7. Advances and applications of ESR
8. Advanced technologies and methods on luminescence, ESR dosimetry and dating
9. Applications in earth and planetary sciences
10. Applications in archaeology
11. Other related topics

We would like to invite you to submit your research article in APLED-2022. The conference includes invited lectures, oral and poster presentations. The presentations will be in sessions covering the conference topics. There will also be Q&A at the end of each session. There will be poster sessions in which a video related to the research can be uploaded. Additionally, sponsors will have a chance to present.

Abstract Submission and Early Registration: 1 August 2022

Abstract Acceptance: within 15-20 days

Please follow the website for announcements: apled2022.org

We hope that you take the opportunity to attend our online conference and meet colleagues.

Looking forward to seeing you in APLED-2022.

Best Regards,

The Local Organizing Committee

Conference Announcements: 14th NWLDW

The US Geological Survey (Denver) is hosting the New World Luminescence Dating Workshop (NWLDW) in Palisade, Colorado. This workshop will take place directly after the Geological Society of America annual meeting in Denver to allow for our academic friends to only be away from their classrooms for one week.

The meeting will be at the **Wine Country Inn of Palisade, Colorado very close to Grand Junction, Colorado**. Wine Country Inn sits in the middle of fruit orchards and vineyards on terraces of the Colorado (Grand) River. Local fruit stands and a small town brewery compliment the warm days and cool nights. Towering mesas capped by the Mesa Verde Group with Mancos Shale beneath offer stunning contrasts to view while you sip your wine grown right on site at 777 Grande River Drive, Palisade CO 81526 (970-464-5777). Colorado National Monument is a short drive away, as is Grand Mesa. Palisade is served by two airports with direct flights from Denver: Montrose, Colorado and Walker Air Field of Grand Junction. It would also be a beautiful drive from Denver through the Rocky Mountains with fall scenery. Denver transportation can also be arranged for car pooling if needed.

The NWDLW has two parts: a one-day calibration of portable gamma spectrometers on either Dept. of Energy drill pads or drill holes on Thursday and more traditional presentations and posters on Friday and Saturday. We have access to a detailed report outlining the drill pad and hole options. You need not have a portable gamma spec to see the facilities and get an idea of contacts or available calibration options.

The day for the gamma spectrometry calibrations is Thursday October 13, 2022.

Presentations are Friday and Saturday October 14 and 15. The meeting will end around 4 pm Saturday for those that need an earlier start back. Or you could join us for a final goodbye to the wine room. Return home Sunday October 16, 2022.

A block of rooms has been set aside for meeting participants. Rooms are \$165/night and can hold 2-3 people. **You will need to book your own rooms with the NWLDW group before September 15 (970-464-5777).** Breakfast is provided by the Inn, as well as complimentary happy hour wine so this is a very good deal indeed. We will have a Friday night dinner hosted by the Inn around \$35-\$40/person. We will set up an Event Brite page for credit card registration and dinner so that we don't have to pester you for IOU's at the workshop.

We anticipate that registration will be \$100/professionals, \$50/early career, and \$25/students. Registration covers conference room rental, complimentary glass of wine/beer at happy hour, and programs. Cost is low due to sponsorship of the meeting, so please encourage students to come.

Abstracts for the program are due August 31. They are limited to one page in any format you desire except please use Times New Roman 12 Font. These abstracts can cover any topic that you think the group will find interesting in dosimetry, luminescence theory, applications, or database archiving. Conference organizers are Shannon Mahan (smahan@usgs.gov), Harrison Gray (hgray@usgs.gov), and Emma Krolczyk (ekrolczyk@usgs.gov). Please e-mail any questions to us.

Conference Announcements: **LED 2023**



17th INTERNATIONAL LUMINESCENCE AND ELECTRON SPIN RESONANCE DATING CONFERENCE (LED2023)



We are pleased to announce that LED2023 will take place from the

26th - 30th June 2023
DGI byen
Copenhagen

in the good old-fashioned “let-us-meet-in-person” style. LED2023 will cover similar scientific themes to previous LED conferences and we hope to attract a large number of students and professionals working in the field of luminescence and ESR dating. We aim to provide a pleasant and stimulating environment for presentations and discussions. The conference homepage will be launched soon and will provide further practical details regarding the conference.

Please send any queries or requests to LED2023@dtu.dk

We look forward to welcoming you in Copenhagen.

The organizing committee, DTU Physics



Ancient TL

ISSN 2693-0935

Aims and Scope

Ancient TL is a journal devoted to Luminescence dating, Electron Spin Resonance (ESR) dating, and related techniques. It aims to publish papers dealing with experimental and theoretical results in this field, with a minimum of delay between submission and publication. Ancient TL also publishes a current bibliography, thesis abstracts, letters, and miscellaneous information, e.g., announcements for meetings.

Frequency

Two issues per annum in June and December

Submission of articles to Ancient TL

Ancient TL has a reviewing system in which direct dialogue is encouraged between reviewers and authors. For instructions to authors and information on how to submit to Ancient TL, please visit the website at:

<http://ancienttl.org/TOC1.htm>

Journal Enquiries

For enquiries please contact the editor:

Regina DeWitt, Department of Physics, East Carolina University, Howell Science Complex, 1000 E. 5th Street, Greenville, NC 27858, USA; Tel: +252-328-4980; Fax: +252-328-0753 (dewittr@ecu.edu)

Subscriptions to Ancient TL

Ancient TL Vol. 32 No.2 December 2014 was the last issue to be published in print. Past and current issues are available for download free of charge from the Ancient TL website:

<http://ancienttl.org/TOC4.htm>